

AD-A134 175 FLIGHT TEST OF ADVANCED DIGITAL CONTROL CONCEPTS(U)  
SYSTEMS TECHNOLOGY INC HAWTHORNE CA  
R F WHITBECK ET AL. MAR 82 AFWAL-TR-82-3821

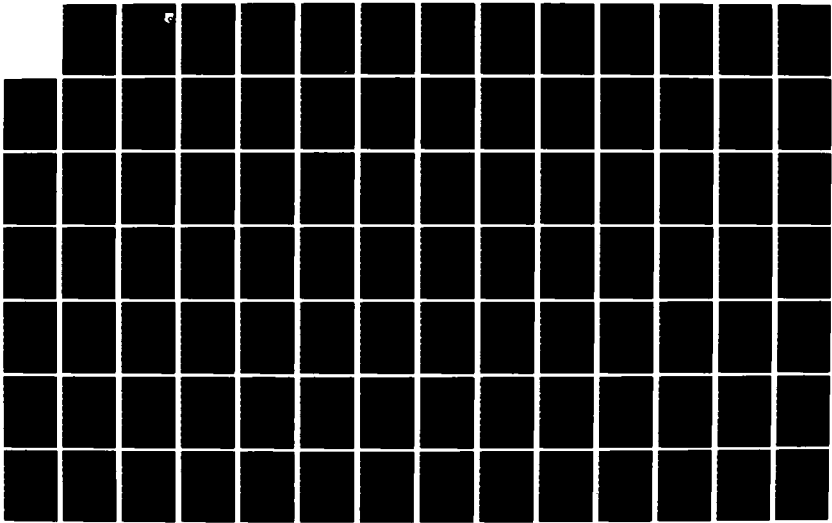
1/2

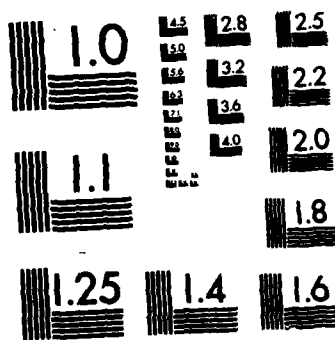
UNCLASSIFIED

F33615-80-C-3612

F/G 1/3

NL





MICROCOPY RESOLUTION TEST CHART  
NATIONAL BUREAU OF STANDARDS-1963-A

2134176-

2

AFWAL-TR-82-3021

FLIGHT TEST OF ADVANCED DIGITAL CONTROL CONCEPTS



Richard F. Whitbeck  
James C. Smith  
Thomas T. Myers

Systems Technology, Inc.  
Hawthorne, CA

March 1982

Final Technical Report for Period June 1980 - February 1982

Approved for public release; distribution unlimited.

FLIGHT DYNAMICS LABORATORY  
AIR FORCE WRIGHT AERONAUTICAL LABORATORIES  
AIR FORCE SYSTEMS COMMAND  
WRIGHT-PATTERSON AIR FORCE BASE, OHIO 45433

DMC FILE COPY

STIC  
ELECTED

OCT 31 1983

A

88 10 16 821

NOTICE

When Government drawings, specifications, or other data are used for any purpose other than in connection with a definitely related Government procurement operation, the United States Government thereby incurs no responsibility nor any obligation whatsoever; and the fact that the government may have formulated, furnished, or in any way supplied the said drawings, specifications, or other data, is not to be regarded by implication or otherwise as in any manner licensing the holder or any other person or corporation, or conveying any rights or permission to manufacture use, or sell any patented invention that may in any way be related thereto.

This report has been reviewed by the Office of Public Affairs (ASD/PA) and is releasable to the National Technical Information Service (NTIS). At NTIS, it will be available to the general public, including foreign nations.

This technical report has been reviewed and is approved for publication.

David K. Bowser

DAVID K. BOWSER  
Project Engineer  
Control Dynamics Branch

R.O. Anderson

RONALD O. ANDERSON, Chief  
Control Dynamics Branch  
Flight Control Division

FOR THE COMMANDER

James D. Lang

JAMES D. LANG, Lt Colonel USAF  
Chief, Flight Control Division  
Flight Dynamics Laboratory

"If your address has changed, if you wish to be removed from our mailing list, or if the addressee is no longer employed by your organization please notify AFWAL/FIGC, N-PAFB, OH 45433 to help us maintain a current mailing list".

Copies of this report should not be returned unless return is required by security considerations, contractual obligations, or notice on a specific document.

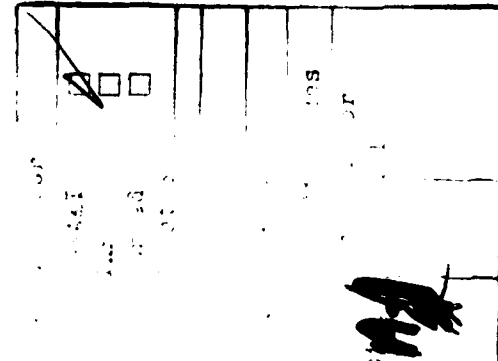
UNCLASSIFIED

**SECURITY CLASSIFICATION OF THIS PAGE (When Data Entered)**

REPORT DOCUMENTATION PAGE		READ INSTRUCTIONS BEFORE COMPLETING FORM
1. REPORT NUMBER  AFWAL-TR-82-3021	2. GOVT ACCESSION NO.  A134175	3. RECIPIENT'S CATALOG NUMBER
4. TITLE (and Subtitle)  FLIGHT TEST OF ADVANCED DIGITAL CONTROL CONCEPTS	5. TYPE OF REPORT & PERIOD COVERED  Final Technical Report June 1980 - February 1982	
	6. PERFORMING ORG. REPORT NUMBER  F33615-80-C-3612	
7. AUTHOR(s) Richard F. Whitbeck James C. Smith Thomas T. Myers	8. CONTRACT OR GRANT NUMBER(s)  F33615-80-C-3612	
9. PERFORMING ORGANIZATION NAME AND ADDRESS Systems Technology, Inc. 13766 South Hawthorne Boulevard Hawthorne, CA 90250	10. PROGRAM ELEMENT, PROJECT, TASK AREA & WORK UNIT NUMBERS  Program Element 62201F 24030543	
11. CONTROLLING OFFICE NAME AND ADDRESS Flight Dynamics Laboratory (AFWAL/FIGC) AF Wright Aeronautical Laboratories, AFSC Wright-Patterson Air Force Base, Ohio 45433	12. REPORT DATE  March 1982	
14. MONITORING AGENCY NAME & ADDRESS (if different from Controlling Office)	13. NUMBER OF PAGES  125	
	15. SECURITY CLASS. (of this report)  Unclassified	
	15a. DECLASSIFICATION/DOWNGRADING SCHEDULE	
16. DISTRIBUTION STATEMENT (of this Report)  Approved for public release; distribution unlimited		
17. DISTRIBUTION STATEMENT (of the abstract entered in Block 20, if different from Report)		
18. SUPPLEMENTARY NOTES		
19. KEY WORDS (Continue on reverse side if necessary and identify by block number)  Aircraft Control Theory Digital Control Systems Flight Control Digital Computers Variable-Stability Aircraft Simulation Airborne Computers Frequency Response Digital Control Flying Qualities Data Holds Flight Test Servo Analysis Sampled Data		
20. ABSTRACT (Continue on reverse side if necessary and identify by block number)  The overall objective of this research is to investigate, via in-flight simulation, new and innovative digital control design concepts for six degree-of-freedom aircraft, including implication to flying qualities of digital mechanization. Factors such as emulation (Tustin transform) versus direct digital to analog coupler (zero-order hold versus slew rate data hold) are the primary digital artifacts considered in this research effort.		

## TABLE OF CONTENTS

	<u>Page</u>
I. INTRODUCTION.....	1
II. TASK DESCRIPTION AND EQUATIONS OF MOTION.....	3
A. Introduction.....	3
B. Description of Task.....	3
C. Description of Baseline Experiment.....	4
D. Baseline Analog Configuration.....	9
E. In-Flight Vehicle Identification.....	9
F. VRA Setup for Analog Direct Force Tests of Ref. 1.....	11
G. YF-16 Bare Airframe Considerations.....	14
H. First-Order Form of Equations of Motion.....	15
I. Discrete First-Order Form (ZOH).....	16
J. Discrete First-Order Form (Slewer).....	16
III. ZOH DIGITAL CONTROLLER.....	18
A. Introduction.....	18
B. Review of the ESD Method.....	19
C. The Digital Controller Case.....	22
D. A Check Computation: Navion + Closed-Loop YF-16.....	25
E. ZOH ESD Control Laws.....	29
F. Defining Equations, in "TOTAL" Notation.....	32
G. Comparison Equations -- State Transition.....	33
H. $w'$ -Comparison.....	33
I. Macros.....	34
J. ZOH, ESD Gains.....	36
K. Validation: Theoretical Controller, TOTAL Model of YF-16.....	36
L. Validation: Microprocessor-Based Control Law, Analog Computer Model of YF-16.....	42
M. Validation: Microprocessor-Based Control Law, Navion as YF-16 Simulator.....	42



	<u>Page</u>
<b>IV. SLEWER CONTROLLER.....</b>	<b>45</b>
A. Introduction.....	45
B. Synthesis Using a Generalized ESD Approach.....	45
C. Solution Via Wiener-Hopf.....	47
D. Spectral Factorization Solution Method.....	47
E. Key Features of the Solution.....	48
F. Illustrative Example.....	49
G. General Procedure.....	54
H. Slewler Control Law.....	55
I. Validation: Theoretical Controller, Theoretical YF-16.....	58
J. Validation: Hardware-Based Slewler, Analog YF-16.....	58
K. Gain Allocation and Noise Problems.....	63
L. The Graceful Entry Problem.....	66
<b>V. CONCLUSIONS AND RECOMMENDATIONS.....</b>	<b>69</b>
A. Conclusions.....	69
B. Recommendations.....	69
<b>REFERENCES.....</b>	<b>70</b>
<b>APPENDIX A. DATA FOR FIRST-ORDER FORMS.....</b>	<b>71</b>
<b>APPENDIX B. VRA HARDWARE AND SOFTWARE SYSTEMS.....</b>	<b>81</b>
<b>APPENDIX C. ANNOTATED TOTAL RUN.....</b>	<b>90</b>
<b>APPENDIX D. VALIDATION OF ZOH CONTROL LAW, FREQUENCY RESPONSE.....</b>	<b>96</b>
<b>APPENDIX E. SLEWER FIRST-ORDER FORM.....</b>	<b>111</b>
<b>APPENDIX F. SLEWER WIENER-HOPF EQUATIONS.....</b>	<b>115</b>
<b>APPENDIX G. PROOF, <math>C_F^{-1}C_B = (\Gamma_1'\Gamma_m)^{-1}\Gamma_1'(\phi_m - \phi_s)</math>.....</b>	<b>117</b>
<b>APPENDIX H. PHYSICAL REALIZATION OF THE SLEWER COUPLER.....</b>	<b>119</b>
<b>APPENDIX I. ADDITIONAL SLEWER DATA AND TABULAR LISTING OF STEP RESPONSES.....</b>	<b>123</b>

## LIST OF FIGURES

	<u>Page</u>
1. Tracking Kinematics and Dynamics Effect of Range.....	5
2. Comparison of Heading Dynamics and Pipper Error Dynamics for Wings Level Turn.....	7
3. Ideal Pilot Input Signal to Roll Autopilot.....	8
4. Navion VRA.....	10
5. VRA as Mechanized for Simulation.....	10
6. Fourier Transformed Heading Responses, Configuration WL1, Minimal Coupling.....	11
7. Analog Test Setup.....	12
8. Lateral VRA System, Prior to Ref. 1 Study.....	12
9. "Analog" Test Configuration.....	14
10. Digital Controller Configuration.....	22
11. Test Configuration.....	30
12. Digital Controller Configuration.....	30
13. Bode Plots: $r/\delta_{cc}$ , $\theta/\delta_{cc}$ .....	40
14. Bode Plots: $p/\delta_{cc}$ , $\phi/\delta_{cc}$ .....	41
15. Comparison of Theoretical Continuous Controllers with ZOH Controller on Hybrid Simulator.....	43
16. VRA Flight Record of Wings Level Turns, ZOH Control Law.....	44
17. Block Diagram for Software Realization.....	55
18. Slever Step Response.....	60
19. YF-16 Model Response to a Step Pedal Input.....	61
20. Zero-Order Hold Gain Configuration.....	63
21. DFCS Gain Configurations Illustrating Within-Loop Placement of Scale Vectors.....	65

	<u>Page</u>
22. Resultant Gain Configuration Illustrating Simplification Brought About by Pre-Multiplication of Matrices.....	65
23. ZOH Auto-Trim Algorithm .....	67
24. Variable Response Research Aircraft (VRA).....	82
25. VRA Analog and Digital Systems -- Data Path Diagrams.....	84
26. DFCS Hardware and Software.....	88
27. Bode Plot $\gamma/\delta_{CC}$ , $\beta/\delta_{CC}$ .....	97
28. Bode Plot $p/\delta_{CC}$ , $\phi/\delta_{CC}$ .....	98
29. Bode Plot $\psi/\delta_R$ , 10 Hz, 50 Hz.....	99
30. Bode Plot $\beta/\delta_R$ .....	100
31. Bode Plot $p/\delta_R$ .....	101
32. Bode Plot $\phi/\delta_R$ .....	102
33. Bode Plot $r/\delta_C$ .....	103
34. Bode Plot $\beta/\delta_C$ .....	104
35. Bode Plot $p/\delta_C$ .....	105
36. Bode Plot $\phi/\delta_C$ .....	106
37. Bode Plot $r/\delta_A$ .....	107
38. Bode Plot $\beta/\delta_A$ .....	108
39. Bode Plot $p/\delta_A$ .....	109
40. Bode Plot $\phi/\delta_A$ .....	110
41. Zero-Order Hold Reconstruction.....	119
42. An Incremental Implementation.....	120
43. A Hardware Slew.....	121
44. Partially Software Implemented Slew.....	122

## LIST OF TABLES

	<u>Page</u>
1. s- and z-Plane Open Loop Plant Representations.....	31
2. ZOH Gains.....	37
3. w'-, s-Plane Comparisons.....	38
4. Step Response.....	39
5. Control Law Scale Factors.....	59
6. VRA Control Characteristics.....	82
7. Data for $\Gamma_1$ , $\Gamma_2$ .....	123
8. Slewer Step Responses.....	125

SECTION I  
INTRODUCTION

Philosophically, aircraft dynamic flying qualities requirements should be independent of the method of control system mechanization. However, from a practical viewpoint, it is known that the type of control mechanization employed does affect the aircraft response characteristics. Consequently, there is a need to practically assess, via in-flight evaluation, the extent of the control response modifications introduced by digital implementation.

All of the significant digital controller implementations (e.g., F-18 and Shuttle) as well as the system presently being developed for the F-5G, have utilized the emulation approach. Emulation is a process wherein an existing analog control law is "digitized" by the use of a so-called "substitution-for-s" rule, usually the Tustin transform. The verisimilitude of this approach is critically dependent on open-loop system bandwidth and sample rate.

In contrast, it is the objective of the present study to use direct digital design procedures and synthesize low data rate control laws for a conventional coupler (zero-order hold) and a more complex coupler which introduces less control roughness (slewer). These control laws will then be flight tested to evaluate the modifications introduced in a particular direct force mode.

Specifically, the analog fly-by-wire system of the Variable Stability Navion will be programmed to simulate an open-loop, lateral-directional YF-16 at  $M = 0.8$  and an altitude of 20,000 ft. A microprocessor-implemented controller is then closed around the bare-airframe YF-16 simulation to force a wings-level turn (WLT) mode. These flight evaluations will replicate a previous, completely analog, in-flight simulation which will serve as a baseline configuration.

An ultimate goal is to make flying qualities assessments, using paired comparisons between analog and the two forms of digital controllers. These assessments are beyond the scope of the present study.

The evaluation of the differences between baseline analog and digital controller cases will constitute a three-stage process. In the first stage the theoretical control law will be tested against an idealized analytical model of the open-loop YF-16. In the second stage the control law will be implemented in the microprocessor-based system and again flown against an idealized model of the open-loop system. Here a TR-48 analog computer will serve as a surrogate YF-16. In the third stage the hardware-implemented control law will be tested against a simulation of the open-loop YF-16, where now the Navion VRA will serve as the host aircraft. This three-stage procedure should be very effective in apportioning the errors introduced by the various interacting elements.

The report is organized into five sections and nine appendices. The heavy use of appendices serves to increase the flow of the development by removing routine developments (e.g., first-order forms of the equations of motion) and detailed theoretical proofs from the main body of the report.

Section II gives a brief description of the task and an overview of the "baseline" analog experiment, the WLT direct side force mode. Section III treats the ZOH control law synthesis and validation in much the same manner as is done for the slewer in Section IV. The report concludes with Section V, conclusions and recommendations.

## SECTION II

### TASK DESCRIPTION AND EQUATIONS OF MOTION

#### A. INTRODUCTION

This section focuses on a description of the baseline analog wings-level turn (WLT) and those facets of the testing approach that are a necessary background for understanding the digital implementation. There is a brief description of the baseline analog task and experiment, together with a description of the feedforward and feedback filter sections used to cross-couple the controller and modify the open-loop dynamics of the simulator aircraft.

First-order forms for the equations of motion are given in the s- and z-domains and for the ZOH and slewer.

#### B. DESCRIPTION OF TASK

The purpose of the baseline analog flight test phase of the Reference 1 program was to fill gaps in the data base as required to develop a handling qualities criterion. A tight tracking task was required to separate good and bad configurations, i.e., to force the pilot to maximum effort and thereby expose deficiencies which may not otherwise have been evident.

The primary task selected in Reference 1 was air-to-air tracking. This task was ideal because the target motions could be tailored to exercise a broad spectrum of frequencies in the tracking aircraft.

The control-configured vehicle (CCV) mode selected was the wings-level turn ( $A_y$ ) mode. This mode was selected because it has considerable potential for future CCV aircraft for air-to-air and air-to-ground applications. The approach of Reference 1 was to generate a series of configurations with adverse and proverse roll and yaw coupling in the wings-level turn mode. These configurations were designed to test the bandwidth hypothesis; that is to say, if the hypothesis is valid then

the pilot ratings should correlate with bandwidth regardless of the type of coupling. Based on this line of reasoning, the following configurations were developed:

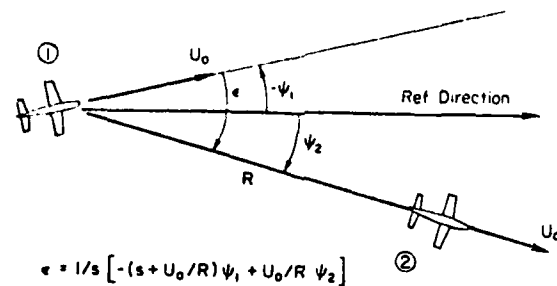
- 1) Wings-level turn with adverse and proverse yaw coupling designed to vary heading bandwidth from zero to nearly 7 rad/sec.
- 2) Wings-level turn configurations with adverse and proverse roll coupling, designed to give the same heading bandwidth as the configurations in Item 1.

If the bandwidth hypothesis is valid, these configurations with similar values of heading bandwidth should receive similar pilot ratings and commentary.

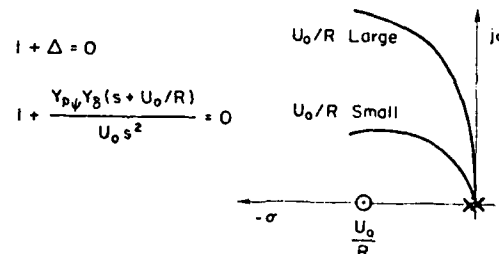
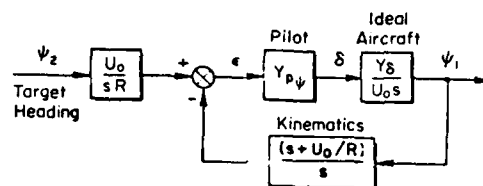
#### C. DESCRIPTION OF BASELINE ANALOG EXPERIMENT

The tracking kinematics for the ideal case (no coupling or uncancelled aircraft modes) in the wings-level turn mode are summarized in Figure 1. The block diagram in Figure 1 indicates the interrelationship between the idealized aircraft dynamics, the air-to-air tracking kinematics, and the target heading,  $\psi_2$ . The tracking kinematics appear in the feedback transfer functions of this block diagram and result in a numerator zero at  $U_0/R$  (aircraft speed/range). The effect of this zero on the piloted loop closure in attempting to null the aim error,  $\epsilon$ , is shown in the root locus plot at the bottom of Figure 1a. The closed-loop characteristic equation is seen to be well damped when  $U_0/R$  is small, that is, at large values of range. At low values of range, or when  $U_0/R$  is large, the closed-loop characteristic roots are seen to be lightly damped. Physically this stems from the fact that  $\epsilon$  is primarily set by heading when  $U_0/R$  is large; whereas, when  $U_0/R$  is small,  $\epsilon$  is strongly affected by lateral displacement (which involves an additional integration). Formation flying represents the limiting case of this with  $R \approx 0$ .

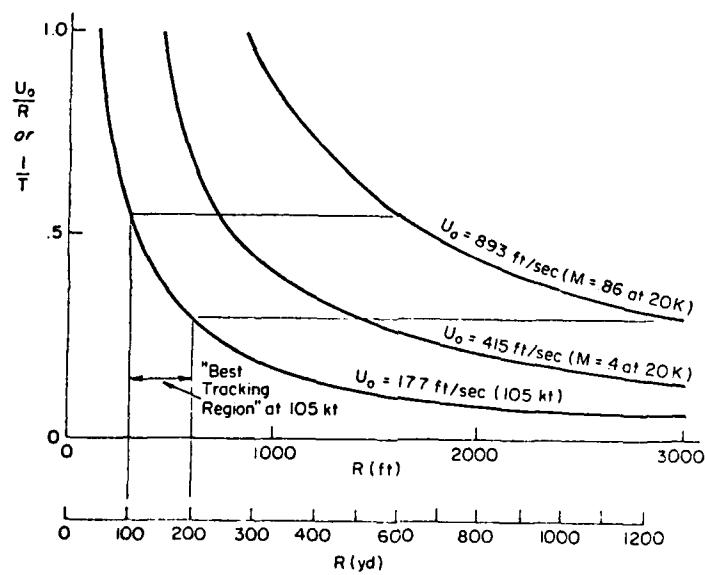
Due to structural limitations of the side force generators, the Princeton University Variable Research Aircraft (VRA) has a maximum maneuvering speed of 105 kt — well below typical air-to-air combat



For Wings Level Turn



a)



R of 100-200 yards in Navion equals R of 600-1200 yards in typical air-to-air encounter

b)

Figure 1. Tracking Kinematics and Dynamics Effect of Range

speeds. It was therefore necessary to adjust the range between the target and attacker in our experiment to make the parameter  $U_0/R$  consistent with a typical air combat encounter. The effect of range on  $U_0/R$  for our test conditions (105 kt TAS) is shown in Figure 1b. Here we can see that typical combat parameters of  $M = 0.86$  at 20,000 ft and a range of 600-1200 yards converts to 100-200 yards at the VRA testing speed (105 kt). Shorter ranges result in relatively large values of  $U_0/R$ , e.g., values which approach the piloted crossover region in the vicinity of 1 rad/sec. The effect of this on sight dynamics is shown in Figure 2 for the baseline configuration (WLT1) used in the flight test experiment. The frequency response phase plot in Figure 2 indicates that for frequencies below  $U_0/R$  the pipper error dynamics are very lightly damped, whereas for a large range of frequencies well above  $U_0/R$  the pipper error dynamics are equivalent to the heading dynamics. Hence, for values of range where  $U_0/R$  is well below the piloted crossover frequency, it is appropriate to use heading as the controlled variable when applying the bandwidth hypothesis. Tracking at close ranges, where  $U_0/R$  is large enough to be near the region of piloted crossover (1 rad/sec), was found to be impractical during initial flight test evaluation because of the very light damping of the pipper error dynamics. The formal runs were conducted so that the safety pilot had control over range and maintained the target aircraft at a nominal range of 150 yards throughout the data runs. This was accomplished by using a series of concentric range circles painted on the aircraft windscreen and sized so that the target aircraft's wingspan would be coincident with the target circle at a range of 150 yards.

The primary disadvantage of testing at speeds well below  $M = 0.8$  is that it is not possible to correctly simulate the aircraft dynamics and the pilot acceleration cues simultaneously. This may be seen from the equation for lateral acceleration:

$$a_{y_{cg}} = U_0(\dot{\beta} + r) - g\dot{\phi}$$

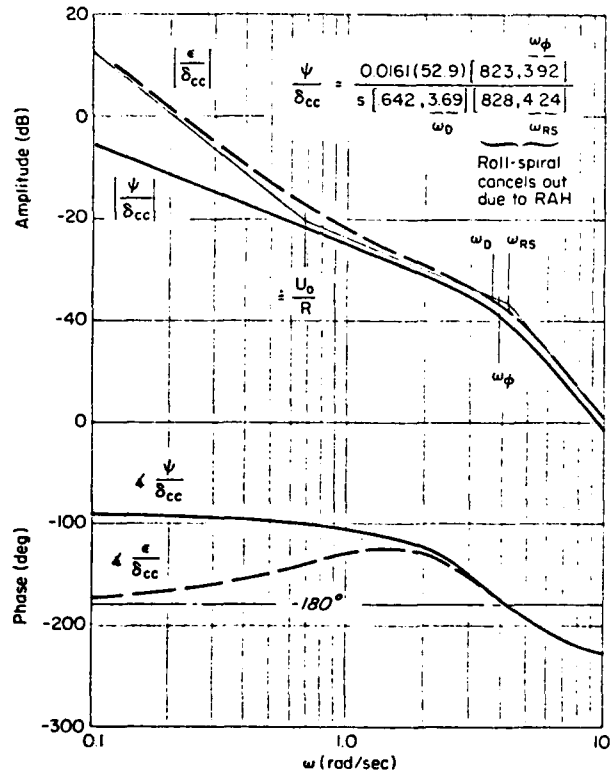


Figure 2. Comparison of Heading Dynamics and Pipper Error Dynamics for Wings Level Turn

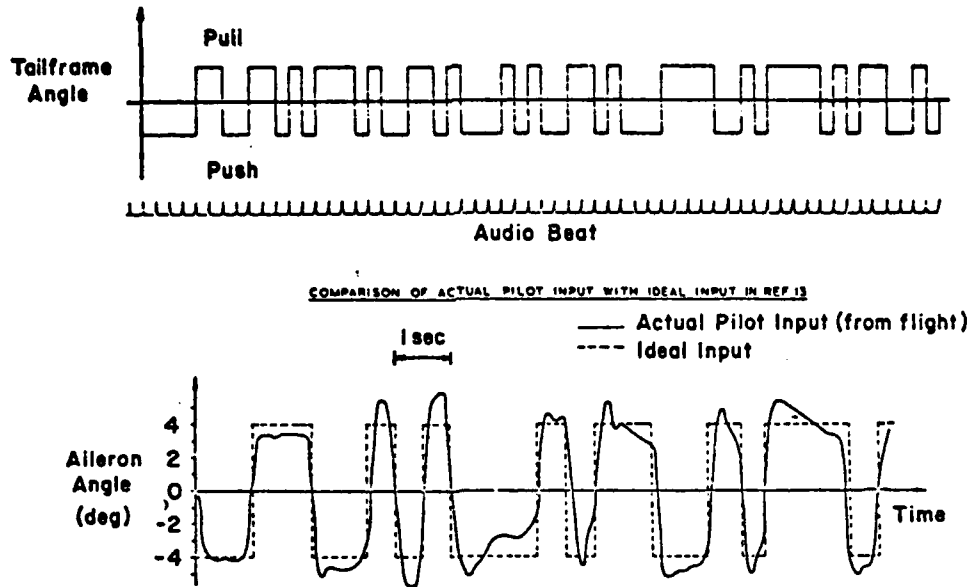


Figure 3. Ideal Pilot Input Signal to Roll Autopilot

If the  $\beta$  and  $r$  responses are correct, the lateral acceleration will be scaled down by the inertial speed  $U_0$ . In the present experiment we elected to maintain the integrity of the sideslip and yaw rate responses at the expense of side acceleration cues, which were about a factor of 5 less than those corresponding to  $M = 0.80$ . This was done in accordance with the notion that visual cues are more dominant than acceleration cues in air-to-air tracking; and with the VRA's maximum lateral acceleration (0.5 g) capacity. Lateral accelerations as high as 0.5 g were utilized frequently during the experiment. This would translate to about 2.5 g at  $M = 0.8$ .

The air-to-air tracking scenario was developed to maximize the probability of exposing deficiencies in the tracking aircraft. This was accomplished by controlling the target aircraft heading ( $\psi_2$  in Figure 1) in a random-appearing fashion which resulted in a power spectrum concentrated in, but evenly spaced over, the frequency range of interest. I. A. M. Hall developed such a signal for the purpose of identifying the frequency response characteristics of aircraft in flight. The signal used is shown in Figure 3. The signal in Figure 3 was played through

the target aircraft lateral autopilot via a switch controlled by the target aircraft pilot. This signal resulted in approximately three-quarters of full aileron travel at the testing speed of 105 kt. The target aircraft was maintained at constant altitude during the run. It was intended to utilize variations in the input series, such as playing it backwards or from the middle to the ends, etc.; however, the evaluation pilots felt that the task remained unlearned (random) and therefore such variations were not utilized.

#### **D. BASELINE ANALOG CONFIGURATION**

The Princeton University Variable Stability Research Aircraft (VRA) is a fly-by-wire response feedback simulation utilizing hydraulically actuated controls. These controls include flaps which move up as well as down and side force generators as sketched in Figure 4. A block diagram of the VRA as mechanized for the in-flight simulation in this program is shown in Figure 5. The  $C_B$  and  $C_F$  matrices in Figure 5 were calculated to allow the VRA to respond like the YF-16 at a flight condition of  $M = 0.8$  at 20,000 ft. The generic variation of roll and yaw coupling in the flight test experiment was achieved via the aileron and rudder crossfeed boxes in Figure 5.

#### **E. IN-FLIGHT VEHICLE IDENTIFICATION**

A primary problem with much of the DFC data generated to date is that the actual controlled element tested was not quantitatively defined. To avoid any uncertainties in defining the controlled element for each configuration tested in this experiment it was decided to run a frequency sweep between the DFC input and the aircraft heading which could then be Fast Fourier Transformed to obtain the frequency response directly. This technique had the secondary advantage of determining whether or not it is practical to write flying qualities criteria in terms of frequency response characteristics. The method for generating the frequency sweep was extremely simple in that the pilot simply exercised the DFC control (rudder pedals) at ever-increasing frequency during a single run. Rudder pedal input and output yaw rate were recorded

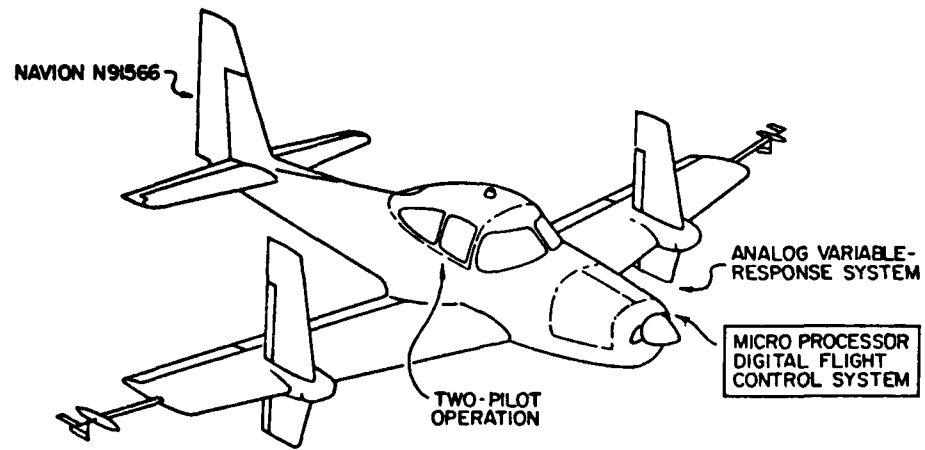


Figure 4. Navion VRA

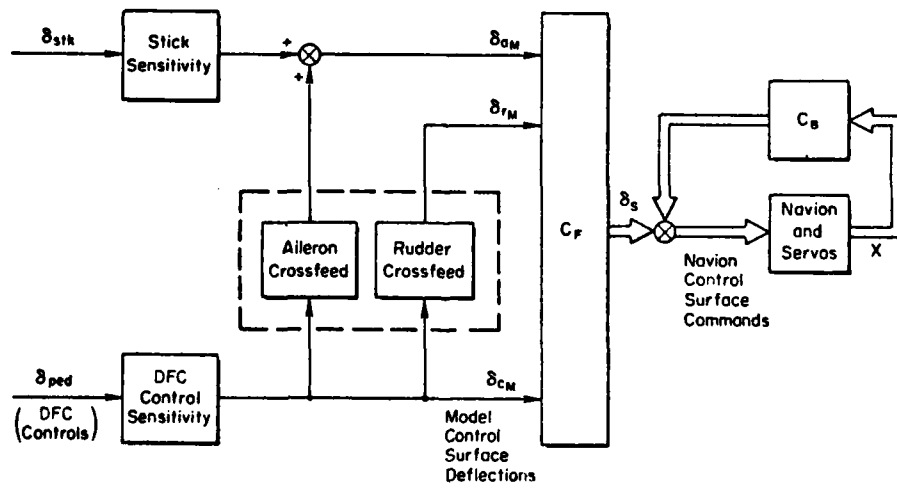


Figure 5. VRA as Mechanized for Simulation

and Fast Fourier Transformed with excellent results, i.e., very little data scatter in the frequency range of interest. An example of a Bode plot generated in this manner is shown in Figure 6.

#### F. VRA SETUP FOR ANALOG DIRECT FORCE TESTS OF REFERENCE 1

The VRA setup for the analog simulation of the YF-16 wings-level turn is shown in Figure 7. In Figure 7, S refers to the simulator (Navion) while M refers to the model (YF-16).

The  $C_F$  and  $C_B$  matrices are a hardwired part of the analog control system; there is a pot to set for each element. However, the matrices do contain zero entries (e.g.,  $\phi + \delta_R$ ,  $p + \delta_{SF}$ ). Some of these were not critical in the analog flight tests and were left at zero.

The "mixing box" and  $C_p$  matrix in Figure 7 need some explanation, which requires, as a prerequisite, a look at the lateral VRA system prior to the Reference 1 study (refer to Figure 8). In Figure 8 the

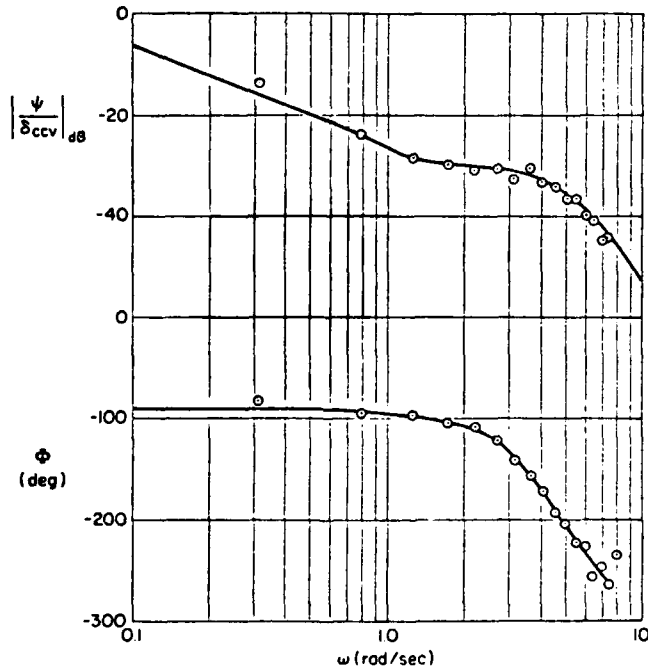
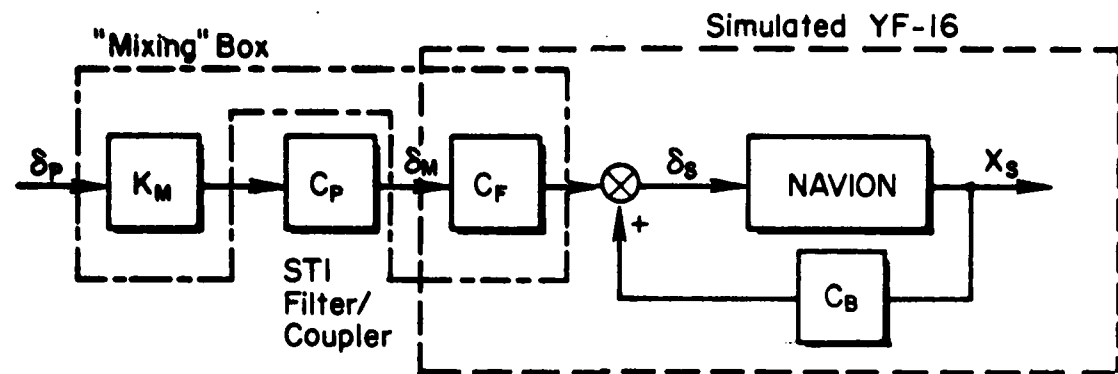


Figure 6. Fourier Transformed Heading Responses,  
Configuration WLT1, Minimal Coupling



$\delta_S = (\delta_R \text{ (rudder)}, \delta_{SF} \text{ (side force)}, \delta_A \text{ (aileron)})_{\text{Navion}}$

$\delta_M = (\delta_R, \delta_{SF}, \delta_A)_{\text{YF-16}}$

$\delta_P$  = Pilot input (rudder pedal deflection in Navion)

$C_B$  = Response feedback (gain) matrix

$C_F$  = Feedforward gain matrix (control crossfeed)

Figure 7. Analog Test Setup

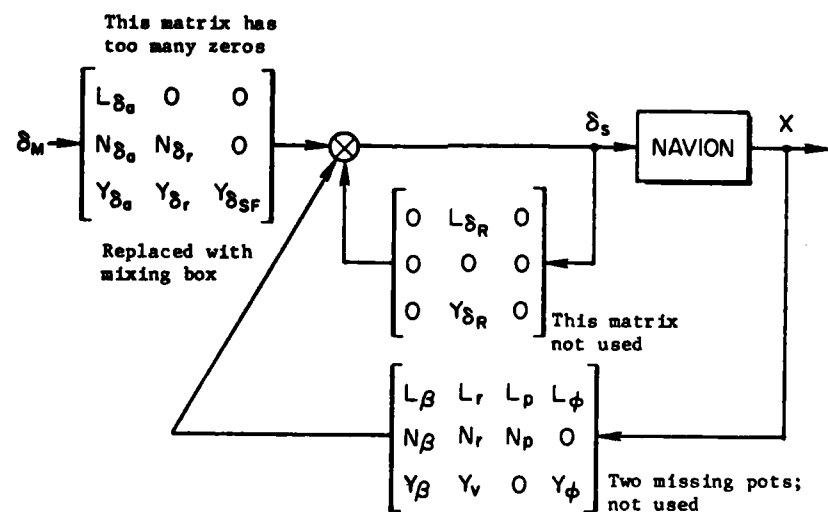


Figure 8. Lateral VRA System, Prior to Ref. 1 Study

limited, existing control coupling gain matrix was not utilized. The feedforward gain matrix had too many zero entries to be useful; to remedy this the VRA personnel installed a "mixing box" to furnish the necessary feedforward gains. This box furnished a  $K_m$  matrix of gains (a  $1 \times 1$  matrix) which interfaced with a  $1 \times 3$  matrix "box" furnished by STI. This box, in turn, coupled with another  $3 \times 3$  matrix of gains,  $C_p$ , furnished by Princeton. The  $K_m$  scalar was utilized as a pure gain during the course of the study; although provision was made for switching in an integrator ( $K_m \rightarrow K_m/s$ ).

The purpose of the STI-furnished box ( $C_p$ ) was to provide control crossfeeds that were functions of frequency; to be specific, a  $1 \times 3$  matrix of first-order filter sections.

With this configuration, the necessary control crossfeeds for the various YF-16 CCV modes could be implemented as filter sections (rather than just pure gains) and thus satisfy the frequency-dependent coupling numerator requirements of Reference 1.

For the present study, two possibilities exist as far as the feedforward matrix is concerned:

- 1) Princeton can expand the "old" CF matrix (with the many zero entries) to a more usable form.
- 2) The mixing box can be reinstalled in the VRA to give a complete gain cross-coupling (feedforward) capability.

Approach 2 was the one ultimately implemented.

The filter break frequencies are very close for the wings-level turn and hence the crossfeeds can be approximated with pure gains.

Another important point concerning the Reference 1 test is that the analog gains (furnished by  $C_B$  and the "mixing box"/STI  $C_p$  filter matrix) were utilized to force the bare airframe Navion to give an equivalent lower-order model of a compensated YF-16 configuration (that is, a bare airframe YF-16 with all the relevant feedforward/feedback loops closed). The term "lower-order model" is used because the YF-16, with compensation networks, is a relatively high-order system. The lower-order

equivalent model was fourth order, which leads to a considerable simplification in the design of the wings-level task (see Section H).

#### G. YF-16 BARE AIRFRAME CONSIDERATIONS

Using the VRA's analog fly-by-wire capability to go directly from the bare airframe Navion to a compensated YF-16 is a reasonable approach for an analog fly-by-wire mechanization. For the digital tests this process would obscure the artifacts introduced by the zero-order hold, variation in the data rate, etc. For the digital tests it is desirable to utilize the analog fly-by-wire system to force the Navion to appear as a bare airframe YF-16. Then the Micro-DFCS can be used to implement the digital controllers. Thus the implementation of Figure 9, where  $C_F$  and  $C_B$  are "analog" gain matrices (furnished by some combination of either existing VRA capabilities or in combination with the mixing box) will allow an exact replication of the bare airframe YF-16 by the Navion. The context of "exact" must wait upon the expository material of a later section.

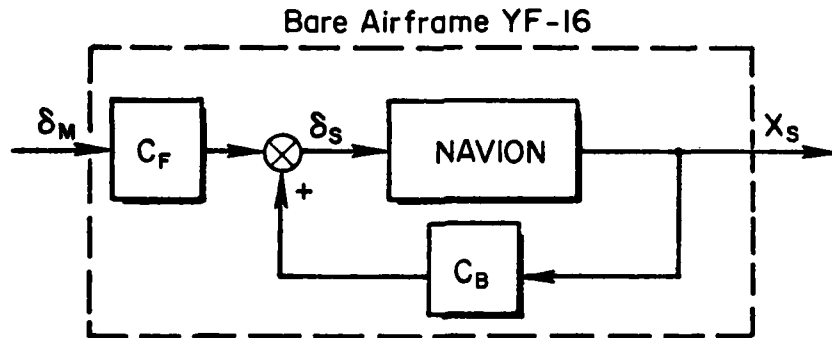


Figure 9. "Analog" Test Configuration

## H. FIRST-ORDER FORM OF EQUATIONS OF MOTION

Let the time invariant model of the aircraft to be simulated (YF-16) be

$$\dot{x}_M = F_M x_M + G_M \delta_M \quad (1)$$

while the simulation aircraft dynamics are modeled as

$$\dot{x}_S = F_S x_S + G_S \delta_S \quad (2)$$

The components of  $x$  are yaw rate ( $\psi$ ), sideslip ( $\beta$ ), roll rate ( $\phi$ ), and roll angle. The control components are rudder ( $\delta_R$ ), side force ( $\delta_{SF}$ ), and aileron ( $\delta_A$ ).

Given the stability axis state vector, the  $F$  matrix has the generic form

$$F = \begin{bmatrix} N_r & N_B & N_p & 0 \\ (Y_r/V) - 1 & Y_B/V & Y_p/V & g/V \\ L_r & L_B & L_p & 0 \\ 0 & 0 & 1 & 0 \end{bmatrix} \quad (3)$$

For the three lateral controllers, the control effectiveness matrix has the generic form

$$G = \begin{bmatrix} N_{\delta_R} & N_{\delta_{SF}} & N_{\delta_A} \\ Y_{\delta_R}/V & Y_{\delta_{SF}}/V & Y_{\delta_A}/V \\ L_{\delta_R} & L_{\delta_{SF}} & L_{\delta_A} \\ 0 & 0 & 0 \end{bmatrix} \quad (4)$$

$F$  is a  $4 \times 4$ , but the control effectiveness matrix is a  $4 \times 3$  (not square). The entries of Equations 3 and 4 are tabulated in Appendix A.

### I. DISCRETE FIRST-ORDER FORM (ZOH)

The discrete version of Equation 1 (or Equation 2) has the format

$$x_{k+1} = \phi x_k + \Gamma \delta_k \quad (5)$$

where

$$\phi = \mathcal{L}^{-1} [I_s - F] \Big|_{t=T}^{-1} \quad (6)$$

$$\Gamma = \mathcal{L}^{-1} \left( \frac{(I_s - F)^{-1}}{s} \right) G \Big|_{t=T} \quad (7)$$

$\phi(t)$  and  $\Gamma(T)$  are tabulated in Appendix A.

### J. DISCRETE FIRST-ORDER FORM (SLEWER)

The discrete version of Equation 1 is

$$x_{k+1} = \phi(T) x_k + \Gamma_1 \delta_k + \Gamma_2 \delta_{k-1} \quad (8)$$

where

$$\phi = \mathcal{L}^{-1} [I_s - F]^{-1} \quad (9)$$

$$\Gamma_1 = \mathcal{L}^{-1} \left. \frac{1}{T} \left( \frac{(I_s - F)^{-1}}{s^2} \right) G \right|_{t=T} \quad (10)$$

$$\Gamma_2 = \Gamma_{ZOH} - \Gamma_1 \quad (\text{See Eq. 7 for } \Gamma_{ZOH}) \quad (11)$$

As an alternative,

$$r_1 = \frac{1}{T} \int_0^t \phi(t - \xi) \xi G \, d\xi \Big|_{t=T} \quad (12)$$

$$r_2 = \frac{1}{T} \int_0^t \phi(t - \xi) [T - \xi] G \, d\xi \Big|_{t=T} \quad (13)$$

See Appendix A for numerical listings.

## SECTION III

### ZOH DIGITAL CONTROLLER

#### A. INTRODUCTION

A digital control law, using a zero-order hold as the coupler between the digital computer and the control actuators is synthesized directly in the z-domain. That is, the "emulation" approach of digitizing an existing analog control law is avoided. The approach is to develop discrete models of the open-loop YF-16 and then apply an extension of the equivalent stability derivative (ESD) approach to synthesize the control law. An overview of the ESD method, and the extension (which uses a pseudo inverse), is described first. After this, the computational details of implementing the approach and validating the control laws are taken up.

An important point concerning the analog baseline experiment (Reference 1) is that analog gains were utilized to force the bare airframe Navion to give an equivalent lower-order model of a compensated YF-16 configuration (that is, a bare airframe YF-16 with all the relevant feedforward/feedback loops closed). The term "lower-order model" is used because the YF-16, with compensation networks, is a relatively high-order system.

The VRA's analog fly-by-wire system was used to go directly from the bare airframe Navion to a compensated YF-16 in the analog tests. For the digital tests it is desirable to utilize the analog fly-by-wire system to force the Navion to appear as a bare airframe YF-16. Then the Micro-DFCS can be used to implement the digital controllers.

The point is a crucial one and deserves elaboration. If the digital control law is designed to force the open-loop Navion to look like a closed-loop YF-16 (at the sampling instants), then (in the inter-sample period) the Navion will respond like a Navion -- not the open-loop YF-16. Consequently, one must first "wrap" an analog fly-by-wire system

around the Navion to insure that the inter-sample aircraft performance resembles that of an open-loop YF-16. This is especially critical if one intends to evaluate the effect of a relatively low data-rate digital control working against a relatively wideband open-loop system.

In view of this, there is an additional requirement to exercise the ESD method and define the (continuous) feedback and feedforward gains that force the Navion to emulate the open-loop YF-16 model.

The validation procedure is a three-step process. First, the theoretically derived control law is tested against a theoretical continuous model of the open-loop YF-16. This was done using the TOTAL program (Reference 5). Various metrics, such as  $w'$ - and  $s$ -plane comparisons, and frequency response and step response comparisons were used to assess the verisimilitude of the results.

Second, the control law was implemented into microprocessor hardware and validated against a theoretical model of the YF-16, that is, flown against an analog computer model of the YF-16.

The last step is the actual flight test, with the Navion VRA simulating the open-loop YF-16. As will be seen, the pseudo inverse generalization of the ESD approach does an excellent job of matching the digitally controlled open-loop YF-16 to the low-order closed-loop model.

#### **B. REVIEW OF THE ESD METHOD**

An important design approach to in-flight simulation is the equivalent stability derivative (ESD) technique. This approach can force the responses of a simulator aircraft to "perfectly" match those of a model aircraft if certain constraints pertaining to the number of controllers and states are satisfied.

Let the time invariant (lateral-directional) model of the aircraft to be simulated be

$$\dot{x}_M = F_M X_M + G_M \delta_M \quad (14)$$

while the simulation aircraft dynamics are modeled as

$$\dot{x}_S = F_S x_S + G_S \delta_S \quad (15)$$

The components of  $x$  are yaw rate ( $\dot{\psi}$ ), sideslip ( $\beta$ ), roll rate ( $\dot{\phi}$ ), and roll angle ( $\phi$ ). The control components are rudder ( $\delta_R$ ), side force ( $\delta_{SF}$ ), and aileron ( $\delta_A$ ).

Given the stability axis state vector, with  $F$  and  $G$  matrices having the literal form

$$F = \begin{bmatrix} N_r & N_B & N_p & 0 \\ (Y_r/V-1) & Y_B/V & Y_p/V & g/V \\ L_r & L_B & L_p & L_\phi \\ 0 & 0 & 1 & 0 \end{bmatrix} \quad (16a)$$

$$G = \begin{bmatrix} N_{\delta_R} & N_{\delta_{SF}} & N_{\delta_A} \\ Y_{\delta_R}/B & Y_{\delta_{SF}}/V & Y_{\delta_A}/V \\ L_{\delta_R} & L_{\delta_{SF}} & L_{\delta_A} \\ 0 & 0 & 0 \end{bmatrix} \quad (16b)$$

it is apparent that three controllers can provide "perfect" model following (subject to control actuator limitations) since the fourth row of Equation 16 is an identity (it requires no "matching") for both model and simulator.

Equation 26 can no longer be forced to look exactly like Equation 23 because  $\Gamma_s^{-1}$  does not exist (it is a  $4 \times 3$ ). Furthermore, the fourth row is non-zero, so that working with a row-reduced version of  $\Gamma_s$  is not feasible. However, the pseudo inverse continues to work and one may define

$$C_F = (\Gamma_s' \Gamma_s)^{-1} \Gamma_s' \Gamma_m, \quad C_B = (\Gamma_s' \Gamma_s)^{-1} \Gamma_s' (\phi_m - \phi_s) \quad (27)$$

as the best mean square fit.

To demonstrate these points, consider a two-state, single-controller example:

$$\begin{aligned} \dot{x}_s &= \begin{bmatrix} 0 & 1 \\ -2 & -3 \end{bmatrix} x_s + \begin{bmatrix} 0 \\ 1 \end{bmatrix} \delta_s \\ \dot{x}_m &= \begin{bmatrix} 0 & 1 \\ -12 & -7 \end{bmatrix} x_m + \begin{bmatrix} 0 \\ -1 \end{bmatrix} \delta_m \end{aligned} \quad (28)$$

A straightforward computation yields

$$\begin{aligned} C_F &= (G_s' G_s)^{-1} G_s' G_m = -1 \\ C_F &= (G_s' G_s)^{-1} G_s' (\phi_m - \phi_s) = [-10 \quad -4] \end{aligned} \quad (29)$$

Clearly,

$$\begin{aligned} \dot{x}_s &= \begin{bmatrix} 0 & 1 \\ -2 & -3 \end{bmatrix} x_s + \begin{bmatrix} 0 \\ 1 \end{bmatrix} \{-\delta_m + [-10 \quad -4] x_s\} \\ &= \begin{bmatrix} 0 & 1 \\ -12 & -7 \end{bmatrix} x_s + \begin{bmatrix} 0 \\ -1 \end{bmatrix} \delta_m \end{aligned} \quad (30)$$

and the simulator exactly matches the model.

However, the discrete models no longer exhibit the s-plane identity in the first component:

$$x_{s_{k+1}} = \begin{bmatrix} 2e^{-T} - e^{-2T} & | & e^{-T} - e^{-2T} \\ \hline - & - & - \\ -2e^{-T} + 2e^{-2T} & | & -e^{-T} + 2e^{-2T} \end{bmatrix} x_{s_k} + \begin{bmatrix} 1/2 - e^{-T} + (1/2)e^{-2T} \\ \hline - & - \\ e^{-T} - e^{-2T} \end{bmatrix} \delta_{s_k} \quad (31)$$

$$x_{m_{k+1}} = \begin{bmatrix} 4e^{-3T} - 3e^{-4T} & | & e^{-3T} - e^{-4T} \\ \hline - & - & - \\ -12e^{-3T} + 12e^{-4T} & | & -3e^{-3T} + 4e^{-4T} \end{bmatrix} x_{m_k} + \begin{bmatrix} -1/12 + (1/3)e^{-3T} - (1/4)e^{-4T} \\ \hline - & - \\ -e^{-3T} + e^{-4T} \end{bmatrix} \delta_{m_k} \quad (32)$$

The pseudo inverse still yields an answer, but it lacks the power of the s-plane result, since the fit is no longer exact (it is a mean-square fit). Thus,

$$\delta_{s_k} = C_F \delta_{m_k} + C_B x_{s_k}$$

with

$$C_F = (\Gamma_s' \Gamma_s)^{-1} \Gamma_1' \Gamma_m, \quad C_B = (\Gamma_s' \Gamma_s)^{-1} \Gamma_1' (\phi_m - \phi_s) \quad (33)$$

will not give Equation 32 "exactly."

**D. A CHECK COMPUTATION: NAVION  $\Rightarrow$  CLOSED-LOOP YF-16**

The "model" for the digital in-flight simulation is the YF-16. A first step is to wrap analog loops around the simulator aircraft (Navion) so that the digital control loops presume an open-loop YF-16. To demonstrate the mathematical process we will first present a check computation to verify the Reference 1 gains used to force the Navion to look like a closed-loop YF-16. The matrices needed (see Appendix A) for both the Navion and YF-16 are tabulated below. The YF-16 flight condition is for 20,000 ft and Mach 0.8.

Navion

$$F_s = \begin{bmatrix} -0.777 & 4.68 & -0.432 & 0 \\ -1.0 & -0.3556 & 0 & 0.172 \\ 1.27 & -12.8 & 1 & 0 \\ 0 & 0 & 1 & 0 \end{bmatrix} \quad (34a)$$

$$G_s = \begin{bmatrix} -6.1 & 2.41 & 0.314 \\ 0.0725 & 0.237 & 0 \\ 0.77 & 0 & 21 \\ 0 & 0 & 0 \end{bmatrix} \quad (34b)$$

The next set gives the F and G matrices for the YF-16, with a vertical canard (CCV vehicle) as per the flight tests of Reference 1 (i.e., the analog flight tests). The 3,4 entry of the F matrix changes dramatically from a value of -0.2077 with no canard to a value of -25.0 with the canard (this is the fourth-order equivalent model used in the Reference 1 tests).

YF-16 with canard, loops closed (the equivalent model)

$$F_m = \begin{bmatrix} -3.105 & 8.917 & -0.272 & 0 \\ -0.9796 & -0.2965 & 0 & 0.03795 \\ 6.564 & -47.71 & -8.359 & -25 \\ 0 & 0 & 1 & 0 \end{bmatrix} \quad (35)$$

$$G_m = \begin{bmatrix} -3.925 & 4.766 & 1.897 \\ 0.02988 & 0.01802 & -0.0336 \\ 7.178 & 5.655 & 49.6 \\ 0 & 0 & 0 \end{bmatrix} \quad (36)$$

Next are the F and G matrices for the bare airframe YF-16 CCV (with canard but no loops closed).

Bare airframe YF-16 with canard

$$F_m = \begin{bmatrix} -0.431 & 10.2 & -0.0416 & 0 \\ -1.0 & -0.306 & 0 & 0.0388 \\ 1.67 & -50 & -2.33 & 0 \\ 0 & 0 & 1 & 0 \end{bmatrix} \quad (37)$$

$$G_m = \begin{bmatrix} -4.17 & 4.62 & 2.17 \\ 0.0318 & 0.0191 & -0.0357 \\ 7.63 & 5.93 & 49.1 \\ 0 & 0 & 0 \end{bmatrix} \quad (38)$$

For all cases, the state vector is

$$\Delta X = [\Delta r \Delta B \Delta P \Delta \phi]' \quad (39)$$

and the control vector is

$$\Delta \delta = [\Delta \delta_R \Delta \delta_{SF} \Delta \delta_A]' \quad (40)$$

First, compute the gains (which determine the pot settings for the analog fly-by-wire computer) which force the Navion to have the ESD (equivalent stability derivative) model of the YF-16 CCV, canard, loops closed. Since this is an s-plane computation we elect to use Equation 20. The first part of Equation 20, which has the form

$$C_B = \hat{G}_s^{-1}(\hat{F}_m - \hat{F}_s) \quad (41)$$

is rewritten in a form suitable for solution using either Cramer's rule or Gaussian elimination. That is,

$$\hat{G}_s C_B = (F_m - F_s)$$

This gives

$$\begin{bmatrix} -6.1 & 2.41 & -0.314 \\ 0.0725 & 0.237 & 0 \\ 0.77 & 0 & 21 \end{bmatrix} C_B = \begin{bmatrix} -2.328 & 4.237 & 0.16 & 0 \\ 0.0204 & 0.0591 & 0 & -0.13405 \\ 5.294 & -34.91 & -1.759 & -25 \end{bmatrix} \quad (42)$$

Gaussian elimination then gives (nine-place accuracy is used only to facilitate checking the answer):

$$C_B = \begin{bmatrix} 0.359857139 & -0.456220933 & -0.019653205 & -0.144939218 \\ -0.024006931 & 0.388928345 & 0.006012056 & -0.521273868 \\ 0.238900576 & -1.645652851 & -0.081612716 & -1.185161753 \end{bmatrix} \quad (43)$$

To compute  $C_F$ , the second part of Equation 20 is also written in a form suitable for Gaussian elimination.

$$\begin{bmatrix} \hat{G}_s C_F & = & \hat{G}_m \end{bmatrix}$$

$$\begin{bmatrix} -6.1 & 2.41 & -0.314 \\ 0.0725 & 0.237 & 0 \\ 0.77 & 0 & 21 \end{bmatrix} C_F = \begin{bmatrix} -3.925 & 4.766 & 1.897 \\ 0.02988 & 0.01802 & -0.0336 \\ 7.178 & 5.655 & 49.6 \end{bmatrix} \quad (44)$$

The solution is

$$C_F = \begin{bmatrix} 0.603820992 & -0.683783153 & -0.436629058 \\ -0.058637225 & 0.285207927 & -0.008204191 \\ 0.319669421 & 0.294357763 & 2.37791449 \end{bmatrix} \quad (45)$$

These gains agree with the Reference 1 results. Next, compute the gains for Navion to bare airframe YF-16. Since the previous sample calculations document the solution procedure for solving  $C_B$  and  $C_F$ , we will dispense with the details and present the results.

$$C_B = \begin{bmatrix} -0.051566838 & -0.653322784 & -0.066549239 & -0.198437737 \\ 0.01577466 & 0.409138817 & 0.020357890 & -0.501321790 \\ 0.020938403 & -1.747473404 & 0.205773472 & 0.007276050 \end{bmatrix} \quad (46)$$

$$C_F = \begin{bmatrix} 0.641584848 & -0.661386936 & -0.478658047 \\ -0.062088192 & 0.282913725 & -0.004207981 \\ 0.339808556 & 0.306631807 & 2.355646033 \end{bmatrix} \quad (47)$$

Next, compute the digital gains which force the bare airframe to match the closed-loop YF-16 (at the sampling instants). First, the plant equations must be properly discretized, taking into account both the sample rate and the data hold. This is done in the next section, where the focus is on the ZOH.

#### E. ZOH ESD CONTROL LAWS

To review, the Navion's analog system will be utilized to force the Navion to appear as the open-loop (bare airframe) YF-16 with canard. (In Figure 11, the subscript C refers to the continuous gain.) In turn, the Navion's Micro-DFCS is then used to implement feedforward and feedback gains to make the open-loop YF-16 appear as a closed-loop YF-16 (Figure 12).

The task now is to find the ESD gains given finite T. Recall that the continuous gains were found very easily; given three controllers and four states (one being an identity), exact matching was possible. For finite T, this fortunate situation no longer pertains; the fourth equation is no longer an identity. This is best illustrated with the aid of Table 1, which describes the ZOH case (T = 0.1, YF-16 CCV canard, bare airframe):

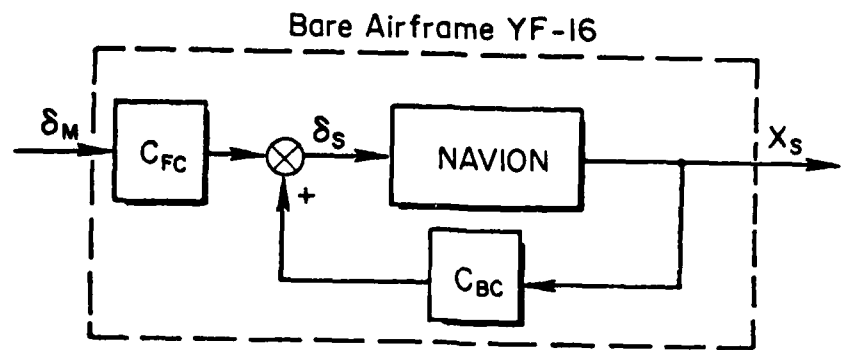


Figure 11. Test Configuration

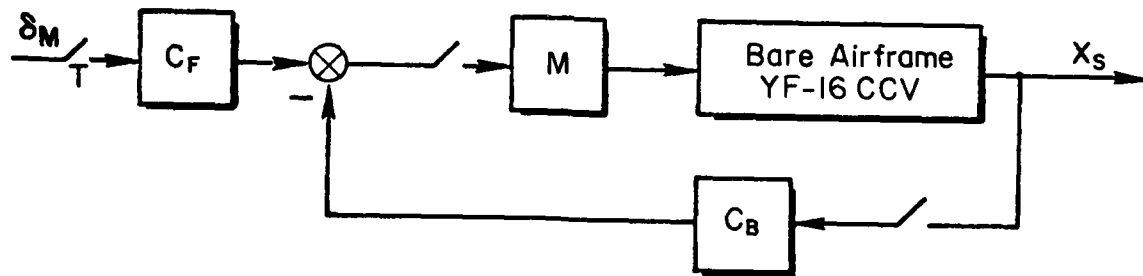


Figure 12. Digital Controller Configuration

TABLE 1.  $s$ - AND  $z$ -PLANE OPEN LOOP PLANT REPRESENTATIONS

$$\dot{x} = Ax + B\delta$$

AMAT(ROW 1)-	-.4310000000	10.20000000	-.4160000000E-01	0.
AMAT(ROW 2)-	-1.00000000	-.3060000000	0.	.3880000000E-01
AMAT(ROW 3)-	1.67000000	-50.00000000	-2.330000000	0.
AMAT(ROW 4)-	0.	0.	1.000000000	0.
BMAT(ROW 1)-	-.4.170000000	4.620000000	2.170000000	
BMAT(ROW 2)-	.3180000000E-01	.1910000000E-01	-.3570000000E-01	
BMAT(ROW 3)-	7.630000000	5.930000000	49.10000000	
BMAT(ROW 4)-	0.	0.	0.	

$$x_{k+1} = Fx_k + G\delta_k$$

FMAT(ROW 1)-	.9085611123	.9755276552	-.3502672856E-02	.1926755760E-02
FMAT(ROW 2)-	-.9471662993E-01	.9204149530	.3626869048E-03	.3756696670E-02
FMAT(ROW 3)-	.36700790570	-.4.234745790	.7912792594	-.8716315341E-02
FMAT(ROW 4)-	.1524291762E-01	-.2246473026	.8917931248E-01	.9997011628
GMAT(ROW 1)-	-.4010594654	.4443513628	-.1978434172	
GMAT(ROW 2)-	.2334360234E-01	-.2042352531E-01	-.1334271711E-01	
GMAT(ROW 3)-	.6097314035	.5949648390	4.419801283	
GMAT(ROW 4)-	.3320928555E-01	.2942249255E-01	.2287260839	

Observe the identities in the fourth row of the  $A$  and  $B$  matrices (0, 0, 1, 0 and 0, 0, 0). The fourth row of  $F$  and  $G$  must take on the numerical values dictated by

$$\phi(T) = \lambda^{-1} [I_s - A]_{t=T}^{-1} \quad (48)$$

and

$$\Gamma(T) = \int_0^T \phi(t - \xi) B \, d\xi \quad (49)$$

and hence the identity is lost. Thus the time domain procedure of throwing away the fourth equation, to obtain a reduced control effectiveness matrix that is invertible, is no longer possible. To preserve the ESD concept we may appeal to the pseudo-inverse, and then check, via  $w'$ , to see how good the result is. The pseudo-inverse equations are described next.

## F. DEFINING EQUATIONS, IN "TOTAL" NOTATION\*

Let the time domain equations for the open-loop YF-16 (the "simulator," subscript s) be

$$\dot{x}_s = (IMAT)_s x_s + (JMAT)_s \delta_s \quad OL YF-16 \quad (50)$$

Let the time domain equations for the closed-loop YF-16 (the "model," subscript m) be

$$\dot{x}_m = (XMAT)_m x_m + (YMAT)_m \delta_m \quad CL YF-16 \quad (51)$$

Use Option 87 to get the discrete (ZOH) form:

$$x_{k+1} = (LMAT)x_k + (MMAT)\delta_k \quad CL YF-16 (Model) \quad (52)$$

$$x_{k+1} = (NMAT)x_k + (OMAT)\delta_k \quad OL YF-16 (Simulator) \quad (53)$$

Since OMAT is the control effectiveness matrix of the "simulator" (OL YF-16), we need its pseudo-inverse. Let

$$PMAT = (OMAT)^\dagger = [0' \ 0]^{-1} 0' \quad (54)$$

where  $\dagger$  indicates the pseudo-inverse.

Clearly, the feedforward gain matrix,  $C_F$ , is given at

$$QMAT = C_F = (PMAT)*(MMAT) \quad (55)$$

In a like manner, the feedback gain matrix,  $C_B$ , is given by

$$UMAT = C_B = (PMAT)[LMAT - NMAT] \quad (56)$$

---

\*For a description of TOTAL matrix notation and analysis options, see Reference 5.

Equations 55 and 56 define the gain matrices. We must now check by substituting Equations 55 and 56 back into the equations for the open-loop system (Equation 53) and see how well the result compares with the model (Equation 52).

#### G. COMPARISON EQUATIONS — STATE TRANSITION

With the control law

$$\delta_{k_s} = C_B x_{k_s} + C_F \delta_{k_m} = (UMAT)x_{k_s} + (QMAT)\delta_{k_m} \quad (57)$$

Equation 53 becomes

$$\begin{aligned} x_{k+1} &= [NMAT + OMAT*UMAT]x_s + (OMAT)(QMAT)\delta_m \\ &= RMATx_s + SMAT\delta_m \end{aligned} \quad (58)$$

Since the model is

$$x_{k_m} = (LMAT)x_{k_m} + (MMAT)\delta_{k_m} \quad (59)$$

compare RMAT with LMAT and SMAT with MMAT (this is done in Appendix C).

#### H. $w'$ -COMPARISON

Given

$$x_{k+1} = \phi x_k + \Gamma \delta_k \quad (60)$$

take the z-transform to form

$$[Iz - \phi]x(z) = \Gamma \delta_k + zx(0) \quad (61)$$

Substituting and clearing gives [for convenience, drop the prime on  $w'$  and set  $x(0) = 0$ ],

$$\left[ Iw + \frac{2}{T} (I + \phi)^{-1}(I - \phi) \right] X(w) = \frac{2}{T} [I + \phi]^{-1} \left( -\frac{w}{2/T} + 1 \right) \Gamma \delta(w) \quad (62)$$

First, generate the  $w'$  format for

$$x_{k+1} = R\text{MAT}x_k + S\text{MAT}\delta_m$$

We can define this to be

$$\left[ Iw + \frac{2}{T} (I + R\text{MAT})^{-1}(I - R\text{MAT}) \right] X = \frac{2}{T} [I - R\text{MAT}]^{-1} S\text{MAT} \left( -\frac{w}{2/T} + 1 \right) \delta(w) \quad (63)$$

$$[Iw' + W\text{MAT}]X = E\text{MAT}\delta_m \left( -\frac{w}{2/T} + 1 \right) \quad (64)$$

This can be compared with the continuous model. That is, compare

$$(I\text{s} - X\text{MAT})X(s) = [Y\text{MAT}]\delta_s \quad (65)$$

against

$$(Iw + W\text{MAT})X(w) = [E\text{MAT}]\delta_s \quad (66)$$

See Appendix C for a specific comparison.

## I. MACROS

Three macros were used to implement the previously described computational algorithms. The first, AKEY, sets up the state transition model, from the time domain model, for both the simulator (Equation 50) and the model (Equation 51).

```
OPTION >CREATE,AKEY,COPY,XMAT,AMAT,COPY,YMAT,BMAT,87,COPY,FMAT,LMAT,  
>COPY,GMAT,MMAT,COPY,IMAT,AMAT,COPY,JMAT,BMAT,87,  
>COPY,FMAT,NMAT,COPY,GMAT,OMAT
```

Next, BKEY computes the pseudo-inverse and the feedback/feedforward gains. It lists LMAT, MMAT, NMAT, OMAT, PMAT, QMAT, UMAT.

```
OPTION >CREATE,BKEY,COPY,OMAT,AMAT,76,COPY,CMAT,FMAT,COPY,CMAT,AMAT,  
>COPY,OMAT,BMAT,74,COPY,CMAT,AMAT,75,COPY,CMAT,AMAT,COPY,FMAT,BMAT,  
>74,COPY,CMAT,FMAT,COPY,FMAT,AMAT,COPY,MMAT,BMAT,74,COPY,CMAT,QMAT,  
>COPY,LMAT,AMAT,COPY,NMAT,BMAT,73,COPY,CMAT,BMAT,  
>COPY,FMAT,AMAT,74,COPY,CMAT,UMAT,LMAT,MMAT,NMAT,OMAT,FMAT,  
>QMAT,UMAT
```

Next use CKEY to check the results.  $C_B$  and  $C_F$  are substituted into the "simulator" equations, and this result is then compared against the "model" equations.

```
OPTION >CREATE,CKEY,COPY,OMAT,AMAT,COPY,UMAT,BMAT,74,COPY,CMAT,BMAT,  
>COPY,NMAT,AMAT,72,COPY,CMAT,RMAT,COPY,QMAT,BMAT,COPY,OMAT,AMAT,  
>74,COPY,CMAT,SMAT,COPY,RMAT,BMAT,COPY,VMAT,AMAT,72,COPY,CMAT,AMAT,  
>75,COPY,CMAT,BMAT,COPY,ZMAT,AMAT,74,COPY,EMAT,TMAT,COPY,VMAT,AMAT,  
>COPY,RMAT,BMAT,73,COPY,CMAT,BMAT,COPY,TMAT,AMAT,74,COPY,CMAT,WMAT,  
>COPY,TMAT,AMAT,COPY,SMAT,BMAT,74,COPY,CMAT,EMAT,COPY,WMAT,BMAT,  
>COPY,HMAT,AMAT,74,COPY,CMAT,AMAT,71
```

An annotated run for the 10 Hz case is given in Appendix C.

## J. ZOH, ESD GAINS

The  $C_B$  and  $C_F$  gains are tabulated in Table 2. The printout rounds the gains to four figures, although the internal precision is much higher. To check the sensitivity to roundoff, we reran CKEY for the 5 Hz and 10 Hz cases using the four-place numbers printed in Table 2. There were no significant changes in the closed-loop plant description, indicating four-place accuracy is sufficient.

## K. VALIDATION: THEORETICAL CONTROLLER, TOTAL MODEL OF YF-16

The first method for validating the theoretical controller against the theoretical YF-16 model was outlined in Section H. For the 10 Hz case,  $C_B$  and  $C_F$  are substituted into the "simulator" equations, resulting in the closed-loop format

$$(I_s - XMAT)X(s) = [YMAT]\delta_s \quad (67)$$

This can be compared against the YF-16 s-plane reference model, given by

$$(I_s + WMAT)(X(w) = [EMAT]\delta_s \quad (68)$$

This is carried out in Table 3. As can be seen, even at 10 Hz the pseudo inverse has done an excellent job of matching the digitally controlled open-loop YF-16 to the desired closed-loop YF-16 configuration.

The second method of validation is to compare the frequency response of the continuous variables of the discretely controlled continuous system against the frequency response of the baseline closed-loop YF-16. A typical (10 Hz) set is given in Figures 13 and 14. The matches are extremely good at low frequencies and exhibit the properties one expects of digitally controlled systems at higher frequencies. A more comprehensive set (10 Hz and 50 Hz) is listed in Appendix D. The third method for comparison is to match step responses (a step of pedal input). These are extremely close and a comparison of printed data is required in order to see the differences (see Table 4).

TABLE 2. ZOH GAINS

1/T (Hz)	T (sec)	C <sub>F</sub>			C <sub>B</sub>			
		C <sub>F1</sub>	C <sub>F2</sub>	C <sub>F3</sub>	C <sub>B1</sub>	C <sub>B2</sub>	C <sub>B3</sub>	
1	1.	-1.620	2.946	2.202	4.891	7.084	-2100	-1.009
	1.672	2.858	1.596	5.188	4.880	-9990E-01	-7243	
	4114	-6572	-1827	-1.527	-7911	-1213E-01	.9032E-01	
5	0.2	1.306	-1428	1.192	1.244	-1.229	-1635	-1.027
	5885	6530	1.156	8593	-2.108	-1410	-8550	
	2070	1836E-01	2113	-3098	.9655	-3590E-01	-3679E-02	
10	0.1	9392	-6880E-01	-6380E-01	6448	3834	-5682E-01	-3444
	1189	8297	-1443	1264	-2180	-3784E-01	-1260	
	6614E-01	1004E-01	7689	-7467E-01	.3024	-8553E-01	-3017	
15	0.06667	9024	-2810E-01	-6322E-01	6040	4744	-6147E-01	-3359
	4333E-01	9125	-1457	4327E-01	-2940E-01	-4578E-01	-1074	
	3659E-01	4270E-05	.8524	-3870E-01	.1800	-9161E-01	-3481	
20	0.05	8991	-1632E-01	-3285E-01	6013	4646	-6573E-01	-3495
	2010E-01	9466	-1137	1992E-01	.9796E-02	-5211E-01	-1171	
	2492E-01	3220E-02	.8879	-2558E-01	.1299	-9415E-01	-3675	
40	0.025	9108	-1416E-01	-2234E-01	6136	4025	-7159E-01	-3782
	1083E-02	9840	-5271E-01	.1856E-02	.2144E-01	-6160E-01	-1414	
	1067E-01	4473E-02	.9409	-1053E-01	.6276E-01	-9812E-01	-3958	
50	0.02	9154	-1631E-01	.3266E-01	6180	3850	-7246E-01	-3841
	6248E-03	9891	-4077E-01	.3107E-03	.1866E-01	-6328E-01	-1466	
	8244E-02	4108E-02	.9520	-8087E-02	.5004E-01	-9900E-01	-4016	
100	0.01	9265	-2346E-01	.5114E-01	6286	3459	-7376E-01	-3954
	2059E-02	9966	-1862E-01	-9408E-03	.9108E-02	-6625E-01	-1567	
	3780E-02	2687E-02	.9752	-3721E-02	.2499E-01	-1009	-4136	
1000	0.001	9388	-3329E-01	.6451E-01	6400	3067	-7433E-01	-4046
	1124E-02	1.000	-1414E-02	-6363E-04	.3503E-02	-6842E-01	-1650	
	2007E-03	5731E-03	.9974	-3571E-03	.2760E-02	-1027	-4248	

TABLE 3.  $w'$ -,  $s$ -Plane Comparisons

ROW	COLUMN			
	1	2	3	4
XMAT	-3.105	8.917	-.2720	0
	-.9796	-.2965	0	.3795E-01
	6.564	-47.71	-8.359	-25.00
	0	0	1.000	0
WMAT	3.140	-9.044	.2562	-.6619E-01
	*.9775	*.3245	-.1929E-02	-.3865E-01
	-6.580	45.39	8.216	23.99
	*.2355E-01	*.1143	-.9845	*.4501E-01
EMAT	-3.925	4.766	1.897	
	*.2988E-01	*.1802E-01	-.3360E-01	
	7.178	5.655	49.60	
	0	0	0	
YMAT	-3.946	4.755	1.768	
	*.4171E-01	*.3806E-02	-.4036E-01	
	6.758	5.557	47.64	
	*.2042E-01	*.4213E-02	*.8822E-01	

TABLE 4. STEP RESPONSE

TIME	CONT.	DISC.	CONT.	DISC.	CONT.	DISC.	CONT.	DISC.
0.0	-0.000000017	-0.000000004	-0.004820652	-0.030651121	-0.030645887	0.000000024	-0.001690086	-0.001416650
	0.018304812	0.004833063	0.004820652	-0.043086926	-0.043473064	-0.005517618	-0.005047682	
	0.035110104	0.0351101039	0.007806208	0.007783140	-0.041094386	-0.041897130	-0.009824885	-0.009275901
	0.049166021	0.0492219275	0.009179154	0.009148255	-0.030114681	-0.031161178	-0.012917862	
0.5	0.05927180	0.0592890768	0.067117145	0.067121251	-0.015287192	-0.016348892	-0.015721016	-0.015305989
	0.067047776	0.067117145	0.088550286	0.07229344	-0.000544843	-0.001425508	-0.016499426	-0.016224603
	0.071179588	0.071247888	0.005757446	0.005714553	0.0116311962	0.011050595	-0.015917003	-0.015784134
	0.072800400	0.072860271	0.004230742	0.004187999	0.020068907	0.019823899	-0.014286232	
	0.072571265	0.072616159	0.002841689	0.002800227	0.024590824	0.02453091	-0.012108355	
1.0	0.071132345	0.071160221	0.001677014	0.001637879	0.025671786	0.025970629	-0.009495707	-0.003619636
	0.069037389	0.069047530	0.000771800	0.000758200	0.024122880	0.024570463	-0.006987841	-0.007129174
	0.067721372	0.066716421	0.000123269	0.000090941	0.020850933	0.021362041	-0.004728490	-0.004862072
	0.064493384	0.064477878	0.000296003	-0.000324572	0.016697052	0.017031326	-0.002844872	-0.002956131
	0.062546517	0.062525830	0.000526751	-0.000551846	0.012344987	0.01293063	-0.001471827	
1.5	0.06097446	0.060956797	0.000614201	-0.000636428	0.008286213	0.00850287	-0.000367884	-0.000409195
	0.059809878	0.059793576	0.000601851	-0.000622036	0.004823887	0.005094543	-0.000273232	
	0.059017764	0.059008774	0.000527622	-0.000546687	0.002099326	0.00281159	0.006621625	0.006640724
	0.058345707	0.058345509	0.0000421964	-0.0000440812	0.000130490	0.0000723994	0.000767731	
	0.058325257	0.0583333969	0.0000307414	-0.000326833	-0.001148624	-0.001100660	0.000670766	0.000727097
	0.058303441	0.058303441	0.000199143	-0.000219741	-0.001852171	-0.001844685	0.000516475	0.000583091
2.0	0.058367189	0.058390114	0.000106075	-0.000128252	-0.002113635	-0.002130740	0.000312066	0.000387727
	0.058514145	0.058541314	0.000032251	-0.000036196	-0.002064921	-0.002064947	0.000104070	0.000179683
	0.058687644	0.05871011	0.000021796	-0.00003922	-0.001822980	-0.001854877	-0.000014995	
	0.058839676	0.058889364	0.000057795	-0.000030450	-0.001482793	-0.001511914	-0.000257278	-0.000181086
	0.059012757	0.059044438	0.000007827	0.000049998	-0.001115241	-0.001138754	-0.000311889	
2.5	0.059137881	0.059164502	0.000088037	0.000058226	-0.000768325	-0.00085471	-0.000481036	-0.00046835
	0.059223332	0.059256341	0.00000889109	0.000038530	-0.000470403	-0.000481760	-0.000542490	-0.000469316
	0.059397635	0.059318871	0.0000055179	0.000024267	0.000147629	0.000145656	-0.000504876	
	0.059349954	0.059362401	0.000084926	0.000053876	-0.00023438	-0.000150073	-0.000553920	-0.000519839
	0.059337819	0.059337819	0.0000049650	0.000019010	0.000061894	-0.000656688	-0.000591498	-0.000520348
	0.059338061	0.059337819	0.0000045539	0.000015178	0.000052669	0.000050445	-0.000591498	
	0.059336368	0.0593378241	0.0000069866	0.000018591	0.0000112436	0.000108231	-0.000527068	-0.000457225
3.0	0.0593163706	0.059326331	0.000062039	0.000010900	0.000011195	0.000081208	-0.000517140	-0.000447485
	0.059359643	0.059372890	0.0000041081	0.000010573	0.0000060364	0.000055249	-0.000440361	
	0.0593404787	0.059317342	0.0000040287	0.000010533	0.0000031983	0.000032753	-0.000504958	-0.000435632
	0.059297652	0.059310617	0.0000040123	0.0000040123	0.0000011374	0.0000006663	-0.00001716	-0.000432981
	0.059292645	0.059308027	0.0000040369	0.0000040369	0.0000011374	0.0000006663	-0.00000500803	-0.000431708
4.0	0.059289497	0.059302662	0.0000040843	0.0000040843				

T = .1, ZOH

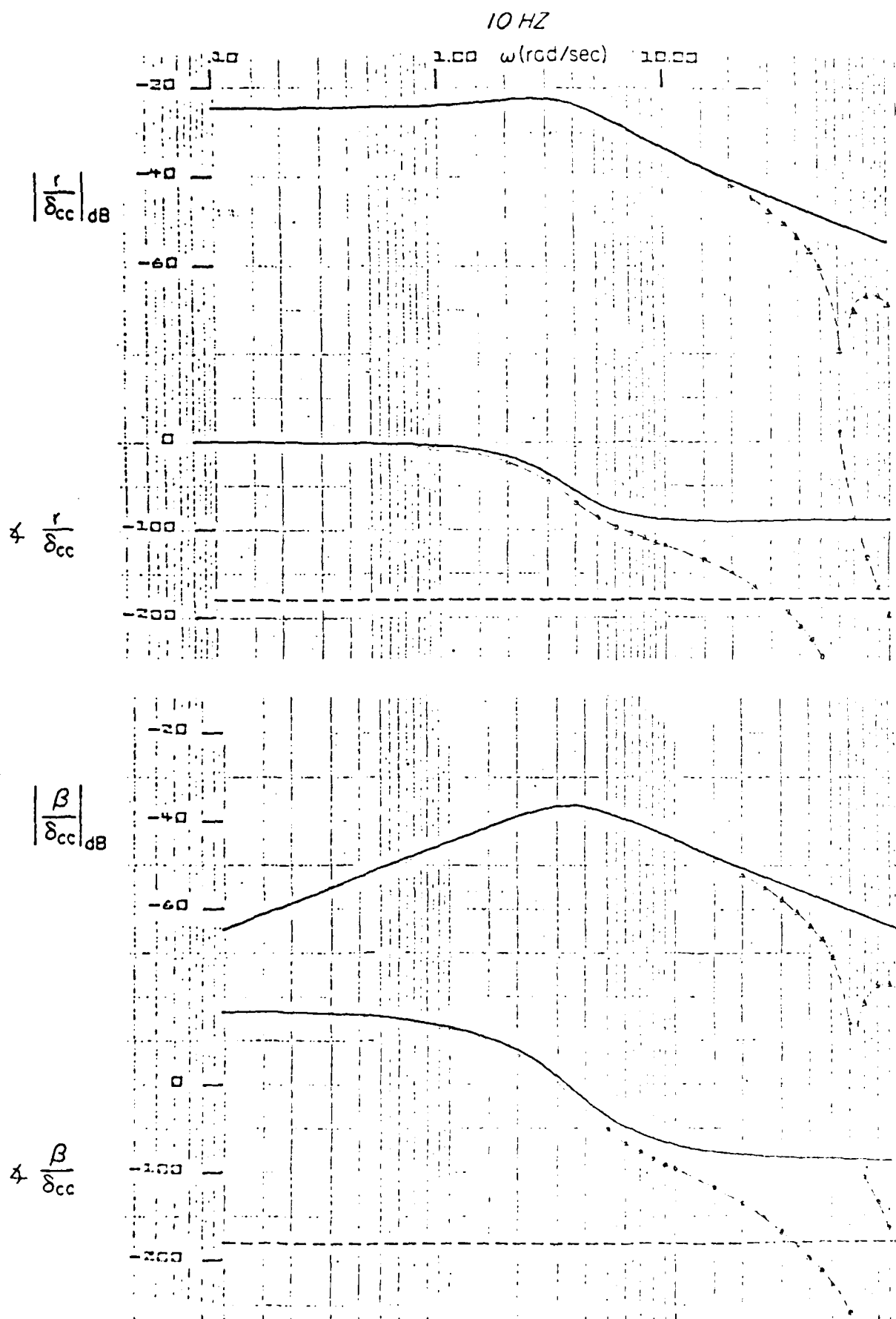


Figure 13. Bode Plots:  $r/\delta_{cc}$ ,  $\beta/\delta_{cc}$

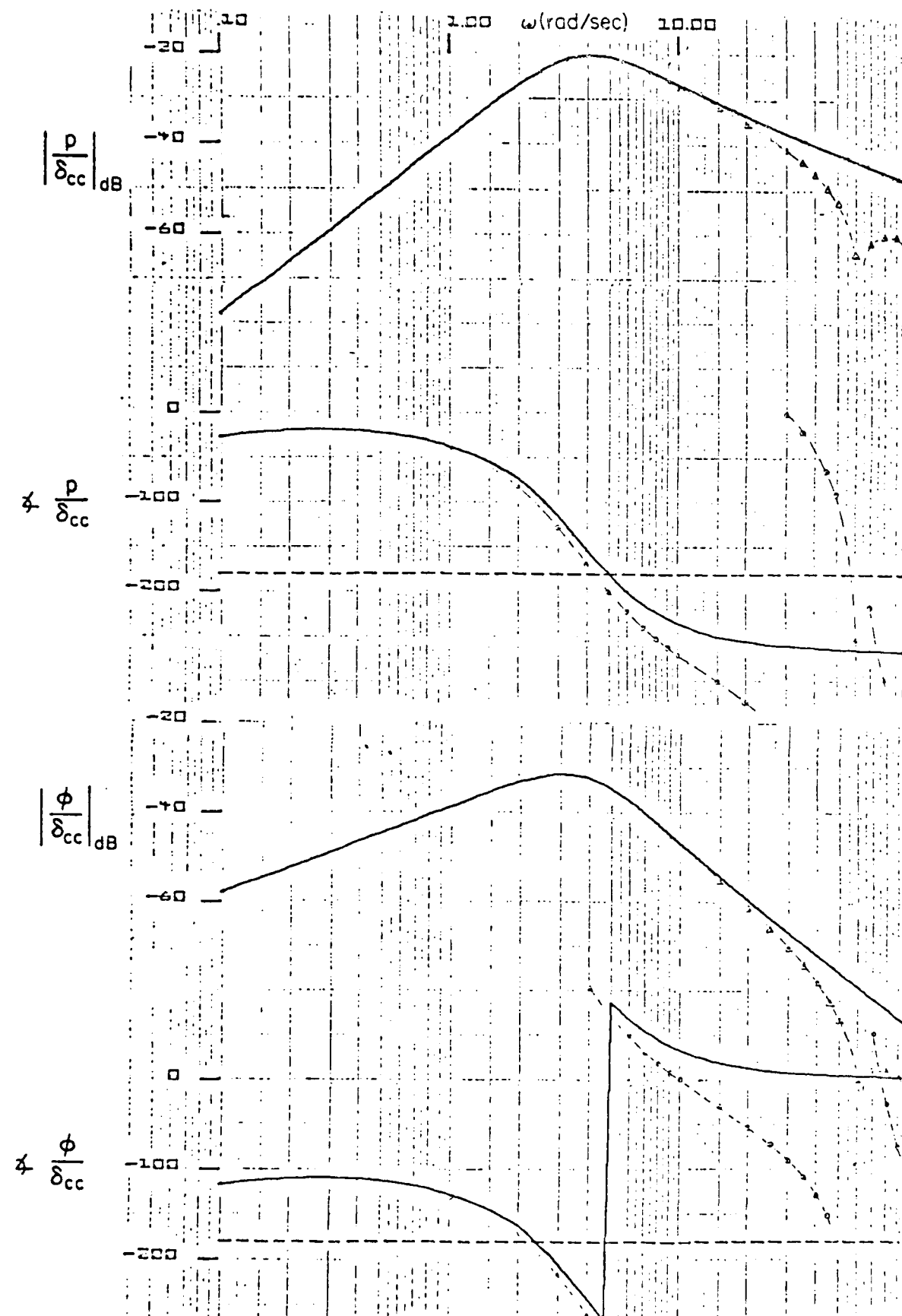


Figure 14. Bode Plots;  $p/\delta_{cc}$ ;  $\phi/\delta_{cc}$

**L. VALIDATION: MICROPROCESSOR-BASED CONTROL LAW,  
ANALOG COMPUTER MODEL OF YF-16**

The ZOH control law was implemented in the microprocessor and validated on the analog computer using an "ideal" aircraft model. The wings-level turn was successfully flown. A comparison between the theoretical response and digital implementation in the hybrid simulation is given in Figure 15.

As can be seen by inspection, the response characteristics of the micro-processor coupled controller closely match those of the continuous model. The magnitude differences between the two sets of curves were due to scaling limitations imposed by the coupling between the micro-processor and the TR-48 bare airframe simulation. The more favorable scaling dynamics of the coupling between the microprocessor and the Navion's analog system assured us that the ZOH would function appropriately under actual flight test.

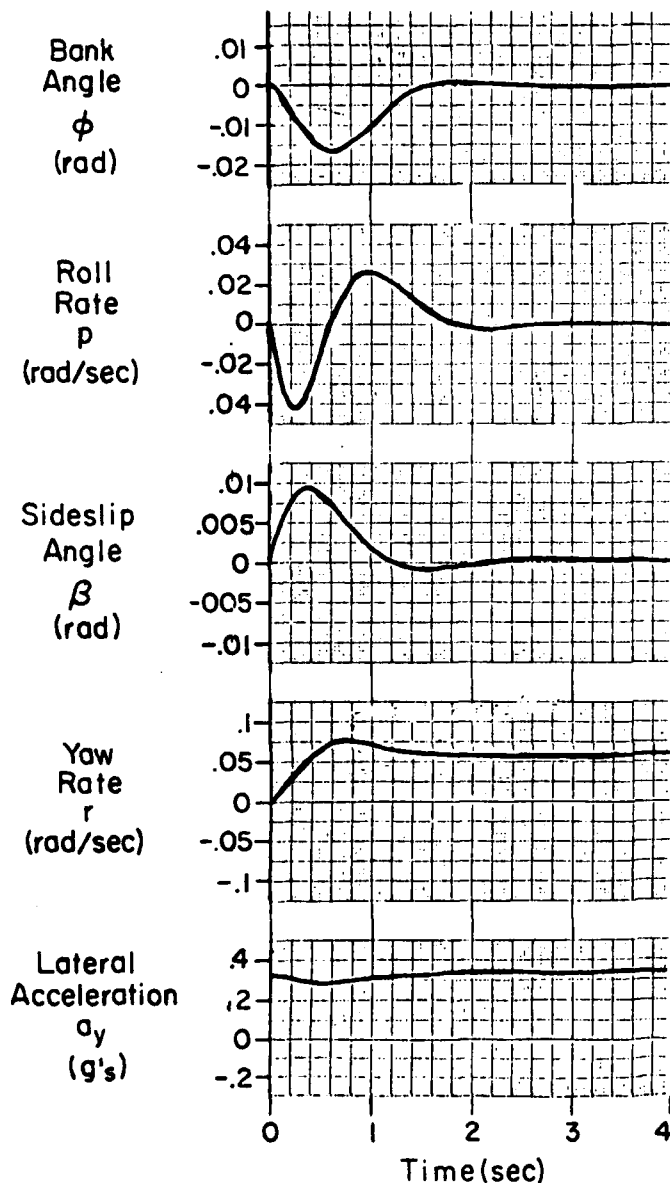
**M. VALIDATION: MICROPROCESSOR-BASED CONTROL LAW,  
NAVION AS YF-16 SIMULATOR**

The microprocessor-based control law was installed in the Navion Variable Stability Aircraft and a wings-level turn successfully flown (see Figure 16). The pedal was ramped in and held at about 70 percent full deflection. A wings level, essentially zero sideslip turn near the Navion limit of  $a_y \approx 1/2 g$  was observed in flight. That the turn is wings level is evidenced by the roll rate trace in Figure 16 which remains near zero throughout the maneuver. For a steady  $1/2 g$  turn

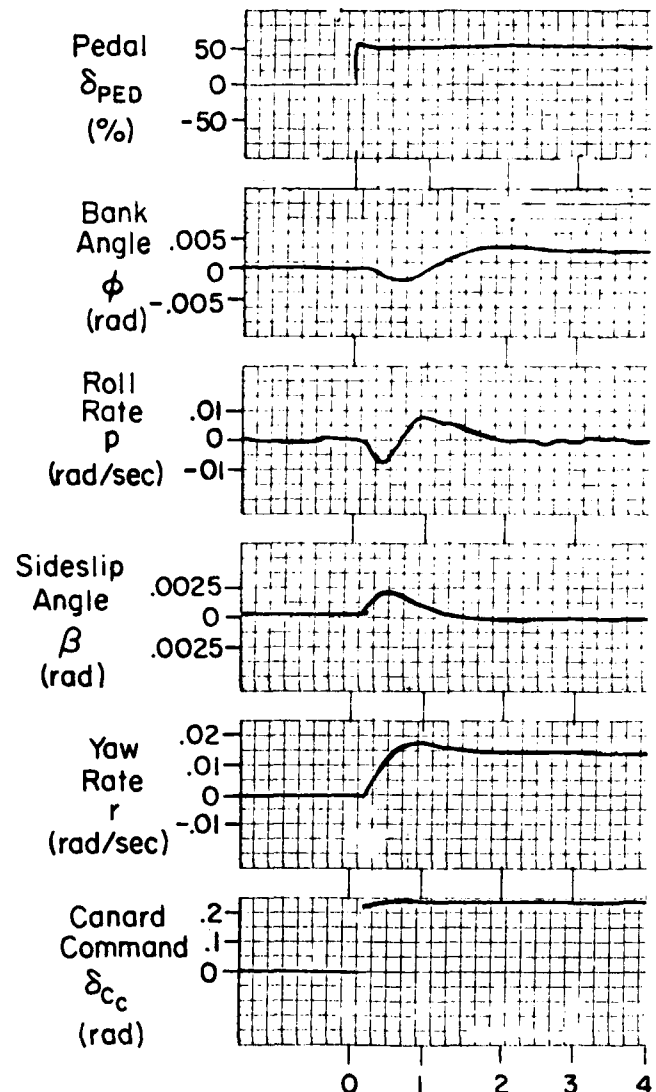
$$r \approx \frac{0.5g}{U_0} = \frac{0.5*32.2 \text{ ft/sec}^2}{177 \text{ ft/sec}} * 57.3 \text{ deg/rad}$$
$$= 5.2 \text{ deg/sec}$$

would be expected. The yaw rate in Figure 16 approaches this, but is effected by limiting in the telemetry system.

In summary, it has been demonstrated that the digital implementation of the ZOH controller performed properly -- both in the hybrid simulation and in VRA flights.



a) Theoretical Response of Continuous Controller to Step Input of Pedal (1 radian Canard Command Step)



b) 10 Hz ZOH Controller with Microprocessor Coupled to TR-48 Analog Computer Response to Pedal Step Input

Figure 15. Comparison of Theoretical Continuous Controllers with ZOH Controller on Hybrid Simulator

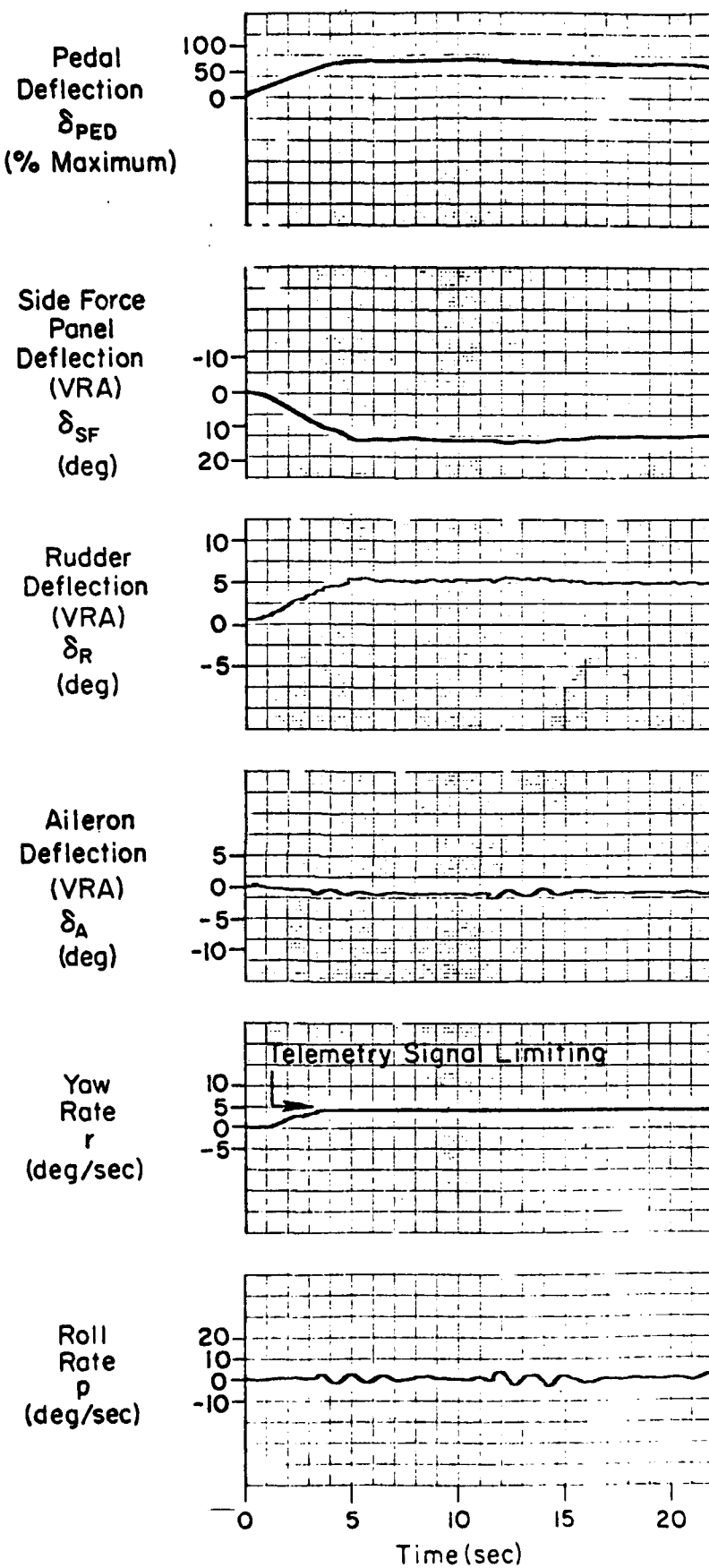


Figure 16. VRA Flight Record of Wings Level Turns, ZOH Control Law

## SECTION IV

### SLEWER CONTROLLER

#### A. INTRODUCTION

This section describes the control law synthesis procedure and validation process for the slew. Because of "structural" differences between the ZOH and slew first-order equations of motion for the YF-16 it was necessary to "invent" a generalization of equivalent stability derivative (ESD) model matching approach. The nature of the solution is described first, with crucial theoretical proofs relegated to appendices. A low-order example is given to illustrate the mathematical process and a general four-step synthesis procedure is outlined.

Next, the control law for the slew/YF-16 combination is given, with the intermediate numerical details given in an appendix. The control law is theoretically validated by running step responses with the theoretical controller working against an analytical model of the open-loop YF-16. The generalized ESD approach does an excellent job of matching the simulator to the model.

Next, the details of validating the hardware (microprocessor) based control law against an analog (TR-48) model of the YF-16 are described. The control law is validated, as is the physical implementation of the slew (in terms of hardware integrators and a "software differencing" format.) Noise problems surfaced in the next stage which prevented the flight validation phase from being carried out. These problems are described in some detail.

#### B. SYNTHESIS USING A GENERALIZED ESD APPROACH

A radical departure in the format of the first-order form occurs when the slew is used as the coupler. The first-order form (see Appendix E for a derivation) becomes

$$x_{s_{k+1}} = \phi_s x_{s_k} + \Gamma_1 \delta_{s_k} + \Gamma_2 \delta_{s_{k-1}} \quad (69)$$

while model equations remain the same

$$x_{m_{k+1}} = \phi_m x_{m_k} + \Gamma_m \delta_{m_k} \quad (70)$$

The pseudo inverse, which was very effective in the ZOH case, will no longer work. To see this, transform the above equations and substitute the control law

$$\delta_s = C_F \delta_m + C_B x_s \quad (71)$$

into the simulator equation. The result is (see Appendix F):

$$[Iz - \phi_s - (\Gamma_1 + \Gamma_2 z^{-1}) C_B] x_s = [\Gamma_1 + z^{-1}] C_F \delta_m \quad (72)$$

$$[Iz - \phi_m] x_m = \Gamma_m \delta_m$$

Thus an exact match requires

$$\begin{bmatrix} C_F \\ C_B \end{bmatrix} = [\Gamma_1 + \Gamma_2 z^{-1}]^{-1} \begin{bmatrix} \Gamma_m \\ \phi_m - \phi_s \end{bmatrix} \quad (73)$$

which is, in general, unattainable for two reasons. The first is that  $[\Gamma_1 + \Gamma_2 z^{-1}]^{-1}$  is not invertible. The second problem is that, even if the inverse exists,  $[\Gamma_1 + \Gamma_2 z^{-1}]^{-1}$  may have poles exterior to the unit circle and therefore produce an unstable controller. Needed is a synthesis procedure that generalizes the ESD approach, can treat non-square matrices, and insures a stable controller. The Wiener-Hopf approach satisfies these criteria and is discussed next.

### C. SOLUTION VIA WIENER-HOPF

Given the equation set (Equation 72) the W-H equation becomes (see Appendix F):

$$\frac{(\Gamma_1' + \Gamma_2 z)(\Gamma_1 + \Gamma_2 z^{-1})}{z} [C_F \mid C_B] - \frac{(\Gamma_1' + \Gamma_2 z)}{z} [\Gamma_m \quad \phi_m - \phi_s] = \psi \quad (74)$$

If one considers  $[C_F \mid C_B]$  as a single matrix, and thus in a certain sense one unknown, the problem posed in Equation 74 becomes clear; there is only one (matrix) equation but two unknowns. That is, treating  $[C_F \mid C_B]$  as one unknown, the other unknown is the matrix  $\psi$ . All we know about  $\psi$  is that it must have poles exterior to the unit circle; that is, a property of  $\psi$  is known. The trick is to "pick" a  $[C_F \mid C_B]$  matrix that is stable, substitute it in Equation 74, and find, after the evaluation, that  $\psi$  has the desired property.

### D. SPECTRAL FACTORIZATION SOLUTION METHOD

Equation 74 has the form

$$\phi Y - N = \psi \quad (75)$$

If a factorization of  $\phi$  exists such that

$$\phi = \phi_{1*} \phi_1 \quad (76)$$

where  $\phi_1$  has the poles interior to the unit circle and  $\phi_{1*} = \phi'(1/z)$  has poles exterior to the unit circle, then the solution can be written as

$$Y = \phi_1^{-1} [\phi_{1*}^{-1} N]_+ \quad (77)$$

where  $[ ]_+$  signifies a partial fraction expansion in which only the terms associated with poles interior to the unit circle are retained. We must verify that Equation 77 produces a  $\psi$ -vector that has all of its poles exterior to the unit circle:

$$\begin{aligned}
 \phi Y - N &= \phi_{1*}\phi_1\phi_1^{-1}[\phi_{1*}^{-1}N]_+ - \phi_{1*}\phi_1^{-1}N = \psi \\
 &= \phi_{1*}[(\phi_{1*}^{-1}N)_+ - \phi_{1*}^{-1}N] = \psi
 \end{aligned} \tag{78}$$

Write

$$\phi_{1*}^{-1}N = [\phi_{1*}^{-1}N]_+ + [\phi_{1*}^{-1}N]_- \tag{79}$$

where  $[\ ]_+$  is the sum of the partial fraction terms interior to the unit circle and  $[\ ]_-$  is the sum of the terms exterior to the unit circle. Thus

$$\phi_{1*}[(\phi_{1*}^{-1}N)_+ - (\phi_{1*}^{-1}N)_+ - (\phi_{1*}^{-1}N)_-] = \psi \tag{80}$$

and

$$\psi = -\phi_{1*}[\phi_{1*}^{-1}N]_- \tag{81}$$

which is guaranteed to have all poles exterior to the unit circle, verifying Equation 77 as a solution of the W-H equation.

The difficulty with the approach is that the spectral matrix  $\phi$  has to be factored into the product of two matrices, one which is analytic in the interior of the unit circle, the other analytic in the exterior of the unit circle. This is a formidable task. However, the factorization approach does give key insights into the properties of our particular W-H equation, a matter to be discussed next.

## E. KEY FEATURES OF THE SOLUTION

From the previous discussion, if the spectral matrix can be written

$$\phi = \phi_{1*}\phi_1 \tag{82}$$

the

$$\det \phi = \det \phi_{1*} \det \phi_1 \tag{83}$$

and we see that the poles of  $\phi$  interior to the unit circle must be the poles of  $\phi_1$  and the poles of  $\phi$  exterior to the unit circle must be the poles of  $\phi_{1*}$ . A key observation is therefore that the poles of the solution vector  $Y$  are already known; we need only determine the zeros of  $Y$ . To do this assume the numerators of  $Y$  are unknown polynomials divided by the "stable" poles of  $\phi$ . Substituting  $Y$  into Equation 75 must lead to a  $\psi$  which has only poles exterior to the unit circle; therefore the numerator polynomials must be selected so that the poles of  $\phi_1$  cancel out of Equation 75. This is the "direct" approach for solving W-H equations that is described in detail in Reference 3.

#### F. ILLUSTRATIVE EXAMPLE

Refocusing our attention on Equation 74, we show how the thought process described earlier can be used to effect a solution. A simple illustrative example is used to facilitate the discussion. Suppose

$$x_{s_{k+1}} = \begin{bmatrix} 1 & 0 \\ -1 & 0 \end{bmatrix} x_{s_k} + \begin{bmatrix} 1 & 1 \\ 0 & 1 \end{bmatrix} \delta_{s_k} + \begin{bmatrix} 1 & 0 \\ .75 & -.25 \end{bmatrix} \delta_{k-1} \quad (84)$$

$$x_{m_{k+1}} = \begin{bmatrix} 2 & 2 \\ 0 & 1 \end{bmatrix} x_{m_k} + \begin{bmatrix} 1 & 2 \\ 2 & 1 \end{bmatrix} \delta_{m_k} \quad (85)$$

Thus

$$\phi_m - \phi_s = \begin{bmatrix} 1 & 2 \\ 1 & 1 \end{bmatrix}, \quad \Gamma_m = \begin{bmatrix} 1 & 2 \\ 2 & 1 \end{bmatrix} \quad (86)$$

and

$$\Gamma_1 + \Gamma_2 z^{-1} = \begin{bmatrix} 1 + z^{-1} & 1 \\ .75z^{-1} & 1 - .25z^{-1} \end{bmatrix} = \frac{\begin{bmatrix} z + 1 & z \\ .75 & z - .15 \end{bmatrix}}{z} \quad (87)$$

$$\Gamma'_1 - \Gamma'_2 z = \begin{bmatrix} z + 1 & .75z \\ 1 & -.25z + 1 \end{bmatrix} \quad (88)$$

The spectral matrix  $\Phi$  is

$$\Phi = [\Gamma'_1 + \Gamma'_2 z][\Gamma_1 + \Gamma_2 z^{-1}] = \frac{\begin{bmatrix} z^2 + 2.5625z + 1 & 1.75z^2 + .8125z \\ .8125z + 1.75 & -.25z^2 + 2.0625z - .25z - .25 \end{bmatrix}}{z} \quad (89)$$

$$\det \Phi = -.25z^4 + 1.0625z^2 - .25 = -.25[z^4 - 4.25z^2 + 1] \quad (90)$$

The roots of Equation 90 are

$$D = (z - .5)(z + .5)(z - 2)(z + 2)$$

and therefore select

$$\Delta = (z - .5)(z + .5) = z^2 - .25 \quad (91)$$

as the poles for all the entries of  $C_F$  and  $C_B$ . Equation 74 has the form, for  $C_F$ :

$$\frac{\begin{bmatrix} z^2 - 2.5625z + 1 & 1.75z^2 + .8125z \\ .8125z + 1.75 & -.25z^2 + 2.0625z - .25 \end{bmatrix}}{z^2} \frac{\begin{bmatrix} a_0z^2 + a_1z + a_2 & b_0z^2 + b_1z + b_2 \\ c_0z^2 + c_1z + c_2 & d_0z^2 + d_1z + d_2 \end{bmatrix}}{(z - .5)(z + .5)}$$

$$- \frac{\begin{bmatrix} 2.5z + 1 & 2.75z + 2 \\ -.5z + 3 & -.25z + 3 \end{bmatrix}}{z^2(z - .5)(z + .5)} z(z - .5)(z + .5) = \psi \quad (92)$$

In Equation 92 the  $(\Gamma_1' \Gamma_2 z) \Gamma_m / z$  has been augmented by a  $z\Delta$  factor, in order to force a common denominator. We must pick the unknown coefficients of  $C_F$  so that each numerator of Equation 92 contains  $z^2(z - .5)$  ( $z + .5$ ), in order that  $\psi$  will be free of poles interior to the unit circle. One property of the solution is therefore immediately apparent; setting  $z = 0$  gives, for the numerator of Equation 92,

$$\begin{bmatrix} 1 & 0 \\ 1.75 & .25 \end{bmatrix} \begin{bmatrix} a_2 & b_2 \\ c_2 & d_2 \end{bmatrix} = 0 \quad (93)$$

Since  $\det \begin{bmatrix} 1 & 0 \\ 1.75 & .25 \end{bmatrix} \neq 0$ , we are assured there is the unique solution

$$\begin{bmatrix} a_2 & b_2 \\ c_2 & d_2 \end{bmatrix} = 0 \quad (94)$$

This is a general result; all numerator entries of  $C_F$  and  $C_B$  must contain a free  $z$ . The free  $z$  in  $C_F$  and  $C_B$  will force a cancellation of one of the  $z$ 's in the first term of Equation 92. This step is of such importance that we emphasize it by simplifying Equation 92:

$$\frac{\begin{bmatrix} z^2+2.5625z+1 & 1.75z^2+.8125z \\ .8125z+1.75 & -.25z^2+2.0625z-.25 \end{bmatrix}}{z} \begin{bmatrix} a_0z+a_1 & b_0z+b_1 \\ c_0z+c_1 & d_0z+d_1 \end{bmatrix} = \frac{\begin{bmatrix} 2.5z+1 & 2.75z+2 \\ .5z+3 & .25z+3 \end{bmatrix}}{z(z-.5)(z+.5)} (z - .5)(z + .5) = \psi \quad (95)$$

There is now only one free  $z$  in the denominator of Equation 95. The numerators of Equation 95 must all contain a free  $z$ , in order for the  $z$  in the denominator to cancel out of  $\psi$ . Setting  $z = 0$  gives

$$\begin{bmatrix} 1 & 0 \\ 1.75 & -.25 \end{bmatrix} \begin{bmatrix} a_1 & b_1 \\ c_1 & d_1 \end{bmatrix} = \begin{bmatrix} 1 & 2 \\ 3 & 3 \end{bmatrix} (-.5)(.5) \quad (96)$$

or

$$\begin{bmatrix} a_1 & b_1 \\ c_1 & d_1 \end{bmatrix} = \begin{bmatrix} -.25 & -.5 \\ 1.25 & -.5 \end{bmatrix} \quad (97)$$

The next step is to pick  $(a_0, b_0, c_0, d_0)$  so that  $\Delta = (z - .5)(z + .5)$  is not a root of  $\psi$ . However, for those values of  $z$  such that  $\Delta(z) = 0$ , Equation 95 simplifies tremendously and we obtain another general result

$$\phi C_F \equiv 0 \quad \text{when} \quad \Delta(z) = 0 \quad (98)$$

This result, however, must be treated with care; it does not mean that  $C_F = 0$  for these values of  $z$  since  $\phi^{-1}$  does not exist. That is,

$$\det \phi \equiv 0 \quad \text{for } z \text{ such that } \Delta(z) = 0 \quad (99)$$

The correct usage of Equation 98 is

$$[\phi] \begin{bmatrix} a_0z + a_1 & b_0z + b_1 \\ c_0z + c_1 & d_0z + d_1 \end{bmatrix} = 0 \quad (100)$$

$$[\phi] \begin{bmatrix} a_0z & b_0z \\ c_0z & d_0z \end{bmatrix} = -\phi \begin{bmatrix} a_1 & b_1 \\ c_1 & d_1 \end{bmatrix} \quad (101)$$

Clearly, since  $\det \phi = 0$  for  $z = 0.5, -0.5$ , the two equations of  $\phi$  are linearly dependent; thus we need only one of them. Suppose we choose the first row:

$$\begin{bmatrix} (z^2 + 2.5625z + 1) & 1.75z^2 + .8125z \end{bmatrix} \begin{bmatrix} a_0z + a_1 & b_0z + b_1 \\ c_0z + c_1 & d_0z + d_1 \end{bmatrix} = 0$$

where  $z = .5, -.5$  (102)

When  $z = 0.5$ ,

$$\begin{bmatrix} 2.53125 & .84375 \end{bmatrix} \begin{bmatrix} .5a_0 + a_1 & .5b_0 + b_1 \\ .5c_0 + c_1 & .5d_0 + d_1 \end{bmatrix} = 0$$

(103)

Solving for  $(a_0, b_0, c_0, d_0)$  in terms of  $(a_1, b_1, c_1, d_1)$  gives

$$c_F = \frac{\begin{bmatrix} -z^2 - .25z & z^2 - .5z \\ 2z^2 + 1.25z & z^2 - .5z \end{bmatrix}}{(z - .5)(z + .5)}$$

(104)

Using the same procedure, except substituting  $\phi_m - \phi_s$  for  $\Gamma_m$ , gives

$$c_B = \frac{\begin{bmatrix} -.25z & z^2 - .5z \\ z^2 + .25z & z^2 - .5z \end{bmatrix}}{(z - .5)(z + .5)}$$

(105)

This illustrative example was chosen so that  $\Gamma_1 + \Gamma_2 z^{-1}$  would be invertible and give the reader an opportunity to verify the answer using Equation 83. However, bear in mind that the W-H approach works when  $\Gamma_1 + \Gamma_2 z^{-1}$  is not invertible.

Before, leaving the example, perform the computation

$$C_F^{-1}C_B = \begin{bmatrix} 1/3 & 0 \\ 1/3 & 1 \end{bmatrix} \quad (106)$$

and observe another property of the solution, namely that  $C_F^{-1}C_B$  is always a matrix of constants. It is given explicitly by the equation (see Appendix G for proof):

$$C_F^{-1}C_B = (\Gamma_1' \Gamma_m')^{-1} \Gamma_1' (\phi_m - \phi_s) \quad (107)$$

#### G. GENERAL PROCEDURE

The steps used in the illustrative example are a good basis for a general procedure. First, let

$$C_F = \frac{z C_F^{\text{adj}}}{\Delta} \quad . \quad C_B = \frac{z C_B^{\text{adj}}}{\Delta} \quad (108)$$

where  $C_F^{\text{adj}}$ ,  $C_B^{\text{adj}}$  are the polynomial adjoint matrices of  $\Delta$ , and rewrite Equation 74 as

$$\frac{[\Gamma_1' + \Gamma_2' z][\Gamma_1 z + \Gamma_2][C_F^{\text{adj}} \mid C_B^{\text{adj}}]}{z\Delta} - [\Gamma_1' + \Gamma_2' z][\Gamma_m(\phi_m - \phi_s)]\Delta = \psi \quad (109)$$

There are four steps in the procedure:

- 1) Evaluate  $\det[(\Gamma_1' + \Gamma_2' z)(\Gamma_1 z + \Gamma_2)]$ , select the interior roots for  $\Delta(s)$ .
- 2) Set up  $C_F^{\text{adj}}$  and  $C_B^{\text{adj}}$  with unknown polynomial entries. The order of each polynomial is equal to the order of  $\Delta(z)$ , with all  $z^0$  terms set to zero.

3) Solve for  $C_F^{\text{adj}}(0)$ ,  $C_B^{\text{adj}}(0)$  using

$$[C_F^{\text{adj}} \mid C_B^{\text{adj}}] = (\Gamma_1' \Gamma_2)^{-1} \Gamma_1' [\Gamma_m] (\phi_m - \phi_s) \Delta(0) \quad (110)$$

4) Find the remaining equations by evaluating appropriate rows of

$$(\Gamma_1' + \Gamma_2' z)(\Gamma_1 z + \Gamma_2) [C_F^{\text{adj}} \mid C_B^{\text{adj}}] = 0, \quad \Delta(z) = 0 \quad (111)$$

Next, we apply the procedure to the slewer controller use and tabulate the  $C_F$  and  $C_B$  matrices.

## H. SLEWER CONTROL LAW

Figure 17a has a matrix  $C_P$  premultiplying the  $C_F$  matrix. As in the case of the ZOH, this is the matrix which couples the model inputs to force a wings-level turn. As in the case of the ZOH, it is a  $3 \times 1$  matrix, but the entries are slightly different.

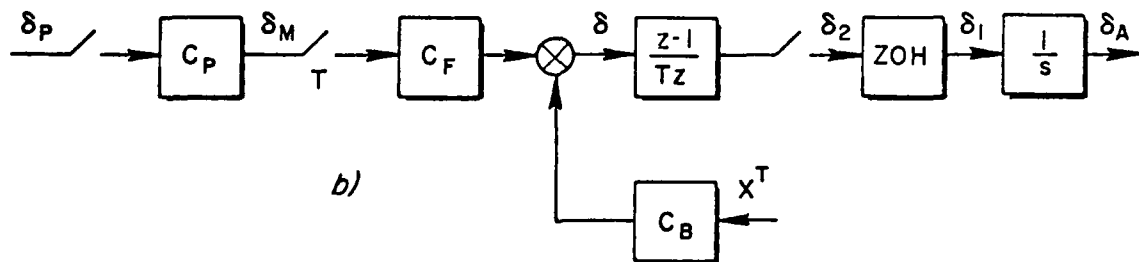
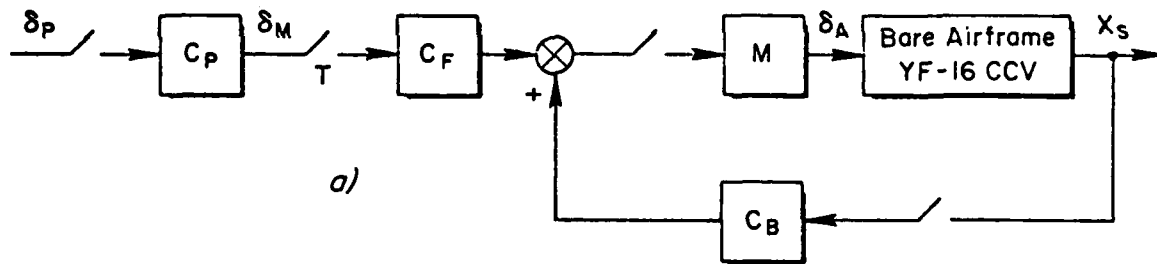


Figure 17. Block Diagram for Software Realization

The idealized configuration of Figure 17a must be modified for the slewer since we have no physical implementation of a completely hardware nature for implementing

$$M = \frac{(1 - e^{-sT})^2}{Ts^2} \quad (112)$$

We choose to implement the slewer by "breaking up" Equation 112 according to Figure 17b. In Figure 17b the basic transfer function of the digital/analog converter as a ZOH has been retained, while the additional  $(1 - e^{-sT})/T$  has been moved back into software as  $(z - 1)/Tz$ . A physical (analog) integrator has been inserted as a prefilter to the controllers. This is an implementation that theoretically matches the characteristics of Equation 112. The theoretical details are discussed in Appendix H.

We will solve for the  $C_F$  and  $C_B$  matrices using the procedure outlined above. The computational details are very extensive and for that reason we relegate the input data and numerical computations to Appendix I. However, we must first discuss the structure of the control law.

Each entry of  $C_B$  and  $C_F$  is a ratio of polynomials in  $z$ . Dividing through by the highest power of  $z$  gives a large number of terms that will be multiplied by delay operators such as  $z^{-1}$ ,  $z^{-2}$ , etc. We will group all such operations involving "past" values of the data in a background computation. We proceed as follows, defining:

$$C_B = \frac{z[B_2z^2 + B_1z + B_0]}{\Delta(z)} \quad (113)$$

$$C_F = \frac{z[C_2z^2 + C_1z + C_0]}{\Delta(z)} \quad (114)$$

$$\Delta(z) = z^3 + a_2z^2 + a_1z + a_0 \quad (115)$$

From Figure 17b,

$$\begin{aligned}\delta &= C_F \delta_P^T + C_B X^T \\ &= \frac{z[C_2 z^2 + C_1 z + C_0]}{\Delta(z)} \delta_P^T + \frac{z[B_2 z^2 + B_1 z + B_0]}{\Delta(z)}\end{aligned}\quad (116)$$

Dividing through by  $z^3$  gives

$$\begin{aligned}[1 + a_2 z^{-1} + a_1 z^{-2} + a_0 z^{-3}] \delta &= (C_2 + C_1 z^{-1} + C_0 z^{-2}) \delta_P^T \\ &\quad + (B_2 + B_1 z^{-1} + B_0 z^{-2}) X^T\end{aligned}\quad (117)$$

The recursion equation is

$$\begin{aligned}\delta_k &= -a_2 \delta_{k-1} - a_1 \delta_{k-2} - a_0 \delta_{k-3} + C_2 \delta_{P_k} + C_1 \delta_{P_{k-1}} + C_0 \delta_{P_{k-2}} \\ &\quad + B_2 X_k + B_1 X_{k-1} + B_0 X_{k-2}\end{aligned}\quad (118)$$

Define the "background" computation as:

$$\begin{aligned}b_k &= -a_2 \delta_{k-1} - a_1 \delta_{k-2} - a_0 \delta_{k-3} + C_1 \delta_{P_{k-1}} + C_0 \delta_{P_{k-2}} \\ &\quad + B_1 X_{k-1} + B_0 X_{k-2}\end{aligned}\quad (119)$$

Thus the "foreground" is

$$\delta_k = C_2 \delta_{P_k} + B_2 X_k + B_k \quad (120)$$

In addition, we need

$$\delta_2 = \frac{1}{T} [\delta_k - \delta_{k-1}] \quad (121)$$

When new data are taken in, the microprocessor will compute the first component of Equations 118 and 121 (the rudder control law), enable an interrupt and output to the rudder. It will then repeat this process for the side force controller and the aileron controller. In the remainder of the frame time, the background computation, Equation 119, will be updated. The data for the matrices are given in Table 5.

#### **I. VALIDATION: THEORETICAL CONTROLLER, THEORETICAL YF-16**

The control law defined by Equations 118, 119, and 120 was theoretically validated by running step responses. These are shown in Figure 18. The agreement between the slewer-based system and the continuous baseline is very good. The step responses are also tabulated in Table I-1 of Appendix H (these can be compared against Table 4 of Section III).

#### **J. VALIDATION: HARDWARE-BASED SLEWER, ANALOG YF-16**

Figure 19 shows a time response from a hybrid simulation of the slewer-controlled YF-16. The control law is implemented in the microprocessor with the YF-16 model on the TR-48 analog computer.

The input to the YF-16 model is a step input of direct force command (pedal) from a switch on the TR-48. This analog signal enters the microprocessor and is processed according to the slewer control law, which puts out canard, rudder, and aileron surface rate signals.

The YF-16 canard rate command,  $\dot{\delta}_C$ , is shown in the top trace of Figure 19. There is a "ringing" noise signal superimposed on the rate command signal. This noise is much larger than the rate signal itself. This suggests an improper scaling of one of the channels which is allowing a noise response of an element of the matrix digital filter to be incorrectly added to the pedal command. We shall have more to say about this noise problem at a later point.

TABLE 5. CONTROL LAW SCALE FACTORS

			$C_2$	$C_1$	$C_0$
$a_2$	2.286091850		1,1    1.533456216	1,1    2.682205102	1,1    1.151205846
$a_1$	1.618495105		2,1    1.667517094	2,1    2.871006820	2,1    1.208809218
$a_0$	0.330906674		3,1    -0.450580559	3,1    -0.774749178	3,1    -0.325123599
			$B_2$		
			1,1    -1.304930639	2,1    -2.374065982	3,1    0.555540645
			1,2    -6.358020110	2,1    -7.722108030	3,2    2.545350641
			1,3    2.299806817	2,3    2.406413878	3,3    -0.8333278666
			1,4    8.929042824	2,4    9.627934872	3,4    -3.240818386
					$\delta_1 = \delta_R$
					$\delta_2 = \delta_{SF}$
			$B_1$		
			1,1    -1.472652250	2,1    -2.894195416	3,1    0.677934236
			1,2    -3.083980375	2,2    -4.717506600	3,2    1.907148562
			1,3    1.687500000	2,3    1.775939779	3,3    -0.726319404
			1,4    6.944045322	2,4    7.681266284	3,4    -2.939232566
					$X_1 = B$
					$X_2 = r$
			$B_0$		
			1,1    -0.072272240	2,1    -0.434231749	3,1    0.092079740
			1,2    2.958707329	2,2    2.614538939	3,2    -0.530540814
			1,3    -0.470633722	2,3    -0.467570771	3,3    0.059743647
			1,4    -1.498452885	2,4    -1.379447161	3,4    0.138754410
					$X_3 = p = \phi$
					$X_4 = \phi$

Note:

$$C_F = \begin{bmatrix} 1.51134 \\ 1.4355 \\ -0.38896 \end{bmatrix}$$

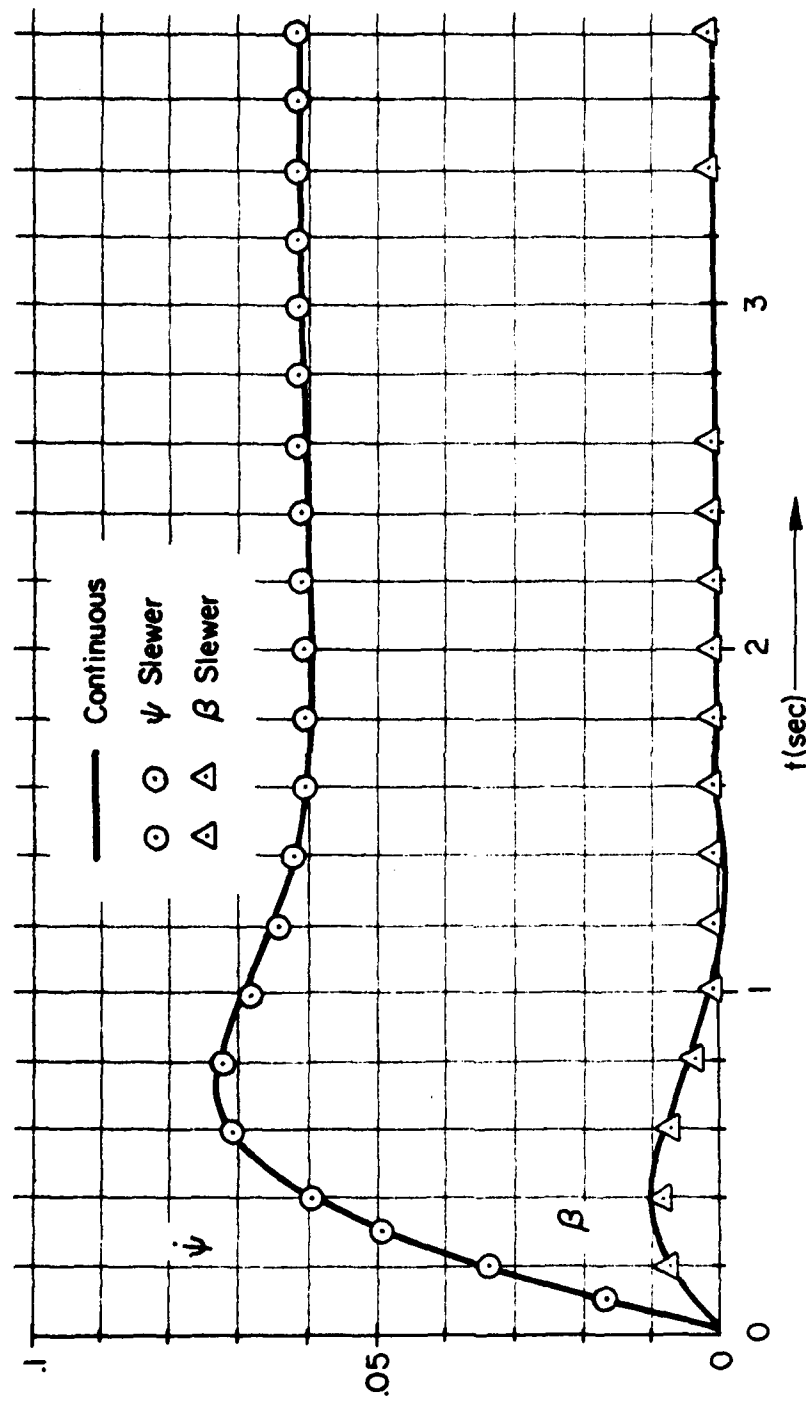


Figure 18. Slewer Step Response

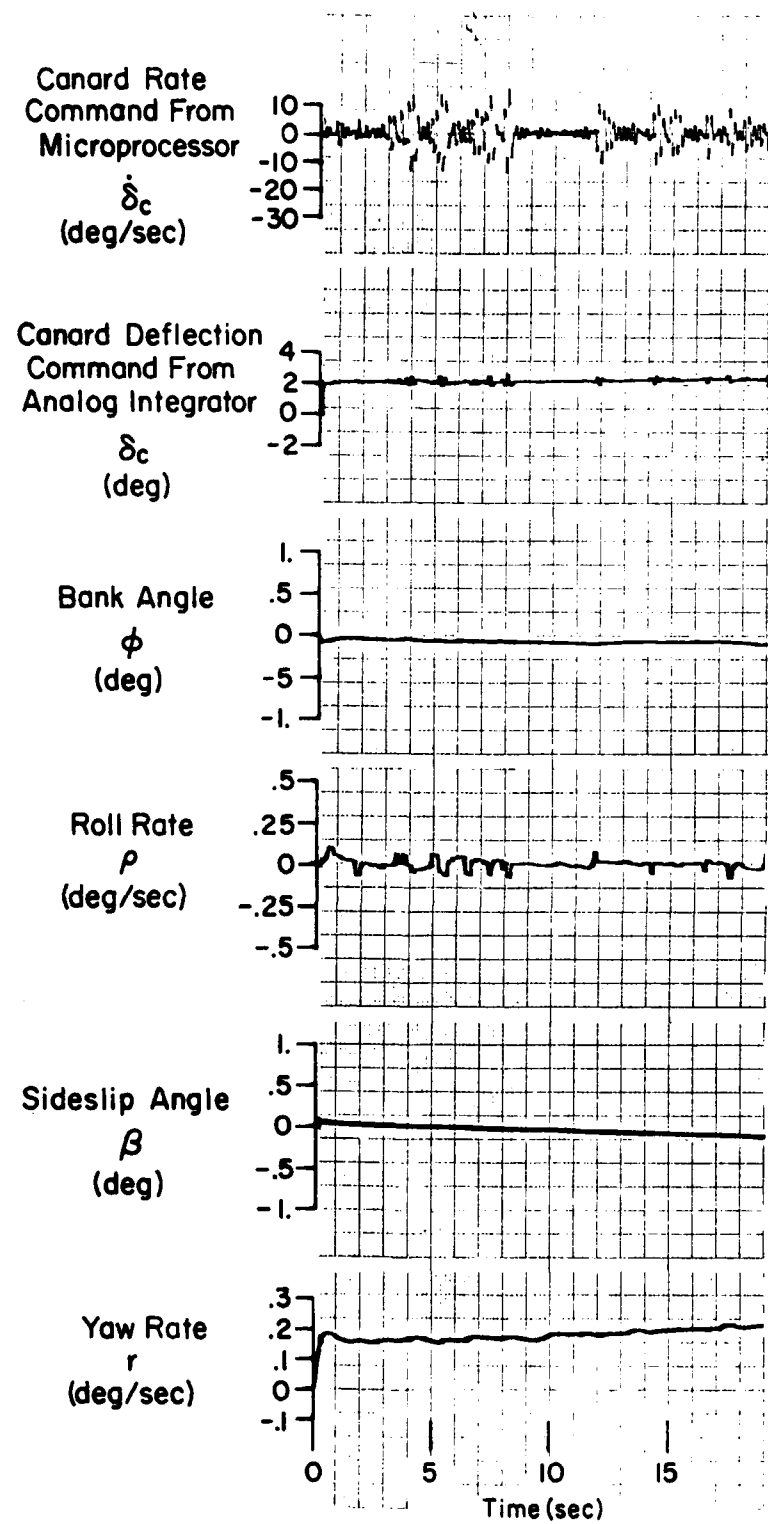


Figure 19. YF-16 Model Response to a Step Pedal Input

The  $C_p$  matrix of Figure 17 breaks the signal up into three components to generate three surface rate signals which are integrated by an analog integrator on the TR-48. This simulates the analog integrators in the VRA "mixing box." The YF-16 canard position command, from its integrator, is shown in the second trace. It is seen that the  $\delta_C$  signal has been properly integrated to a step, with a small 10 Hz noise component superimposed. The slow drift in  $\delta_C$  (and the response signals) is due to the bias in the D/A converters, which input the analog integrators. This bias could not be completely eliminated by the integrator balancing circuits.

The yaw rate response shown in the bottom trace has a "steady-state" value of

$$\frac{r}{\delta_C}_{ss} = 0.08 \text{ (deg/sec)/deg}$$

which compares well with the calculated value of 0.059 (deg/sec)/deg (considering the drift). The transient response shows the appropriate rise time and overshoot.

The sideslip, roll rate, and bank angle traces remain essentially zero (when the integrator drift is allowed for) as required for the wings-level coordinated turn.

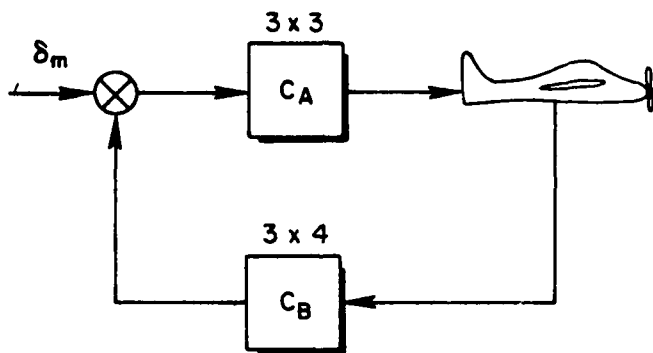
It was necessary to keep signal levels low because larger inputs caused the noise component to limit the surface rate channels. However, because the simulation is linear, it can be seen that the slewer controller performs properly over the frequency region of interest for control of the YF-16 dynamics.

In essence, the problems noted in the traces, such as the unusually sensitive response to digital noise, are not properties of the slewer control law but properties of any recursive control law. That is, D/A and A/D interfaces imply a ratioing between physical variables and machine variables. If the gain of a machine variable is too high, the system will always be responding to digital noise or bit dither. Thus

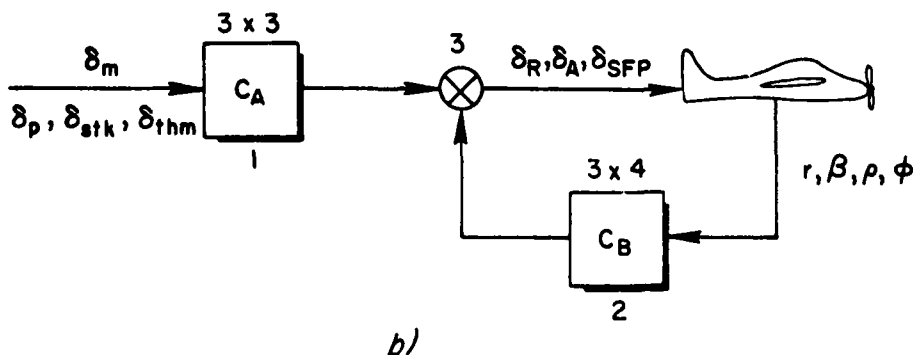
the problem is to properly proportion physical variables and machine variables, a process which requires a systematic technique for performing the scaling. Unfortunately, our original plan for gathering the data needed for the scaling was not workable. The microprocessor speed prevented a real-time printout of the states and controllers, since we were working with a TR-48, which would only work in real time. These problems are described next.

#### K. GAIN ALLOCATION AND NOISE PROBLEMS

One of the major obstacles to successful evaluation of the slewer control law and, in fact, a major consideration in any digital control environment, may be termed the gain allocation problem. Consider, for illustration, the zero-order hold case (Figure 20a).



a)



b)

Figure 20. Zero-Order Hold Gain Configurations. a) Standard Nomenclature, b) Equivalent Configuration vs. Implemented in DFCS Control Hardware/Software

In the present digital implementation the computations are structured according to the alternative form (Figure 20b).

If, for checkout purposes and computational convenience, one desires to enter the gains for  $C_F$  and  $C_B$  in physical units, it is necessary to introduce additional scale vectors (Figure 21), where A and B are vectors of dimension 3 and 4, respectively, which convert command and state A/D voltages to physical units; and C is a vector of dimension 3, which converts control and physical units to the correct voltage units for driving the servo buffer amplifiers.

This particular form worked well in earlier assembly code versions of the control program. However, in the later, more computationally advanced versions, performing the vector-matrix operations

$$\delta_x \times B \times C_B \times C \quad \text{and} \quad \delta_m \times A \times C_F \times C$$

could not be reliably accomplished within the 100 msec time frame. This problem was solved by premultiplying the scaling vectors prior to entering the control loop, thus:

$$\hat{C}_F = A \times C_F \times C \quad \text{and} \quad \hat{C}_B = B \times C_B \times C$$

Now the real-time calculations revert to the simplified form (Figure 22) and are easily accomplished within the designated time frame. Although the slewer case is intrinsically more complex, the same operational principles apply to the digital code.

In the ZOH case the magnitudes of  $\hat{C}_F$  and  $\hat{C}_B$  fell between  $\pm 1.2$ . In the slewer case, however, the presence of the hardware integrators forced the conditioned gains ( $\hat{C}_0$ ,  $\hat{C}_1$ ,  $\hat{C}_2$ ) to vary over a much wider range ( $\pm 40$ ). While the range of intermediate products was not observed, we estimate that transient values exceeding  $10^3$  may have occurred during slewer control law operations. The presence of high gains and uneven gain distributions makes digital systems highly vulnerable to digital artifacts such as bit dither, roundoff, and truncation errors. In the slewer case, additional problems of analog noise sensitivity in the A/D

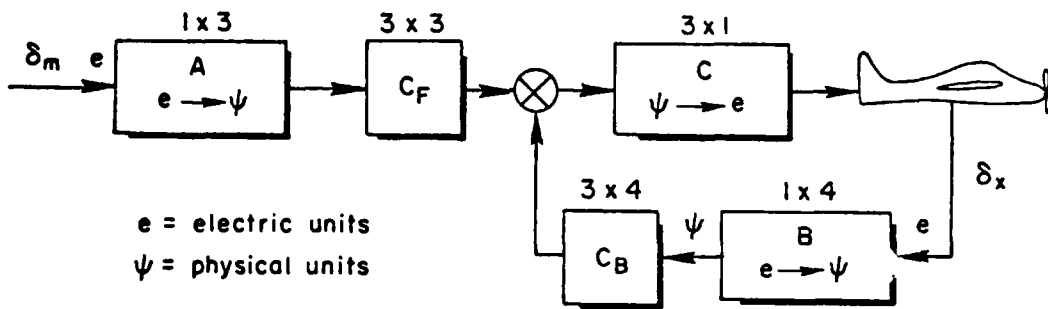


Figure 21. DFCS Gain Configurations Illustrating Within-Loop Placement of Scale Vectors

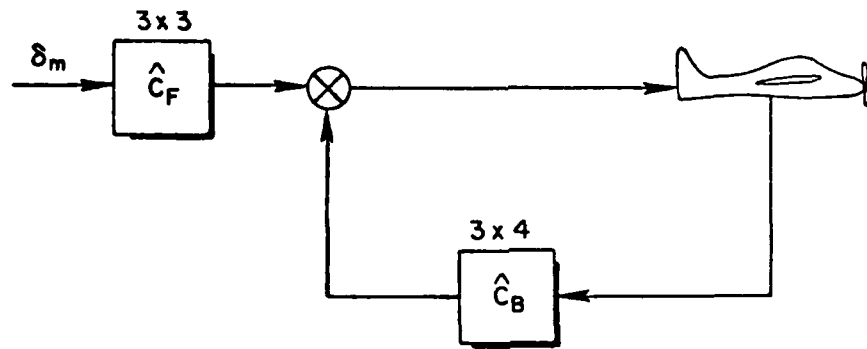


Figure 22. Resultant Gain Configuration Illustrating Simplification Brought About by Pre-Multiplication of Matrices

converters and offset sensitivity in the hardware integrators compounded our difficulties.

It should be noted here that sensitivity problems of this nature are extremely hard to identify, especially due to the dynamic requirements of the slewer. It is nearly impossible to capture intermediate values with the slewer running in real time due to the intolerance of the frame epoch for additional code, especially I/O. Another approach would be to slow down the TR-48 to match the frame rate of a modified slewer with I/O in the control loop. This procedure, however, is resisted by operational limitations of the TR-48. A general solution of minimizing the range of conditioned gains ( $\hat{C}_0$ ,  $\hat{C}_1$ ,  $\hat{C}_2$ ) was attempted by using internal analog scaling to reduce the internal gain distribution from  $\pm 40$  to  $\pm 9$ . This was somewhat successful in that it resulted in the only stable data obtained on the slewer. However, analog noise external to the digital system was exacerbated.

Future efforts would definitely include a systematic attack on scaling problems of this type, since they appear to be the root of many digital control system problems.

#### **L. THE GRACEFUL ENTRY PROBLEM**

Although it is generally considered appropriate to trim an aircraft to stable level flight prior to engaging an autopilot, it has long been recognized that some sort of autotrim mechanism is necessary for smooth engagement since perfect level flight is seldom extant at engage time.

The Princeton VRA represents no exception to this rule. Minimization of engage transients is extremely critical to the Navion due to the high angular accelerations available at the control servos.

The VRA's analog system has an active continuous autotrim which is highly effective. For the micro-DFCS, however, it is necessary to implement the autotrim in software. The Figure 23 flow diagram illustrates how this is done, again, using the zero-order hold case as an example. An important consideration in dealing with control law calculations on the micro-DFCS is that the numerical basis for the A/D and

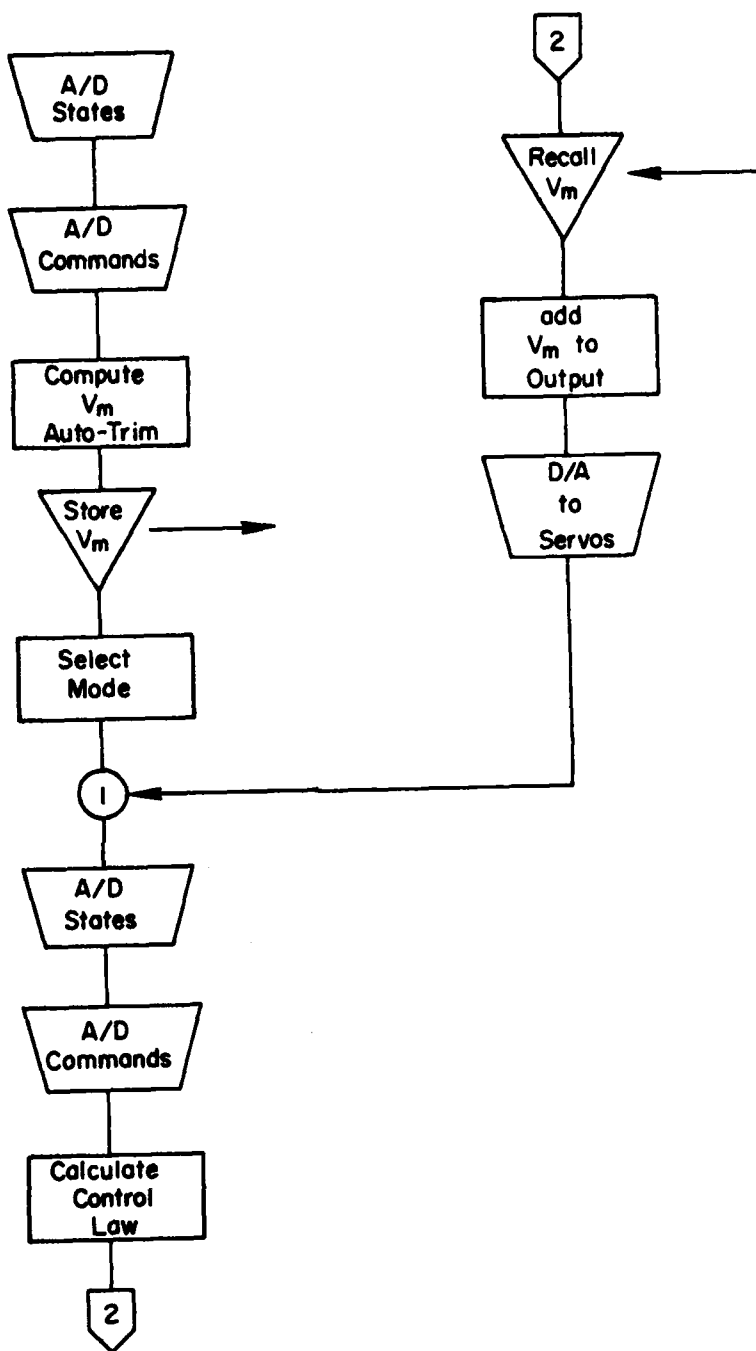


Figure 23. ZOH Auto-Trim Algorithm

D/A peripherals is offset binary, i.e.,  $0 = -10V$ ,  $2048_{10} = 2^{11} = 0V$ ,  $4096_{10} = 2^{12} = +10V$ . Since the same numerical basis is used for both A/D and D/A operations it is considerably more efficient to perform control law calculations with the offset in place. This means, using the ZOH case as an example, for small state and command perturbations centering around  $0 \pm 2.0$  VDC, control law products are in the range  $1.0 \times 10^3 < P < 5.0 \times 10^3$  or 11-13 bits. Since the autotrim calculations which are applied to the ZOH case operate in the same magnitude range they pose no threat of digital saturation even with the binary offset present.

In the slewer case, however, an entirely different set of parameters was found to apply. First, there is an order of magnitude differential between A/D incoming volts and D/A output volts due to the present of the hardware integrators. Second, the presence of the 11 bit binary offset, coupled with the relatively larger gains and greater number of computational terms produced intermediate products which apparently caused saturation of the 9511 match chip. For these reasons, the ZOH autotrim algorithm would not work for the slewer. Additionally, it was found that the slewer control loop computations were numerically incorrect when performed in offset binary. Although modifying the control loop routine to take out the offset immediately following A/D input, and reinserting it immediately prior to D/A turned out to be fairly simple, modifying the autotrim required a major code rework which could not be accomplished in the remaining time at Princeton.

The slewer was evaluated on the TR-48 by initializing the analog computer in a manner that simulated autotrim. (Digital autotrim was disabled for these test runs.) An analogous simulation in the VRA could not be accomplished due to the design of the VRA analog system. This was the major impediment to flight testing the slewer on the VRA.

SECTION V  
CONCLUSIONS AND RECOMMENDATIONS

**A. CONCLUSIONS**

From a theoretical viewpoint, both the direct synthesis ZOH and slewer control laws achieve the design objective of emulating the baseline wings-level-turn direct side force mode. In the ZOH case the equivalent stability derivative (ESD) model follower simulator approach was enhanced by the innovative use of a pseudo inverse.

A major theoretical addition to in-flight simulator technology was achieved in the slewer design with the introduction of a Wiener-Hopf optimization algorithm for augmenting the basic ESD approach. This is of great value in that other configurations (other than the slewer) lead to the same class of problem. For example, digital controllers utilizing ZOHs, wherein computer throughput delay is of concern, produce the exact same problem formulation.

The ZOH control law was hardware validated against both the TR-48 (functioning as a surrogate YF-16) and the Navion VRA (with analog closures to simulate an open-loop YF-16).

The slewer controller was validated in hardware against a surrogate YF-16 (TR-48). This is significant in that the input to the actuators, from the hardware integrators, possessed all the correct attributes even though a "continuous" slewer term,  $1 - e^{-sT}$ , was implemented in software as  $(z - 1)/Tz$ . Thus, one possible physical realization of the slewer coupler was realized.

On the negative side, largely unanticipated problems involving the scaling of physical and machine variables between the A/D computer and D/A modules led to an inordinate and unacceptable level of digital noise (bit dither, rounding, etc.). This noise was a major impediment to flight validation of the slewer. Another major obstacle was the lack of an adequate digital autotrim algorithm for the slewer. This created an engage-transient or "graceful entry" problem which precluded flight test of the slewer.

**B. RECOMMENDATIONS**

There are four recommendations. First, two software routines need to be written for the slewer/microprocessor/Navion combination:

- 1) An autotrim algorithm for the YF-16 program that provides graceful entry into the test run.
- 2) A program for optimizing the relative ratios between physical variables and machine variables so as to eliminate or minimize the digital noise problem.

With the control of the digital noise, the integrator drift problem will probably disappear. If it remains, then we need:

- 3) A slew rate realization that resets the integrator every T seconds.

Implementation of Recommendations 1 and 2 should be straightforward since both issues underwent preliminary attack immediately prior to the termination of our last flight test effort at Princeton. The autotrim problem is easily solved, but was unanticipated until our last minute review of slew rate computations was made. The realization of the first two recommendations (and if necessary the third) would set the stage for carrying out the fourth recommendation:

- 4) Pilot evaluation flights to furnish paired comparisons between the ZOH, slew rate, and baseline analog configurations.

#### REFERENCES

1. Hoh, Roger H., Thomas T. Myers, Irving L. Ashkenas, Robert F. Ringland, and Samuel J. Craig, Development of Handling Quality Criteria for Aircraft with Independent Control of Six Degrees of Freedom, AFWAL/TR-81-3027, Apr. 1981.
2. Whitbeck, R. F., Wiener-Hopf Approaches to Regulator, Filter/Observer and Optimal Coupler Problems, ONR-CR215-260-1, Jan. 1980.
3. Whitbeck, R. F., "'Direct' Wiener-Hopf Solution of Filter/Observer and Optimal Coupler Problems," J. Guidance and Control, Vol. 4, No. 3, May-June 1981, pp. 329-336.
4. Whitbeck, R. F., "Digital Controller Effects on the ESD Approach to Model Following," Proc. of Joint Automatic Control Conference, Vol. I, Charlottesville, VA, 17-19 June 1981.
5. Larimer, Stanley J., An Interactive Computer Aides Design Program for Digital and Continuous Control System Analysis and Synthesis, AFIT/GGC/EE/78-2, Mar. 1978.

APPENDIX A  
DATA FOR FIRST-ORDER FORMS

This appendix gives data for the first-order forms of the equations of motion. The continuous system has the form

$$\dot{X} = (AMAT)X + (BMAT)\delta$$

whereas the ZOH forms are

$$X_{k+1} = (FMAT)X_k + (GMAT)\delta_k$$

Data are for open-loop Navion, YF-16 CCV with canard (the bare airframe), and the YF-16 CCV with canard and FCS loop in (the closed-loop, reduced-order model). Sample rate varies from 1 to 100 Hz.

## NAVION

CASE I -- T=1

AMAT(ROW 1)=	-.7770000000	4.680000000	-.4320000000	0.
AMAT(ROW 2)=	-1.000000000	-.3556000000	0.	.1720000000
MAT(ROW 3)=	1.270000000	-12.80000000	-6.600000000	0.
MAT(ROW 4)=	0.	0.	1.000000000	0.
BMAT(ROW 1)=	-6.100000000	2.410000000	-.3140000000	0.
BMAT(ROW 2)=	.7250000000E-01	.2370000000	0.	21.00000000
BMAT(ROW 3)=	.7700000000	0.	0.	0.
BMAT(ROW 4)=	0.	0.	0.	0.
FMAT(ROW 1)=	-.4075412400	.9390138680	.4293097259E-01	.2046989908
FMAT(ROW 2)=	-.1551241565	-.3838344962	.2389389190E-01	.5992906255E-01
FMAT(ROW 3)=	.3669224081	.6128786254	-.4385726603E-01	-.9280900090E-01
FMAT(ROW 4)=	.4186501074	-.5395872145	.1201782102	.9301757677
GMAT(ROW 1)=	-.1526753013	.9162311377	-.2970684949	0.
GMAT(ROW 2)=	1.371944289	-.4438240609	.4585820142	0.
GMAT(ROW 3)=	-2.500348506	.8810645890	2.392286281	0.
GMAT(ROW 4)=	-1.014895194	.3290076095	2.421418515	0.

YF-16 CCV Canard Bare A/F

CASE III -- T=1

AMAT(ROW 1)=	-.4310000000	10.20000000	-.4160000000E-01	0.
AMAT(ROW 2)=	-1.000000000	-.3060000000	0.	.3880000000E-01
AMAT(ROW 3)=	1.670000000	-.50.00000000	-2.330000000	0.
AMAT(ROW 4)=	0.	0.	1.000000000	0.
BMAT(ROW 1)=	-4.170000000	4.620000000	2.170000000	0.
BMAT(ROW 2)=	.3180000000E-01	.1910000000E-01	-.3570000000E-01	0.
BMAT(ROW 3)=	7.630000000	5.930000000	49.10000000	0.
BMAT(ROW 4)=	0.	0.	0.	0.
FMAT(ROW 1)=	-.6572296784	-.3871536087	.2385575652E-01	.6403866666E-01
FMAT(ROW 2)=	.5950769285E-01	-.7476665798	.4549435916E-02	.8276581092E-03
FMAT(ROW 3)=	2.119849638	7.661676086	.7858333945E-02	-.9944693746E-01
FMAT(ROW 4)=	2.363943008	-.2.563065399	.3446968122	.9093419354
GMAT(ROW 1)=	-.4684180033E-01	.1989741296	.2045705577	0.
GMAT(ROW 2)=	.6623635154	-.6763966931	-.1374128646	0.
GMAT(ROW 3)=	-7.309111147	12.91651424	22.14587124	0.
GMAT(ROW 4)=	-1.949465070	5.642783658	14.37868337	0.

YF-16 CCV Canard FCS Loops Closed

CASE II -- T=1

AMAT(ROW 1)=	-3.105000000	8.917000000	-.2720000000	0.
AMAT(ROW 2)=	-.979600000	-.2965000000	0.	.3795000000E-01
AMAT(ROW 3)=	6.564000000	-.47.71000000	-.8.359000000	-25.00000000
AMAT(ROW 4)=	0.	0.	1.000000000	0.
BMAT(ROW 1)=	-3.925000000	4.766000000	1.897000000	0.
BMAT(ROW 2)=	.2988000000E-01	.1802000000E-01	-.3360000000E-01	0.
BMAT(ROW 3)=	7.178000000	5.655000000	49.60000000	0.
BMAT(ROW 4)=	0.	0.	0.	0.
FMAT(ROW 1)=	-.1647293396	.1684792288	.5506900077E-02	-.2931554793E-01
FMAT(ROW 2)=	-.2779410484E-01	-.1025779173	-.1693009604E-02	-.2654919693E-01
FMAT(ROW 3)=	-.4343475822	1.263840151	-.6278117903E-02	-.5307241723E-01
FMAT(ROW 4)=	.1520723612	-.2465090960E-01	.2085476608E-02	.5251806333E-01
GMAT(ROW 1)=	-.2115582524	.3495927831	.2256656150	0.
GMAT(ROW 2)=	.4262370630	-.4745105578	-.1272278461	0.
GMAT(ROW 3)=	-.5826510360	.7361260345	.3927491796	0.
GMAT(ROW 4)=	-.4549428843	1.060727086	2.201845451	0.

## NAVION

## CASE I -- T=.2

AMAT(ROU 1)	-.7770000000	4.680000000	-.4320000000	0.
AMAT(ROU 2)	-1.000000000	-.3556000000	0.	.1720000000
AMAT(ROU 3)	1.270000000	-12.80000000	-6.600000000	0.
AMAT(ROU 4)	0.	0.	1.000000000	0.
BMAT(ROU 1)	-.6100000000	2.410000000	-.3140000000	
BMAT(ROU 2)	.7250000000E-01	.2370000000	0.	
BMAT(ROU 3)	.7700000000	0.	21.00000000	
BMAT(ROU 4)	0.	0.	0.	
FMAT(ROU 1)	.7638201656	.8734526537	-.4088771668E-01	.1554957149E-01
FMAT(ROU 2)	-.1720708623	.8410590820	.7465474683E-02	.3215391975E-01
FMAT(ROU 3)	.2779824494	-1.226753688	.2575694151	-.2739705798E-01
FMAT(ROU 4)	.2763312714E-01	-.1592852208	.1103686365	.9979399271
GMAT(ROU 1)	-.1088635063	.4524869698	-.1685774105	
GMAT(ROU 2)	.1251228024	.3970933440E-03	.1753197902E-01	
GMAT(ROU 3)	-.9512640391E-01	.2884523906E-01	2.309064565	
GMAT(ROU 4)	-.1650785217E-02	.1560467561E-02	.2817568625	

## YF-16 CCV Canard Bare A/F

## CASE III -- T=.2

AMAT(ROU 1)	-.4310000000	10.20000000	-.4160000000E-01	0.
AMAT(ROU 2)	-1.000000000	-.3060000000	0.	.3880000000E-01
AMAT(ROU 3)	1.670000000	-50.00000000	-2.330000000	0.
AMAT(ROU 4)	0.	0.	1.000000000	0.
BMAT(ROU 1)	-.4.170000000	4.620000000	2.170000000	
BMAT(ROU 2)	.3180000000E-01	.1910000000E-01	-.3570000000E-01	
BMAT(ROU 3)	7.630000000	5.930000000	49.10000000	
BMAT(ROU 4)	0.	0.	0.	
FMAT(ROU 1)	.7318284667	1.798616821	-.5428346869E-02	.7372047226E-02
FMAT(ROU 2)	-.1730440775	.7523851752	.1287590071E-02	.7027636713E-02
FMAT(ROU 3)	1.024821400	-6.888606229	.6225241588	-.3081227258E-01
FMAT(ROU 4)	.8309475710E-01	-.7941307365	.1595835351	.9978105376
GMAT(ROU 1)	-.7447458733	.8261207402	.3495396442	
GMAT(ROU 2)	.8316230277E-01	-.8098278965E-01	-.4190035662E-01	
GMAT(ROU 3)	.8458638785	1.315060244	8.044217665	
GMAT(ROU 4)	.1094266806	.1232560490	.8575517720	

## YF-16 CCV Canard FCS Loops Closed

## CASE II -- T=.2

AMAT(ROU 1)	-.3.105000000	8.917000000	-.2720000000	0.
AMAT(ROU 2)	-.9796000200	-.2965000000	0.	.3795000000E-01
AMAT(ROU 3)	6.564000000	-47.71000000	-8.359000000	-25.00000000
AMAT(ROU 4)	0.	0.	1.000000000	0.
BMAT(ROU 1)	-.3.925000000	4.766000000	1.897000000	
BMAT(ROU 2)	.2988900000E-01	.1802000000E-01	-.3360000000E-01	
BMAT(ROU 3)	7.178000000	5.655000000	49.60000000	
BMAT(ROU 4)	0.	0.	0.	
FMAT(ROU 1)	.4074418431	1.309025344	-.1275477179E-01	.6458359475E-01
FMAT(ROU 2)	-.1314973514	.7988423546	.2674845925E-02	.1373731217E-02
FMAT(ROU 3)	.7113296577	-2.922093678	.1131844369E-01	-.2.047166570
FMAT(ROU 4)	.9096334565E-01	-.4705547884	.8117236063E-01	.7145802362
GMAT(ROU 1)	-.5585048934	.6523271267	.1419336178	
GMAT(ROU 2)	.6692142842E-01	-.6804147674E-01	-.2395987392E-01	
GMAT(ROU 3)	.2115638959	.8840816074	4.214517195	
GMAT(ROU 4)	.5394908806E-01	.9566196556E-01	.5774663642	

## NAVION

## CASE -T-.1

AMAT(ROW 1)=	-.7770000000	4.680000000	-.4320000000	0.
AMAT(ROW 2)=	-1.000000000	-.3556000000	0.	.1720000000
AMAT(ROW 3)=	1.270000000	-12.80000000	-6.600000000	0.
AMAT(ROW 4)=	0.	0.	1.000000000	0.
BMAT(ROW 1)=	-.6100000000	2.410000000	-.3140000000	
BMAT(ROW 2)=	.7250000000E-01	.2370000000	0.	
BMAT(ROW 3)=	.7700000000	0.	21.00000000	
BMAT(ROW 4)=	0.	0.	0.	
FMAT(ROW 1)=	.9005375284	.4598270385	-.2987563193E-01	.3990407457E-02
FMAT(ROW 2)=	-.9363477977E-01	.9418349233	.2364184296E-02	.1676410940E-01
FMAT(ROW 3)=	.1378664855	-.8863597096	.5142138486	-.8645289826E-02
FMAT(ROW 4)=	.6760554231E-02	-.5026331294E-01	.7311505762E-01	.9996937882
GMAT(ROW 1)=	-.5814275833	.2353585281	-.6556590545E-01	
GMAT(ROW 2)=	.3637102593E-01	.1154709769E-01	.3265167507E-02	
GMAT(ROW 3)=	.1141512336E-01	.4380530530E-02	1.533293396	
GMAT(ROW 4)=	.1636999808E-02	.1147306212E-03	.8514173945E-01	

## YF-16 CCV Canard Bare A/F

## CASE III -- T=.1

AMAT(ROW 1)=	-.4310000000	10.20000000	-.4160000000E-01	0.
AMAT(ROW 2)=	-1.000000000	-.3060000000	0.	.3880000000E-01
AMAT(ROW 3)=	1.670000000	-.50.00000000	-2.330000000	0.
AMAT(ROW 4)=	0.	0.	1.000000000	0.
BMAT(ROW 1)=	-.4.170000000	4.620000000	2.170000000	
BMAT(ROW 2)=	.3180000000E-01	.1910000000E-01	-.3570000000E-01	
BMAT(ROW 3)=	7.630000000	5.930000000	49.10000000	
BMAT(ROW 4)=	0.	0.	0.	
FMAT(ROW 1)=	.9085611123	.9755276552	-.3502672856E-02	.1926755760E-02
FMAT(ROW 2)=	-.9471662993E-01	.9204149530	.3626869048E-03	.3756696670E-02
FMAT(ROW 3)=	.3670070570	-.4.234745790	.7912792594	-.8716315341E-02
FMAT(ROW 4)=	.1524291762E-01	-.2246473026	.8917931248E-01	.9997011628
GMAT(ROW 1)=	-.4010594654	.4443513628	.1978434172	
GMAT(ROW 2)=	.2334360234E-01	-.2042352531E-01	-.1334271711E-01	
GMAT(ROW 3)=	.6097314035	.5949648390	4.419801283	
GMAT(ROW 4)=	.3320928555E-01	.2942249255E-01	.2287260839	

## YF-16 CCY Canard FCS Loops Closed

## CASE -T=.1

AMAT(ROW 1)=	-3.105000000	8.917000000	-.2720000000	0.
AMAT(ROW 2)=	-.9796000000	-.2965000000	0.	.3795000000E-01
AMAT(ROW 3)=	6.564000000	-.47.71000000	-8.359000000	-25.0000000
AMAT(ROW 4)=	0.	0.	1.000000000	0.
BMAT(ROW 1)=	-3.925000000	4.760000000	1.897000000	
BMAT(ROW 2)=	.2988000000E-01	.1802000000E-01	-.3360000000E-01	
BMAT(ROW 3)=	7.178000000	5.655000000	49.60000000	
BMAT(ROW 4)=	0.	0.	0.	
FMAT(ROW 1)=	.6913530975	.7847112229	-.1445263004E-01	.2438014138E-01
FMAT(ROW 2)=	-.8143829476E-01	.9306333501	.1026091597E-02	.2738524359E-02
FMAT(ROW 3)=	.5050937166	-.2.793147507	.3561891237	-1.626384125
FMAT(ROW 4)=	.2782330729E-01	-.1696021813	.6479790890E-01	.9054019678
GMAT(ROW 1)=	-.3369331513	.3982455362	.1136179162	
GMAT(ROW 2)=	.2023112757E-01	-.1874449879E-01	-.9625423529E-02	
GMAT(ROW 3)=	.3508569708	.4959675280	3.272450037	
GMAT(ROW 4)=	.2310227340E-01	.2585590160E-01	.1892645608	

## NAVION

CASE I T=1/15

AMAT(ROW 1)	- .7770000000	4.680000000	- .4320000000	0.
AMAT(ROW 2)	- 1.000000000	- .3956000000	0.	.1720000000
AMAT(ROW 3)	1.270000000	-12.800000000	-6.600000000	0.
AMAT(ROW 4)	0.	0.	1.000000000	0.
BMAT(ROW 1)	-6.100000000	2.410000000	- .3140000000	
BMAT(ROW 2)	.7250000000E-01	.2370000000	0.	
BMAT(ROW 3)	.7700000000	0.	21.00000000	
BMAT(ROW 4)	0.	0.	0.	
FMAT(ROW 1)	.9383143219	.3096458333	- .2253006438E-01	.1782414534E-02
FMAT(ROW 2)	- .6393779430E-01	.9661950935	.1138803461E-02	.1129209760E-01
FMAT(ROW 3)	.9034754103E-01	- .6675638125	.6428389070	- .4159728345E-02
FMAT(ROW 4)	.2958693533E-02	- .2418446712E-01	.5390706991E-01	.9999037240
GMAT(ROW 1)	- .3946575033	.1984265226	- .3746658817E-01	
GMAT(ROW 2)	.1797272883E-01	.1034727325E-01	.1232907956E-02	
GMAT(ROW 3)	.2170703941E-01	.1398732707E-02	1.131119438	
GMAT(ROW 4)	.1047484156E-02	.2422028064E-04	.4048356976E-01	

YF-16 CCV Canard Bare A/F

CASE III -- T=1/15

AMAT(ROW 1)	- .4310000000	10.20000000	- .4160000000E-01	0.
AMAT(ROW 2)	- 1.000000000	- .3060000000	0.	.3880000000E-01
AMAT(ROW 3)	1.670000000	-50.00000000	-2.330000000	0.
AMAT(ROW 4)	0.	0.	1.000000000	0.
BMAT(ROW 1)	-4.170000000	4.620000000	2.170000000	
BMAT(ROW 2)	.3180000000E-01	.1910000000E-01	- .3570000000E-01	
BMAT(ROW 3)	7.630000000	5.930000000	49.10000000	
BMAT(ROW 4)	0.	0.	0.	
FMAT(ROW 1)	.9494344256	.6627364428	- .2492658100E-02	.8656843351E-03
FMAT(ROW 2)	- .6454926763E-01	.9575563303	.1671091565E-03	.2541175261E-02
FMAT(ROW 3)	.2042464420	- .2995950275	.8558111402	- .4021544870E-02
FMAT(ROW 4)	.5820256384E-02	- .1036480637	.6174066395E-01	.9999090099
GMAT(ROW 1)	- .2719177536	.3012317087	.1364919874	
GMAT(ROW 2)	.1119295553E-01	- .8788073625E-02	- .6878441879E-02	
GMAT(ROW 3)	.4435147884	.3910320437	3.047796792	
GMAT(ROW 4)	.1554396657E-01	.1302126060E-01	.1040095882	

CASE II -- T=1/15

YF-16 CCV Canard FCS Loops Closed

AMAT(ROW 1)	- 3.105000000	8.917000000	- .2720000000	0.
AMAT(ROW 2)	- .9796000000	- .2965000000	0.	.3795000000E-01
AMAT(ROW 3)	6.564000000	-47.71000000	-8.359000000	-25.00000000
AMAT(ROW 4)	0.	0.	1.000000000	0.
BMAT(ROW 1)	- 3.925000000	4.766000000	1.897000000	
BMAT(ROW 2)	.2988000000E-01	.1802000000E-01	- .3360000000E-01	
BMAT(ROW 3)	7.178000000	5.655000000	49.60000000	
BMAT(ROW 4)	0.	0.	0.	
FMAT(ROW 1)	.7929440685	.5494393477	- 1.207281251E-01	.1234319886E-01
FMAT(ROW 2)	- .5792803295E-01	.9620117449	.5219054695E-03	.2179316420E-02
FMAT(ROW 3)	.3710752075	- 2.248227289	.5314737971	- 1.255750750
FMAT(ROW 4)	.1312179935E-01	- .8467970511E-01	.5010148620E-01	.9538412096
GMAT(ROW 1)	- .2373145125	.2825025632	.8965247920E-01	
GMAT(ROW 2)	.9948800860E-02	- .8340187072E-02	- .5406877956E-02	
GMAT(ROW 3)	.3055951759	.3443364719	2.512771007	
GMAT(ROW 4)	.1199475075E-01	.1181732408E-01	.9206478638E-01	

## NAVION

CASE I -- T=.04

AMAT(ROW 1)=	-.7770000000	4.680000000	-.4320000000	0.
AMAT(ROW 2)=	-1.000000000	-.3556000000	0.	.1720000000
AMAT(ROW 3)=	1.270000000	-12.80000000	-6.600000000	0.
AMAT(ROW 4)=	0.	0.	1.000000000	0.
BMAT(ROW 1)=	-6.100000000	2.410000000	-.3140000000	
BMAT(ROW 2)=	.7250000000E-01	.2370000000	0.	
BMAT(ROW 3)=	.7700000000	0.	21.00000000	
BMAT(ROW 4)=	0.	0.	0.	
FMAT(ROW 1)=	.9653025756	.1867461509	-.1491312120E-01	.6432824454E-03
FMAT(ROW 2)=	-.3904748090E-01	.9821326052	.4375688368E-03	.6822711531E-02
FMAT(ROW 3)=	.5311019486E-01	-.4417088909	.7675373788	-.1596940856E-02
FMAT(ROW 4)=	.1048205181E-02	-.9284539859E-02	.3514969324E-01	.9999781788
GMAT(ROW 1)=	-.2398825142	.9567140852E-01	-.1893215507E-01	
GMAT(ROW 2)=	.7683918776E-02	.7503300938E-02	.3728614911E-03	
GMAT(ROW 3)=	.1999808306E-01	.3257385388E-03	.7378144217	
GMAT(ROW 4)=	.4712947284E-03	.3376613923E-05	.1540865728E-01	

YF-16 CCV Canard Bare A/F

CASE III -- T=.04

AMAT(ROW 1)=	-.4310000000	10.20000000	-.4160000000E-01	0.
AMAT(ROW 2)=	-1.000000000	-.3000000000	0.	.3880000000E-01
AMAT(ROW 3)=	1.670000000	-50.00000000	-2.330000000	0.
AMAT(ROW 4)=	0.	0.	1.000000000	0.
BMAT(ROW 1)=	-4.170000000	4.620000000	2.170000000	
BMAT(ROW 2)=	.3180000000E-01	.1910000000E-01	-.3570000000E-01	
BMAT(ROW 3)=	7.630000000	5.930000000	49.10000000	
BMAT(ROW 4)=	0.	0.	0.	
FMAT(ROW 1)=	.9748103413	.4025218296	-.1566478786E-02	.3139188721E-03
FMAT(ROW 2)=	-.3930584452E-01	.9797568870	.6184057166E-04	.1538349980E-02
FMAT(ROW 3)=	.1013990812	-.1.879432731	.9109187967	-.1489813099E-02
FMAT(ROW 4)=	.1803056655E-02	-.3839724481E-01	.3819146932E-01	.9999799274
GMAT(ROW 1)=	-.1649053236	.1826802021	.8396093475E-01	
GMAT(ROW 2)=	.4566014355E-02	-.2892618326E-02	-.3091213386E-02	
GMAT(ROW 3)=	.2826611323	.2340721474	1.880484558	
GMAT(ROW 4)=	.5808274716E-02	.4694081842E-02	.3815443411E-01	

YF-16 CCV Canard FCS Loops Closed

AMAT(ROW 1)=	-.3.105000000	8.917000000	-.2720000000	0.
AMAT(ROW 2)=	-.9795000000	-.2965000000	0.	.3795000000E-01
AMAT(ROW 3)=	5.564000000	-.47.71000000	-.8.359000000	-.25.0000000
AMAT(ROW 4)=	0.	0.	1.000000000	0.
BMAT(ROW 1)=	-.3.925000000	4.765000000	1.897000000	
BMAT(ROW 2)=	.2988000000E-01	.1802000000E-01	-.3360000000E-01	
BMAT(ROW 3)=	7.178000000	5.655000000	49.60000000	
BMAT(ROW 4)=	0.	0.	0.	
FMAT(ROW 1)=	.8755142184	.3413154467	-.8577719870E-02	.4920022584E-02
FMAT(ROW 2)=	-.3652123063E-01	.9814276240	.2087635817E-03	.1433196768E-02
FMAT(ROW 3)=	.2389593799	-.1.556608858	.6985810643	-.8451940165
FMAT(ROW 4)=	.4938820713E-02	-.3339426577E-01	.3375706817E-01	.9820997563
GMAT(ROW 1)=	-.1483598848	.1778481148	.6168577304E-01	
GMAT(ROW 2)=	.4142719572E-02	-.2834450828E-02	-.2608657566E-02	
GMAT(ROW 3)=	.2219255433	.2138328753	1.684841571	
GMAT(ROW 4)=	.4858124306E-02	.4355657517E-02	.3562179926E-01	

## NAYION

## CASE I -- T=.05

AMAT(ROW 1)	- .7770000000	4.680000000	-.4320000000	0.
AMAT(ROW 2)	- 1.000000000	-.3556000000	0.	.1720000000
AMAT(ROW 3)	1.270000000	-12.80000000	-6.600000000	0.
AMAT(ROW 4)	0.	0.	1.000000000	0.
BMAT(ROW 1)	-6.100000000	2.410000000	-.3140000000	
BMAT(ROW 2)	.7250000000E-01	.2370000000	0.	
BMAT(ROW 3)	.7700000000	0.	21.00000000	
BMAT(ROW 4)	0.	0.	0.	
FMAT(ROW 1)	.9555316015	.2330558656	-.1796767751E-01	.1004345292E-02
FMAT(ROW 2)	-.4849401955E-01	.9765307325	.6671421219E-03	.8507226727E-02
FMAT(ROW 3)	.6695093648E-01	-.5322224088	.7182447813	-.2435565041E-02
FMAT(ROW 4)	.1648367882E-02	-.1416026187E-01	.4257594997E-01	.9999581460
GMAT(ROW 1)	-.2984446796	.1193158269	-.2540478969E-01	
GMAT(ROW 2)	.1106887586E-01	.8769265325E-02	.6255871934E-03	
GMAT(ROW 3)	.2170181841E-01	.6165845330E-03	.8935773618	
GMAT(ROW 4)	.6808687877E-03	.7988999976E-05	.2357427800E-01	

## YF-16 CCV Canard Bare A/F

## CASE III -- T=.05

AMAT(ROW 1)	- .4310000000	10.20000000	-.4160000000E-01	0.
AMAT(ROW 2)	- 1.000000000	-.3060000000	0.	.3880000000E-01
AMAT(ROW 3)	1.676000000	-50.00000000	-2.330000000	0.
AMAT(ROW 4)	0.	0.	1.000000000	0.
BMAT(ROW 1)	-4.170000000	4.620000000	2.170000000	
BMAT(ROW 2)	.3180000000E-01	.1910000000E-01	-.3570000000E-01	
BMAT(ROW 3)	7.630000000	5.930000000	49.10000000	
BMAT(ROW 4)	0.	0.	0.	
FMAT(ROW 1)	.9660797195	.5010062428	-.1925524494E-02	.4892360520E-03
FMAT(ROW 2)	-.4887522366E-01	.9722327856	.9564466181E-04	.1917067339E-02
FMAT(ROW 3)	.1368891187	-2.311075252	.8898722311	-.2303271656E-02
FMAT(ROW 4)	.2991324989E-02	-.5936267154E-01	.4719503489E-01	.9999611015
GMAT(ROW 1)	-.2053658134	.2275011297	.1040021563	
GMAT(ROW 2)	.6721352123E-02	-.4738986258E-02	-.4358271650E-02	
GMAT(ROW 3)	.3457365581	.2925526513	2.325886636	
GMAT(ROW 4)	.8952949095E-02	.7326948138E-02	.5919413131E-01	

## YF-16 CCV Canard FCS Loops Closed

## CASE II -- T=.05

AMAT(ROW 1)	-3.105000000	8.917000000	-.2720000000	0.
AMAT(ROW 2)	-.9796000000	-.2965000000	0.	.3795000000E-01
AMAT(ROW 3)	6.564000000	-.47.71000000	-8.359000000	-25.00000000
AMAT(ROW 4)	0.	0.	1.000000000	0.
BMAT(ROW 1)	-3.925000000	4.766000000	1.897000000	
BMAT(ROW 2)	.2988000000E-01	.1802000000E-01	-.3360000000E-01	
BMAT(ROW 3)	7.178000000	5.655000000	49.50000000	
BMAT(ROW 4)	0.	0.	0.	
FMAT(ROW 1)	.8444610734	.4213275315	-.1007440058E-01	.7401204421E-02
FMAT(ROW 2)	-.4482256768E-01	.9747742525	.3136369660E-03	.1739461895E-02
FMAT(ROW 3)	.2910955121	-.1845387524	.6329338519	-1.012203501
FMAT(ROW 4)	.7591677878E-02	-.5043493463E-01	.4041157983E-01	.9727991840
GMAT(ROW 1)	-.1826709617	.2183750549	.7323600726E-01	
GMAT(ROW 2)	.6051094183E-02	-.4583226766E-02	-.3580530460E-02	
GMAT(ROW 3)	.2587699885	.2638005832	2.020510386	
GMAT(ROW 4)	.7267305823E-02	.6744890998E-02	.5417478726E-01	

## NAVION

## CASE I -- T=.02

AMAT(ROW 1)	- .7770000000	4.680000000	- .4320000000	0.
AMAT(ROW 2)	- 1.000000000	-.3556000000	0.	.1720000000
AMAT(ROW 3)	1.270000000	-12.80000000	-6.600000000	0.
AMAT(ROW 4)	0.	0.	1.000000000	0.
BMAT(ROW 1)	- 6.100000000	2.410000000	-.3140000000	
BMAT(ROW 2)	.7250000000E-01	.2370000000	0.	
BMAT(ROW 3)	.7700000000	0.	21.00000000	
BMAT(ROW 4)	0.	0.	0.	
FMAT(ROW 1)	.9835451199	.9356434665E-01	-.8026174145E-02	.1609741472E-03
FMAT(ROW 2)	-.1976761620E-01	.9919767251	.1149278250E-03	.3426722506E-02
FMAT(ROW 3)	.2603042592E-01	-.2377387318	.8762314076	-.4191740962E-03
FMAT(ROW 4)	.2582943506E-03	-.2437058699E-02	.1873548183E-01	.9999971709
GMAT(ROW 1)	-.1210102458	.4803255323E-01	-.7956939811E-02	
GMAT(ROW 2)	.2655609736E-02	.4243415067E-02	.7860836784E-04	
GMAT(ROW 3)	.1267403872E-01	.4490647334E-04	.3933640141	
GMAT(ROW 4)	.1357845151E-03	.2350923155E-06	.4020525562E-02	

## YF-16 CCV Canard Bare A/F

## CASE III -- T=.02

AMAT(ROW 1)	- .4310000000	10.20000000	-.4160000000E-01	0.
AMAT(ROW 2)	- 1.000000000	-.3060000000	0.	.3880000000E-01
AMAT(ROW 3)	1.670000000	-.50.00000000	-2.330000000	0.
AMAT(ROW 4)	0.	0.	1.000000000	0.
BMAT(ROW 1)	- 4.170000000	4.620000000	2.170000000	
BMAT(ROW 2)	.3180000000E-01	.1910000000E-01	-.3570000000E-01	
BMAT(ROW 3)	7.630000000	5.930000000	49.10000000	
BMAT(ROW 4)	0.	0.	0.	
FMAT(ROW 1)	.9893772443	.2027706864	-.8083110994E-03	.7884315984E-04
FMAT(ROW 2)	-.1983944718E-01	.9918682480	.1577175559E-04	.7731044228E-03
FMAT(ROW 3)	.4226453740E-01	-.3700397241	.9544504647	-.3802625596E-03
FMAT(ROW 4)	.3934530725E-03	-.9800581432E-02	.1954103847E-01	.9999974520
GMAT(ROW 1)	-.8298243611E-01	.9193036413E-01	.4271056099E-01	
GMAT(ROW 2)	.1464060722E-02	-.5379547149E-03	-.1137872572E-02	
GMAT(ROW 3)	.1471457657	.1175089202	.9606686627	
GMAT(ROW 4)	.1489947893E-02	.1178197980E-02	.9677019529E-02	

## YF-16 CCV Canard FCS Loops Closed

## CASE II -- T=.02

AMAT(ROW 1)	- 3.105000000	8.917000000	-.2720000000	0.
AMAT(ROW 2)	-.9796000000	-.2965000000	0.	.3795000000E-01
AMAT(ROW 3)	6.564000000	-.47.71000000	-8.359000000	-25.00000000
AMAT(ROW 4)	0.	0.	1.000000000	0.
BMAT(ROW 1)	- 3.925000000	4.766000000	1.897000000	
BMAT(ROW 2)	.2988000000E-01	.1802000000E-01	-.3360000000E-01	
BMAT(ROW 3)	7.178000000	5.655000000	49.60000000	
BMAT(ROW 4)	0.	0.	0.	
FMAT(ROW 1)	.9377770289	.1746757479	-.4840832552E-02	.1325894921E-02
FMAT(ROW 2)	-.1892568168E-01	.9923652712	.5640188019E-04	.7467331653E-03
FMAT(ROW 3)	.1254679558	-.8631235396	.8412450672	-.4599560387
FMAT(ROW 4)	.1274224413E-02	-.8929501842E-02	.1838468656E-01	.9952692512
GMAT(ROW 1)	-.7636796768E-01	.9210287677E-01	.3420301581E-01	
GMAT(ROW 2)	.1349787841E-02	-.5512878322E-03	-.1013843279E-02	
GMAT(ROW 3)	.1266971358	.1098774464	.9145976885	
GMAT(ROW 4)	.1322227582E-02	.1109280185E-02	.9399519380E-02	

## NAVION

## CASE I -- T=.0125

AMAT(ROW 1)	-.7770000000	4.680000000	-.4320000000	0.
AMAT(ROW 2)	-1.000000000	-.3556000000	0.	.1720000000
AMAT(ROW 3)	1.270000000	-12.80000000	-6.600000000	0.
AMAT(ROW 4)	0.	0.	1.000000000	0.
BMAT(ROW 1)	-.6100000000	2.410000000	-.3140000000	
BMAT(ROW 2)	.7250000000E-01	.2370000000	0.	
BMAT(ROW 3)	.7700000000	0.	21.00000000	
BMAT(ROW 4)	0.	0.	0.	
FMAT(ROW 1)	.9899286253	.5849783390E-01	-.5156843442E-02	.6288951048E-04
FMAT(ROW 2)	-.1241007876E-01	.9951990693	.4573793149E-04	.2144966566E-02
FMAT(ROW 3)	.1612929741E-01	-.1527613544	.9207685898	-.1667802128E-03
FMAT(ROW 4)	.1002925153E-03	.9696524003E-03	.1199808842E-01	.9999992997
GMAT(ROW 1)	-.7586926797E-01	.3006175147E-01	-.4592816955E-02	
GMAT(ROW 2)	.1378562340E-02	.2768182511E-02	.2844749554E-04	
GMAT(ROW 3)	.8556443942E-02	.1189734304E-04	.2519283650	
GMAT(ROW 4)	.5569746412E-04	.3953238250E-07	.1596280616E-02	

## CASE III -- T=.0125

## YF-16 CCV Canard Bare A/F

AMAT(ROW 1)	-.4310000000	10.20000000	-.4160000000E-01	0.
AMAT(ROW 2)	-1.000000000	-.3060000000	0.	.3880000000E-01
AMAT(ROW 3)	1.670000000	-50.00000000	-2.330000000	0.
AMAT(ROW 4)	0.	0.	1.000000000	0.
BMAT(ROW 1)	-.4.170000000	4.620000000	2.170000000	
BMAT(ROW 2)	.3180000000E-01	.1910000000E-01	-.3570000000E-01	
BMAT(ROW 3)	7.630000000	5.930000000	49.10000000	
BMAT(ROW 4)	0.	0.	0.	
FMAT(ROW 1)	.9938280622	.1270405060	-.5108504318E-03	.3084586472E-04
FMAT(ROW 2)	-.1243920345E-01	.9953876977	.6206153958E-05	.4839450630E-03
FMAT(ROW 3)	.2436901531E-01	-.6133245727	.9712884452	-.1496768819E-03
FMAT(ROW 4)	.1450813907E-03	-.3857651595E-02	.1231969689E-01	.9999993744
GMAT(ROW 1)	-.5197017096E-01	.5757545600E-01	.2685873820E-01	
GMAT(ROW 2)	.7215721478E-03	-.1213981239E-03	-.6129946312E-03	
GMAT(ROW 3)	.9327162452E-01	.7365239741E-01	.6053496619	
GMAT(ROW 4)	.5873774656E-03	.4612306361E-03	.3800817208E-02	

## CASE II -- T=.0125

## YF-16 CCV Canard FCS Loops Closed

AMAT(ROW 1)	-.3.105000000	8.917000000	-.2720000000	0.
AMAT(ROW 2)	-.979600000	-.296500000	0.	.3795000000E-01
AMAT(ROW 3)	6.564000000	-47.71000000	-8.359000000	-25.00000000
AMAT(ROW 4)	0.	0.	1.000000000	0.
BMAT(ROW 1)	-.3.925000000	4.766000000	1.897000000	
BMAT(ROW 2)	.2988000000E-01	.1802000000E-01	-.3360000000E-01	
BMAT(ROW 3)	7.178000000	5.655000000	49.60000000	
BMAT(ROW 4)	0.	0.	0.	
FMAT(ROW 1)	.9611317743	.1100587149	-.3162405534E-02	.5325623816E-03
FMAT(ROW 2)	-.1198467995E-01	.9956241283	.2267550034E-04	.4709993003E-03
FMAT(ROW 3)	.7979469095E-01	-.5603306928	.8988316140	-.2966565147
FMAT(ROW 4)	.5034431973E-03	-.3576340101E-02	.1186083171E-01	.9981132427
GMAT(ROW 1)	-.4823415613E-01	.5831561560E-01	.2222406262E-01	
GMAT(ROW 2)	.6695383975E-03	-.1342553646E-03	-.5575070930E-03	
GMAT(ROW 3)	.8305417439E-01	.6940796792E-01	.5893724494	
GMAT(ROW 4)	.5328398624E-03	.4364282181E-03	.3746696550E-02	

## NAVION

CASE I -- T=.01

AMAT(ROW 1)=	-.7770000000	4.680000000	-.4320000000	0.
AMAT(ROW 2)=	-1.000000000	-.3556000000	0.	.1720000000
AMAT(ROW 3)=	1.270000000	-12.80000000	-6.60000000	0.
AMAT(ROW 4)=	0.	0.	1.000000000	0.
BMAT(ROW 1)=	-6.1880000000	2.4100000000	-.3140000000	0.
BMAT(ROW 2)=	.7250000000E-01	.2370000000	0.	
BMAT(ROW 3)=	.7700000000	0.	21.00000000	
BMAT(ROW 4)=	0.	0.	0.	
FMAT(ROW 1)=	.9920000036	.4680115171E-01	-.4153647039E-02	.4025012640E-04
FMAT(ROW 2)=	-.9942633432E-02	.9962162200	.2945506434E-04	.1716811258E-02
FMAT(ROW 3)=	.1286448839E-01	-.1233444327	.9361034362	-.1073975789E-03
FMAT(ROW 4)=	.6405413975E-04	-.6244045283E-03	.9677050337E-02	.9999996398
GMAT(ROW 1)=	-.5675759491E-01	.2405998227E-01	-.3570163506E-02	
GMAT(ROW 2)=	.1927569263E-02	.2245565580E-02	.1771492273E-04	
GMAT(ROW 3)=	.7015329178E-02	.6386603604E-05	.2031979441	
GMAT(ROW 4)=	.3621511445E-04	.1714434361E-07	.1027204472E-02	

YF-16 CCV Canard Bare A/F

CASE III -- T=.01

AMAT(ROW 1)=	-.4310000000	10.20000000	-.4160000000E-01	0.
AMAT(ROW 2)=	-1.000000000	-.3060000000	0.	.3880000000E-01
AMAT(ROW 3)=	1.670000000	-.50.00000000	-2.330000000	0.
AMAT(ROW 4)=	0.	0.	1.000000000	0.
BMAT(ROW 1)=	-4.170000000	4.620000000	2.170000000	
BMAT(ROW 2)=	.3180000000E-01	.1910000000E-01	-.3570000000E-01	
BMAT(ROW 3)=	7.630000000	5.930000000	49.10000000	
BMAT(ROW 4)=	0.	0.	0.	
FMAT(ROW 1)=	.9951875200	.1017103534	-.4101666451E-03	.1975111292E-04
FMAT(ROW 2)=	-.9961500945E-02	.9964358261	.3981578242E-05	.3873411156E-03
FMAT(ROW 3)=	.1894283792E-01	-.4925337505	.9769652730	-.9603515182E-04
FMAT(ROW 4)=	.9099833036E-04	-.2475132779E-02	.9884386482E-02	.9999996791
GMAT(ROW 1)=	-.4160268085E-01	.4609019745E-01	.2153024875E-01	
GMAT(ROW 2)=	.5255320796E-03	-.3965890725E-04	-.4639650323E-03	
GMAT(ROW 3)=	.7495969660E-01	.5898754909E-01	.4856992049	
GMAT(ROW 4)=	.3770519690E-03	.2954250251E-03	.2436981830E-02	

YF-16 CCV Canard FCS Loops Closed

CASE II -- T=.01

AMAT(ROW 1)=	-.3.105000000	8.917000000	-.2720000000	0.
AMAT(ROW 2)=	-.9796000000	-.2965000000	0.	.3795000000E-01
AMAT(ROW 3)=	6.564000000	-.47.71000000	-8.359000000	-25.00000000
AMAT(ROW 4)=	0.	0.	1.000000000	0.
BMAT(ROW 1)=	-3.925000000	4.766000000	1.897000000	
BMAT(ROW 2)=	.2988000000E-01	.1802000000E-01	-.3360000000E-01	
BMAT(ROW 3)=	7.178000000	5.655000000	49.60000000	
BMAT(ROW 4)=	0.	0.	0.	
FMAT(ROW 1)=	.9689126343	.8827758866E-01	-.2567176464E-02	.3440086304E-03
FMAT(ROW 2)=	-.9629390870E-02	.9966056658	.1465171999E-04	.3776502744E-03
FMAT(ROW 3)=	.6419997708E-01	-.4539311793	.9185902417	-.2398168580
FMAT(ROW 4)=	.3234115495E-03	-.2307934166E-02	.9589170877E-02	.9987840890
GMAT(ROW 1)=	-.3872084600E-01	.4685342750E-01	.1801119674E-01	
GMAT(ROW 2)=	.4887348029E-03	-.5060593333E-04	-.4248695386E-03	
GMAT(ROW 3)=	.6749271715E-01	.5572655178E-01	.4763139338	
GMAT(ROW 4)=	.3445490309E-03	.2799897326E-03	.2414096702E-02	

## APPENDIX B

### VRA HARDWARE AND SOFTWARE SYSTEMS

#### VRA SYSTEMS OVERVIEW

The Princeton Flight Research Laboratory's Variable Response Research Aircraft (VRA) (Figure 24) consists of a modified NAVION aircraft with independent control of lift, sideforce, thrust, pitch, roll and yaw. Mediating between the evaluation pilot and actual aircraft control are a specially constructed analog computer system and a digital microprocessor (Micro-DFCS), which, in the present research application, accepts 8 channels of analog sensor and command data and supplies three channels of output control which, in turn, drive control surfaces actuators.

Independent control of three forces and three moments is provided by commands to the elevator, ailerons, rudder, throttle, direct-lift flaps and side-force panels. The control surfaces are driven by hydraulic servos capable of high surface accelerations (some were originally fitted to the B-58 aircraft). The modified VRA units incorporate solenoid actuated valves with force-override features for quick disengagement. Characteristics of the control surface effectors are summarized in Table 6. Surface rate limits are seen to range from 60 to 110 deg/sec. Bandwidths are given for flat response and 6 db attenuation (in parentheses), except that the thrust bandwidth is specified by the frequency for 3 dB attenuation. The aircraft's normal operating speed range is 65 to 120 kt; maximum specific forces and moments ("control power") are given for 70 kt airspeed. At IAS = 105 kt maximum direct lift and side-force accelerations are 1 g and 0.5 g, respectively.

#### SENSORS AND COMMAND SIGNALS

The sensors used for most flight testing include angular rate gyros and linear accelerometers for all three axes, vertical and heading

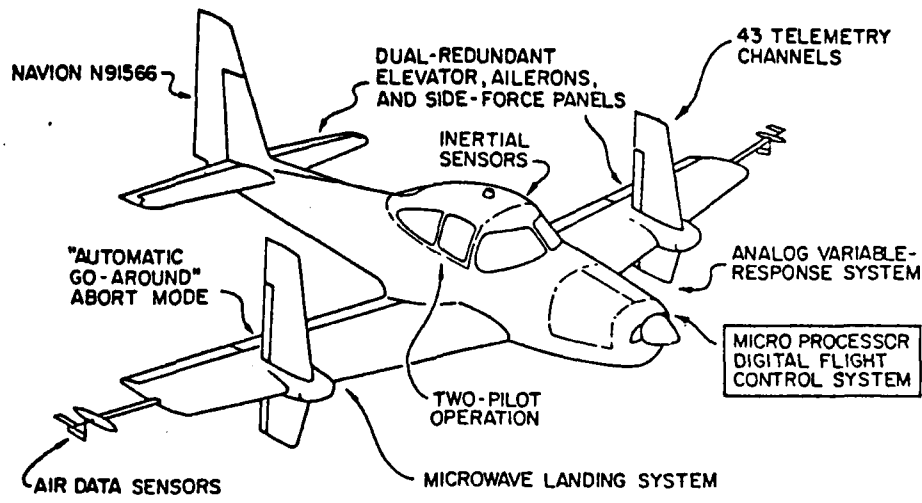


Figure 24. Variable Response Research Aircraft (VRA)

TABLE 6. VRA CONTROL CHARACTERISTICS

CONTROL	DISPLACEMENT LIMIT (deg)	RATE LIMIT (deg/sec)	BANDWIDTH (Hz)	MAXIMUM SPECIFIC FORCE OR MOMENT (IAS = 70 kt)
Roll	±30	70	5 (10)	4.1 rad/sec <sup>2</sup>
Pitch	+15 -30	70	5 (10)	4.4 rad/sec <sup>2</sup>
Yaw	±15	70	5 (10)	1.9 rad/sec <sup>2</sup>
Thrust	---	---	0.6	0.1 g
Side Force	±35	60	2 (3)	0.25 g
Normal Force	±30	110	2 (3)	0.5 g

gyros, dual angle-of-attack and sideslip angle vanes, radar altimeter, indicated airspeed, control surface positions and cockpit control positions.

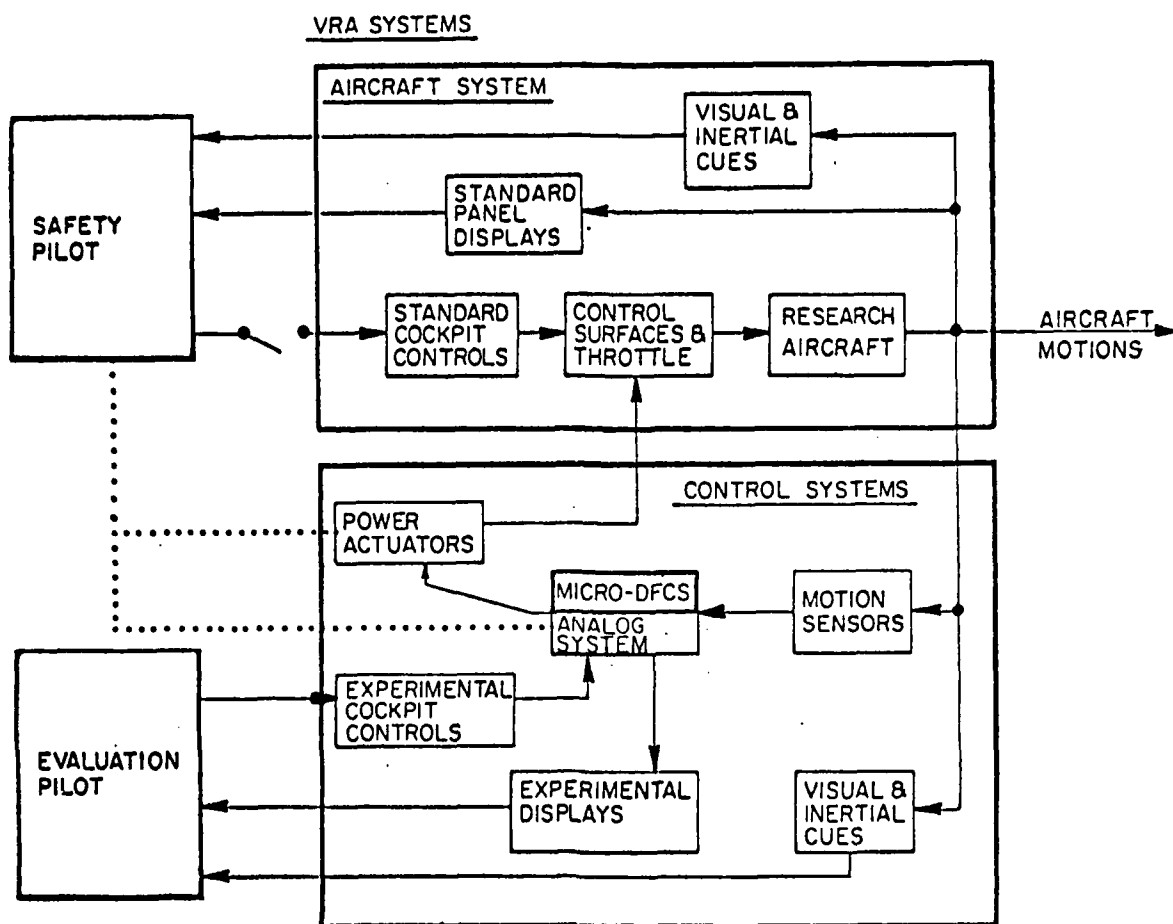
In conventional application of the VRA (Figure 25a), aircraft sensor signals and command signals from the evaluation pilot's controls are fed into the VRA analog system which can be set with the necessary gains and crossfeeds to emulate performance characteristics of a variety of other aircraft. The Micro-DFCS was originally conceived as a research tool for the evaluation of digital systems in flight control. As presently implemented in the VRA, the Micro-DFCS operates in parallel with the analog system. Although capable of exerting full 6-axis control, the digital system is usually enabled in only 3 axes, with the analog system supplying the remaining vectors.

For the present research application, the VRA's analog simulation and the Micro-DFCS serve complementary roles. The analog system is set to emulate the lateral directional characteristics of the bare-airframe YF-16; however, the gains mediating pilot commands through it are reduced to zero. Thus, all of the command augmentation for the present problem is supplied by the digital system, while the analog system, responding only to feedback, maintains the bare-airframe YF-16 configuration. This relationship is summarized graphically in Figure 25b.

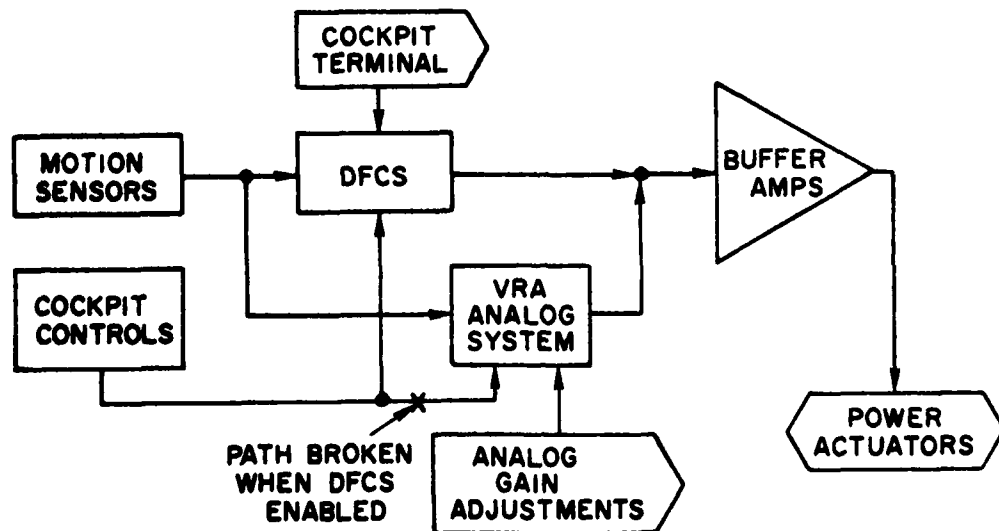
#### **MICROPROCESSOR DIGITAL FLIGHT CONTROL SYSTEM**

The Micro-DFCS has undergone substantial evolution since the beginning of the contract period, due largely to FRL's recognition of deficiencies in the original system in terms of throughput delay and program memory. They have also expanded program development capability and facilities. Concomitantly, STI has become increasingly sophisticated in the use of the software development resources available.

Initially, the Micro-DFCS was configured with Intel SBC family boards. The processor board (iSBC 80-05) contained an 8085 microprocessor running from a 2 mHz system clock. In order to perform floating point operations, an Intel iSBC-310 "high speed math unit" (a separate



a) VRA System Modules



b) DFCS Module Interconnections

Figure 25. VRA Analog and Digital Systems — Data Path Diagrams

multibus board) was also installed. In addition, several boards of RAM (memory) were also required. Control software, a 6K byte assembly language program (CAS-1) was written to operate in this environment.

In September 1980, the Intel 80-05 board was replaced with a Monolithic Systems 80-04 processor board containing a Z-80 microprocessor with 32K bytes of onboard RAM, a 4 mHz clock and a single-chip floating point math unit (AMD 9511), with capabilities considerably beyond the iSBC-310 math unit. By this time, the CAS-1 control program had evolved to CAS-4 which, like its predecessors, still accessed the iSBC-310 math board for floating point calculations. An upgraded version called CAS-6 was written for the new Z-80 based system; however, the enormous inconvenience of adapting the assembly code to accommodate the different coding convention required by the AMD-9511 math chip dictated that CAS-6 also use the ponderously slow iSBC-310 math board.

#### **SOFTWARE DEVELOPMENT SYSTEM**

STI's initial adaptations of FRL's software to the YF-16 problem centered around the CAS-6 program. However, when certain subtle discrepancies in the responses of the YF-16 zero-order-hold problem were observed, an extensive static check of the longitudinal modes of CAS-6 was performed by J. Smith and T. Myers of STI. In the course of this check, it was discovered that a serious "scramble" existed in the gain selection algorithm of CAS-6 and that, apparently, the program had not been thoroughly static-checked by its original author. This discovery hastened FRL's decision to abandon the assembly language code and pursue the installation of higher level language software which would support the onboard floating point capability of the MSC 8004 hardware.

Up to this point, program development for the CAS series of assembly language programs had been accomplished using a FORTRAN cross assembler resident on Princeton's IBM 3033 timesharing system. Assembly code would be written using the 3033 system editor facilities and the resulting source code assigned as an input file to one of several disk resident cross assemblers. The cross assembler, in turn, created an output file in standard Intel hex format which was then loaded on to the 80-04

microprocessor over a standard voice-grade phone link at 300 baud. When the relative inefficiency of this system became obvious, FRL, with some counsel from STI, made the decision to implement a local disk-based development system using a processor compatible with the Z-80 on the 80-04 board. They acquired a MSC-80-09 processor board from Monolithic systems, which represented one of the most advanced single-board computers available. The 80-09 contained a Z-80 processor, 9511 math unit, floppy disk controller, ROM with bootstrap for a standard CP/M operating system, two serial RS-232 ports and 32K of RAM on a single multibus board. Additional elements included dual 8 in. floppies (adapted from an earlier system), a LSI ADM-31 CRT terminal, and an Anadex DP-9501 matrix printer.

#### **MONITOR AND LANGUAGE SELECTION**

The selection of CP/M as the operating monitor for the development system opened a choice among a number of higher level languages which could be used to generate Z-80 code acceptable to the MSC 80-04 board which remained as the heart of the Micro-DFCS. Two versions of the PASCAL language, FORTRAN and a compiler version of BASIC, were evaluated for suitability and benchmarked for object code efficiency. The definitive winner was PASCAL/MT v. 3.2, created by MT Microsystems of Carlsbad, CA. At the time of the benchmark runs, PASCAL/MT 3.2 had already been obsoleted by PASCAL/MT v. 5.x. The latter, however, while containing more convenience features than its predecessor, generated markedly less compact object code. Even using the less replete of the two PASCAL, the execution module for a PASCAL equivalent of CAS-6 still contained 2-3 times the number of instructions of the assembly code CAS-6. Nevertheless, the introduction of the PASCAL-based system rendered floating point operations and program logic much more accessible than was possible with the assembly language code. This permitted much more flexibility in terms of control algorithms, and, in general, saved considerable time and effort in the development of the revised ZOH and slewver code.

## SOFTWARE DEVELOPMENT FOR SLEWER CONTROL LAW

During the course of the contract period, two major efforts at Slewler implementation were mounted. The first effort (February 1981) centered around a formulation which had the capability of handling three model input vectors. This formulation was coded into an adaptation of the FRL CAS-6 assembly language code. Although it was immune from the gain selection glitch inherent in the Zero Order Hold, it nevertheless proved extremely resistant to static check. This served as a beginning object lesson in the validation of slewers, i.e., that careful formalized validation procedures whose numerical performance can be compared to theoretical check cases are a prime necessity.

The second major onslaught against the Slewler occurred after the decision had been reached to abandon the assembly language version of CAS-6 in favor of the framework of R.V. Walters' PASCAL language code (pCAS). Groundwork was laid by first adapting the Zero Order Hold within the pCAS framework, and performing extensive validation work to assure ourselves that the software was indeed performing to specification. The first PASCAL slewler embodied the February 1981 Slewler algorithm; however, that effort was truncated when the excessive computational load of that model became apparent. A second (October 1981) slewler formulation proved to be computationally more congenial for two reasons. First, it utilized only pedal command input; second, it had a more balanced distribution of foreground and background computation than its predecessor. Rough-out code for this latter version of the Slewler were completed and a preliminary compiled version generated.

Overall structure of the software is shown in Figure 26. The slewler control program SLEW2 contains two functional modes of operation which can be selected by the evaluation pilot using the cockpit Termiflex control console. Mode "E" initiates ZOH operation and mode "S" initiates slewler operation. Because of the RAM space required by the additional gains and constants associated with the Slewler, it was necessary to strip out all of the longitudinal axis setup and control routines as well as some of the analog test utilities from the currently operational

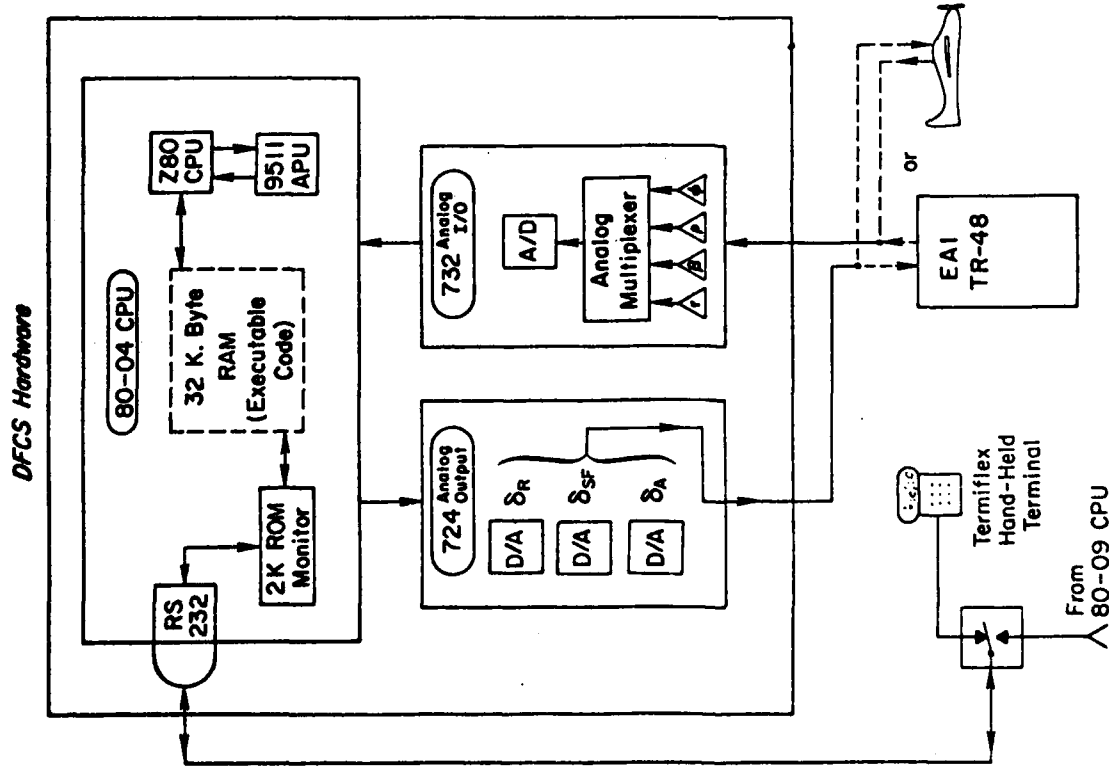
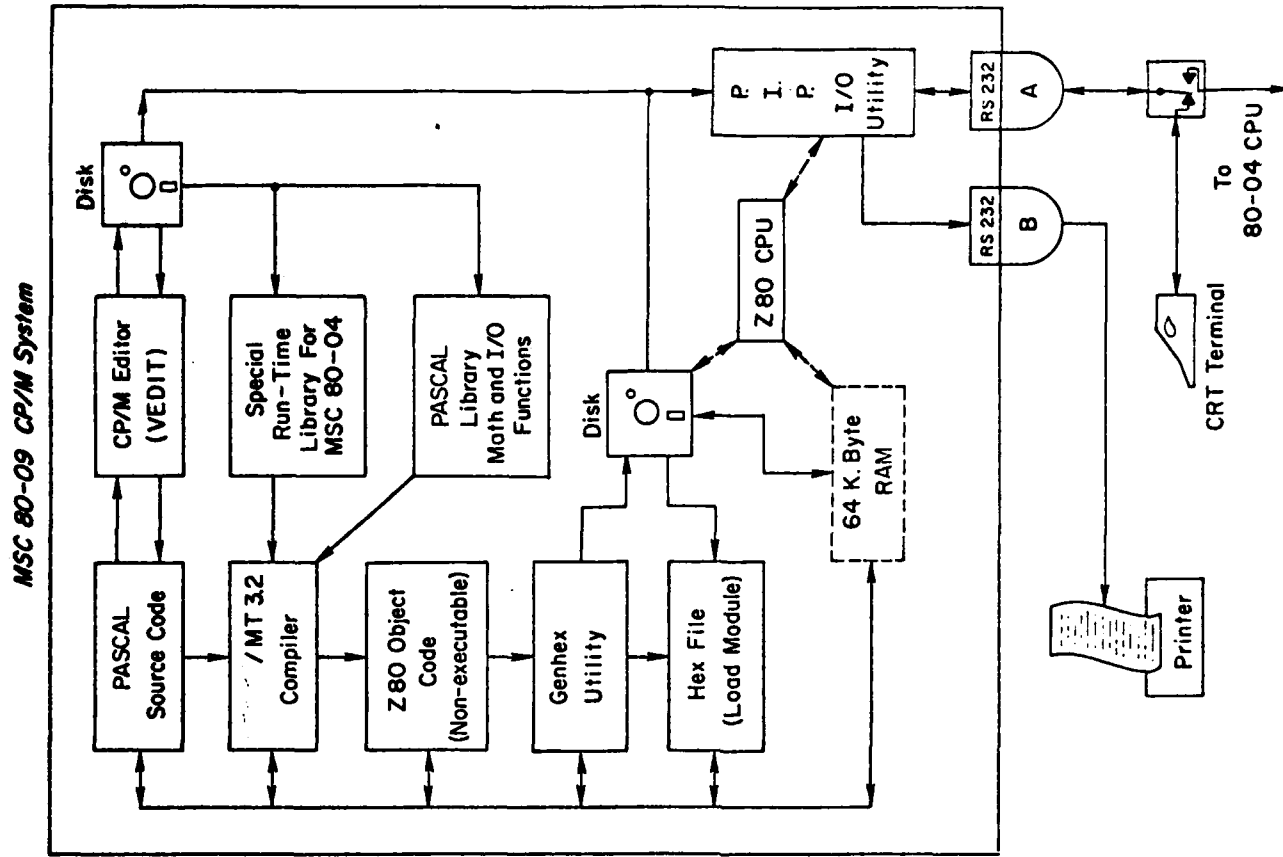


Figure 26. DFCS Hardware and Software

version of pCAS (ver. 4.3). In addition, several alternative versions of the slewer control program had to be compiled in order to address certain validation problems. These will be discussed later on. It should be noted that the pCAS control program containing the ZOH controller also contained an operational slewer. However, the scaling and graceful entry problems discussed earlier in the text made it too hazardous to engage mode "S" during any of our last three flights.

#### **NUMERICAL VALIDATION OF THE SLEWER ALGORITHM**

Due to the dynamic structure of the Slewer algorithm, a static end-to-end I/O check was not possible using the procedures developed for the ZOH case. It was necessary, therefore, to compile a special validation version of the Slewer in order to verify the internal calculations of the real-time flight controller program (SLEW2). The validation program (SLTST) differed from the real-time controller in three regards:

1. The analog drivers were disabled so that the program could function using the 80-04 processor in a stand-alone environment.
2. LPRINT statements (PASCAL printer output commands) were inserted into the control loop section of the source code in order to print out intermediate and output variables at every sample frame.
3. Unity values were substituted for the front- and back-end conversion scale factors so that values in pure physical units would be displayed.

In order to validate the numerical output of the Micro-DFCS, a validation case consisting of output values for three controllers were worked out using the discrete model with constant pedal input and fixed (constant) feedback variables. Numerical validation of the October 1981 algorithm was obtained after resolving some tricky problems resulting from uninitialized variables in the PASCAL code.

## **APPENDIX C**

### **ANNOTATED TOTAL RUN**

This run checks verisimilitude of pseudo inverse, ZOH matching of continuous system by comparing s-plane matrices (continuous model) against w'-matrices (simulator).

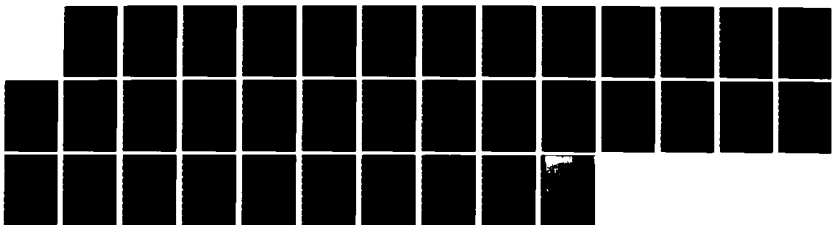
AD-A134 175 FLIGHT TEST OF ADVANCED DIGITAL CONTROL CONCEPTS(U)  
SYSTEMS TECHNOLOGY INC HAWTHORNE CA  
R F WHITBECK ET AL. MAR 82 AFWAL-TR-82-3021

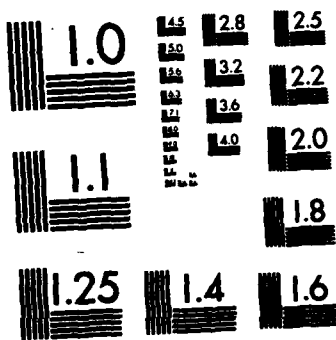
2/2

UNCLASSIFIED F33615-88-C-3612

F/G 1/3

NL





MICROCOPY RESOLUTION TEST CHART  
NATIONAL BUREAU OF STANDARDS-1953-A



(CMAT) = (AMAT) \* (BMAT)

[ CMAT ] MATRIX:  $\rightarrow$  P [L-M]  $\rightarrow$  C8  $\rightarrow$  UMAT

(CMAT) = (AMAT) \* (BMAT)

COL > 1 (10 Hz)

ROW	1	2	3	4
1	.6448	.3834	-.5682E-01	-.3444
2	.1264	-.2180	-.3784E-01	-.1260
3	-.7367E-01	.3024	-.8533E-01	-.3017

COPY COMPLETE

COL > 1	2	3	4	
ROW 1	.6914	.7847	-.1445E-01	.2438E-01
2	-.8144E-01	.9306	.1026E-02	.2739E-02
3	.3051	-.2793	.3562	-.1.626
4	-.2782E-01	-.1696	.6480E-01	.9054

92 COL > 1

ROW	1	2	3	4
1	-.3369	.3982	.1136	
2	.3507	-.1874E-01	-.9622E-02	
3	.2310E-01	.4960	.3.272	
4		.2588E-01	.1893	

COL > 1

ROW	1	2	3	4
1	.9036	.9755	-.3503E-02	.1927E-02
2	-.9472E-01	.9704	.3622E-03	.3757E-02
3	.3667	-.4.235	.7913	-.8716E-02
4	.1524E-01	-.2246	.8713E-01	.9997

OPTION CMAT

COL	1	2	3	4
ROW 1	-.4011	.4444		
2	.2334E-21	-.1942E-01	.1978	
3	.6027	.1956	.4.410	
4	.3321E-01	.2942E-01	.2.787	

OPTION

check on Results - subblocks  $C_B$   
and  $C_P$  into simulator equations  
 $C_{MAT} \rightarrow A$   
 $C_{MAT} \rightarrow B$   
 $(C_{MAT}) \cdot (AMAT) \rightarrow AMAT$   
( $C_{MAT} \cdot (AMAT) \rightarrow AMAT$ ) - compare against  
"Model" equations.

$(AMAT) \cdot (AMAT)$

COL > 1 2 3 4  
ROW  
1 -2172 -1908 -1095E-01 .2247E-01  
2 .1542E-01 .9366E-02 .5876E-03 -.1422E-02  
3 .1383 1.441 -.4352E-01 -.1618  
4 .8053E-02 .7548E-01 -.2256E-01 -.8414E-01

$C_{MAT}$

$AMAT$

$AMAT</$

(AMAT) \* (BMAT)

E CHAT 1 MATRIX:

$$\frac{1}{4} [I + \alpha \omega \tau]^{-1} [IP - \alpha MMAT]$$

COL > 1 2 3 4  
 ROW 1 3.140 -9.044 .2562 -.4619E-01  
 2 .9775 .3245 -.1929E-02 -.3865E-01  
 3 -6.580 45.39 8.216 23.99  
 4 .2355E-01 .1143 -.9845 .4501E-01

COPY COMPLETE C = MMAT  
 COPY COMPLETE T  $\rightarrow$  A  
 COPY COMPLETE T  $\rightarrow$  B  
 (CHAT) = (AMAT) \* (BMAT)

E CHAT 1 MATRIX:

COL > 1 2 3 E MAT  
 ROW 1 -3.946 4.755 1.768  
 2 .4171E-01 .3806E-02 -.4036E-01  
 3 6.758 5.557 47.64  
 4 .2042E-01 .4213E-02 .8822E-01

COPY COMPLETE ~~W MAT  $\rightarrow$  B~~  
 COPY COMPLETE ~~-Z  $\rightarrow$  MMAT  $\rightarrow$  A~~  
 (CMAT) = (EMAT) \* (EMAT)

E CHAT 1 MATRIX: — MMAT

COL > 1 2 3 4  
 ROW 1 -3.140 9.044 -.2562 .6619E-01  
 2 -.9775 -.3245 .1929E-02 .3865E-01  
 3 6.580 45.39 -8.216 -23.99  
 4 -.2355E-01 -.1143 .9845 -.4501E-01

COPY COMPLETE ~~W MAT  $\rightarrow$  B~~  
 COPY COMPLETE ~~-Z  $\rightarrow$  MMAT  $\rightarrow$  A~~

STORING CHARACTERISTIC EQU & EIGENVALUES OF (AMAT)

TO POLYA AND ROOTS RESPECTIVELY:

CHARACTERISTIC EQU  
 POLYA COEFFICIENTS

EIGENVALUES OF AMAT  
 POLYA ROOTS (ROOTA)

COL > 1 2 3 4  
 ROW 1 1.000 1S\*\* 4  
 2 11.73 1S\*\* 3  
 3 64.25 1S\*\* 2  
 4 178.2 1S\*\* 1  
 5 236.7

POLYNOMIAL CONSTANT= 1.0000

Compare with continue

-2.374j 8.857 pure

-3.515j 3.3381

OPTION >RMAT,LMAT

COL > 1 2 3 4  
 ROW 1 .6913 .7847 -.1445E-01 .2439E-01  
 2 -.8125E-01 .9298 -.9503E-03 .2315E-02  
 3 .5053 -2.794 .3561 -.1.627  
 4 .23330E-01 -.1492 .6662E-01 .9156

Compare

COL > 1 2 3 4  
 ROW 1 .6914 .7847 -.1445E-01 .2439E-01  
 2 -.8144E-01 .9306 .1026E-02 .2773E-02  
 3 .5051 -2.793 .3562 -.1.626  
 4 .2782E-01 -.1696 .6480E-01 .9054

Compare

OPTION >

SMAT

COL > 1 2 3 4  
 ROW 1 -.3369 .3982 -.1868E-01 .8801E-02  
 2 .2038E-01 -.1956E-01 .2442E-01 .1.695  
 3 .3510 .4960 .3.273  
 4 .1956E-01

Compare

SMAT

COL > 1 2 3 4  
 ROW 1 -.3369 .3982 -.1874E-01 .1136  
 2 .2028E-01 -.19509 .4960 .3.272  
 3 .3509 .2310E-01 .2586E-01 .1893  
 4

MMAT

OPTION >

WFLUN, VFLUN, YFLU

WHAT, XMAT

COL >	1	2	3	4
ROW	5.140	-9.044	.2562	-4619E-01
1	.9775	.3245	.1929E-02	-3865E-01
2	-6.380	45.39	8.216	23.99
3	.2355E-01	.1143	.9845	.4501E-01
4				

↓ Compare

check input data

COL >	1	2	3	4
ROW	-3.105	8.917	-2.220	0.
1	-9776	-2965	0.	-3795E-01
2	6.354	-47.71	-8.359	-25.00
3	0.	0.	1.000	0.
4				

OPTION : EMAT, YMAT

COL >	1	2	3	4
ROW	-3.946	4.755	1.768	EMAT
1	.4171E-01	.3605E-02	-4036E-01	
2	6.758	5.557	47.64	
3	.2042E-01	.4213E-02	.8822E-01	
4				

↓ Compare

COL >	1	2	3	4
ROW	-3.725	4.766	1.897	YMAT
1	.2738E-01	.1693E-01	-.3360E-01	
2	7.178	5.575	49.60	
3	0.	0.	0.	
4	0.	0.	1.000	

IMAT, JMAT

COL >	1	2	3	4
ROW	-4.310	10.20	-.4160E-01	0.
1	-1.000	-.3050	0.	-3880E-01
2	1.270	-.5000	-2.330	check Input data
3	0.	0.	1.000	
4	0.	0.	0.	

↓ Compare  
check input data

option : note ZMAT must be changed such  
here a new sample rate is used

It affects only CKEY.

check input data

check input data

check input data

COL >	1	2	3	4
ROW	-3.925	4.766	1.897	ZMAT, UMAT, VMAT,
1	.2988E-01	.1802E-01	-.3360E-01	
2	7.178	5.655	49.60	
3	0.	0.	0.	
4	0.	0.	0.	

COL >	1	2	3	4
ROW	20.00	0.	0.	ZMAT, UMAT, VMAT,
1	0.	20.00	0.	
2	0.	0.	20.00	
3	0.	0.	0.	
4	0.	0.	0.	

COL >	1	2	3	4
ROW	1.000	0.	0.	ZMAT, UMAT, VMAT,
1	0.	1.000	0.	
2	0.	0.	1.000	
3	0.	0.	0.	
4	0.	0.	0.	

COL >	1	2	3	4
ROW	-1.000	0.	0.	ZMAT, UMAT, VMAT,
1	0.	1.000	0.	
2	0.	0.	1.000	
3	0.	0.	0.	
4	0.	0.	0.	

**APPENDIX D**

**VALIDATION OF ZOH CONTROL LAW, FREQUENCY RESPONSE**

A comparison of the theoretical controller working against an ideal model of the open-loop aircraft was carried through using the frequency response concepts of Reference 2. A comprehensive set, at 10 Hz and 50 Hz, follows.

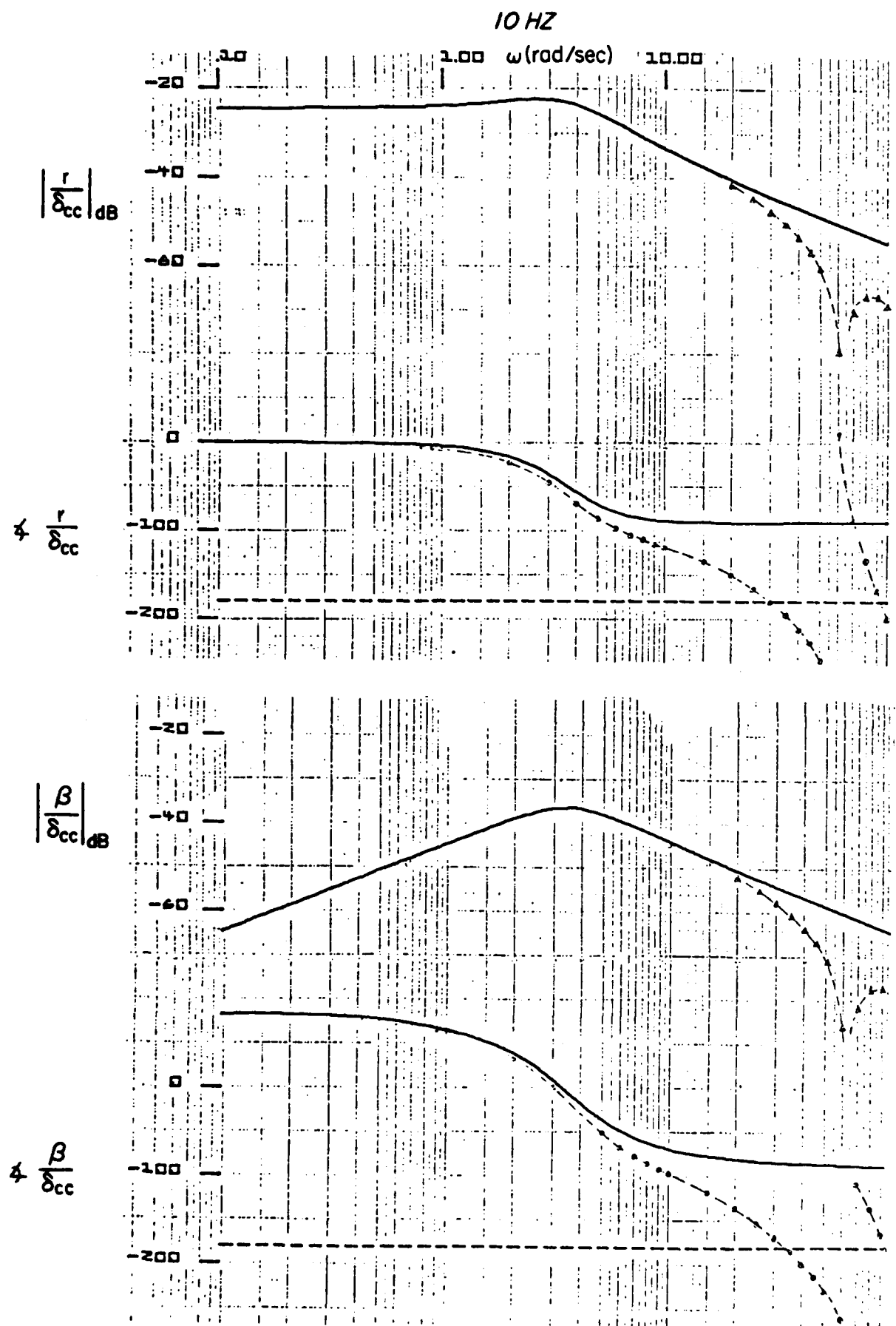


Figure 27. Bode Plot  $\gamma/\delta_{CC}$ ,  $\beta/\delta_{CC}$

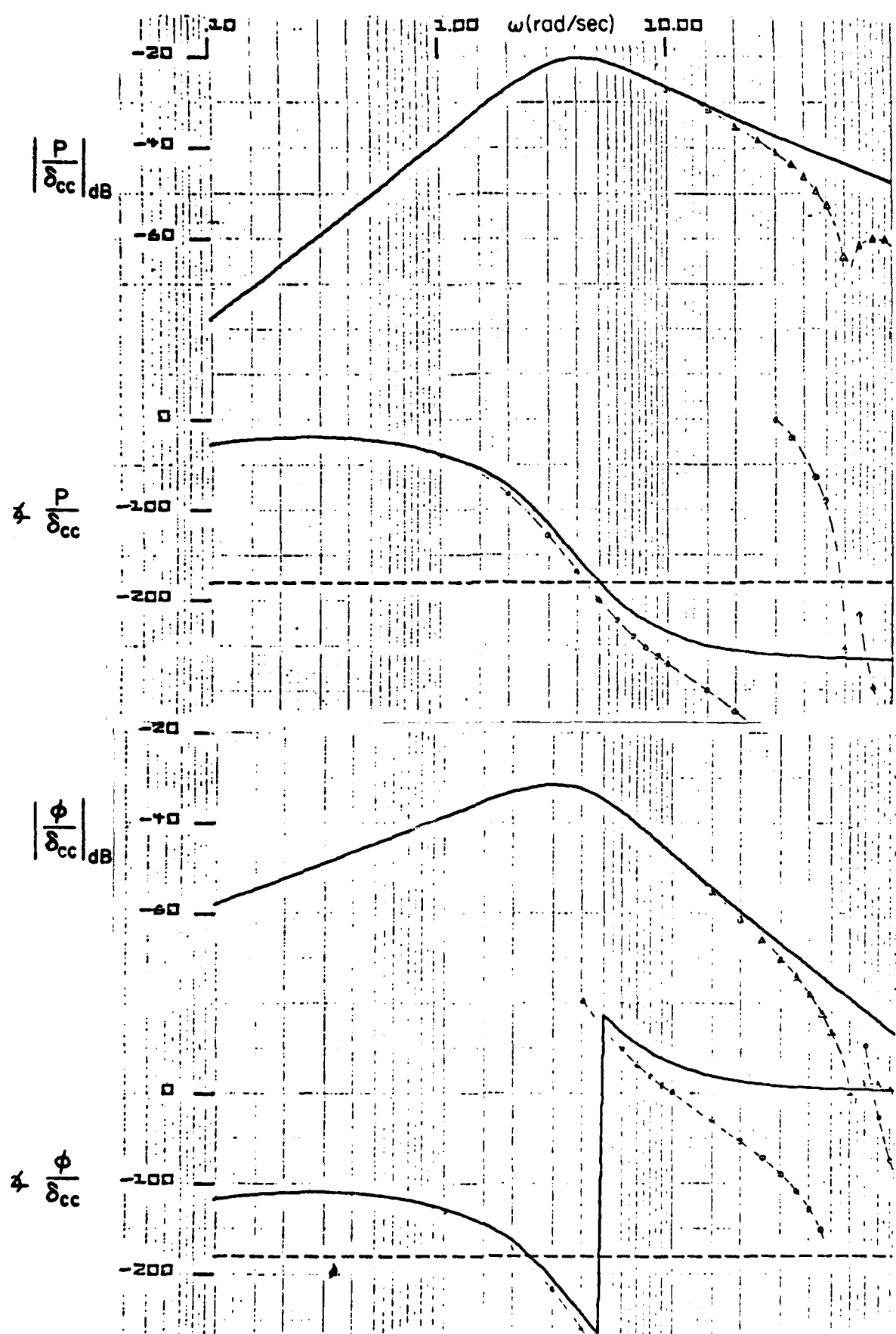


Figure 28. Bode Plot  $p/\delta_{CC}$ ,  $\phi/\delta_{CC}$

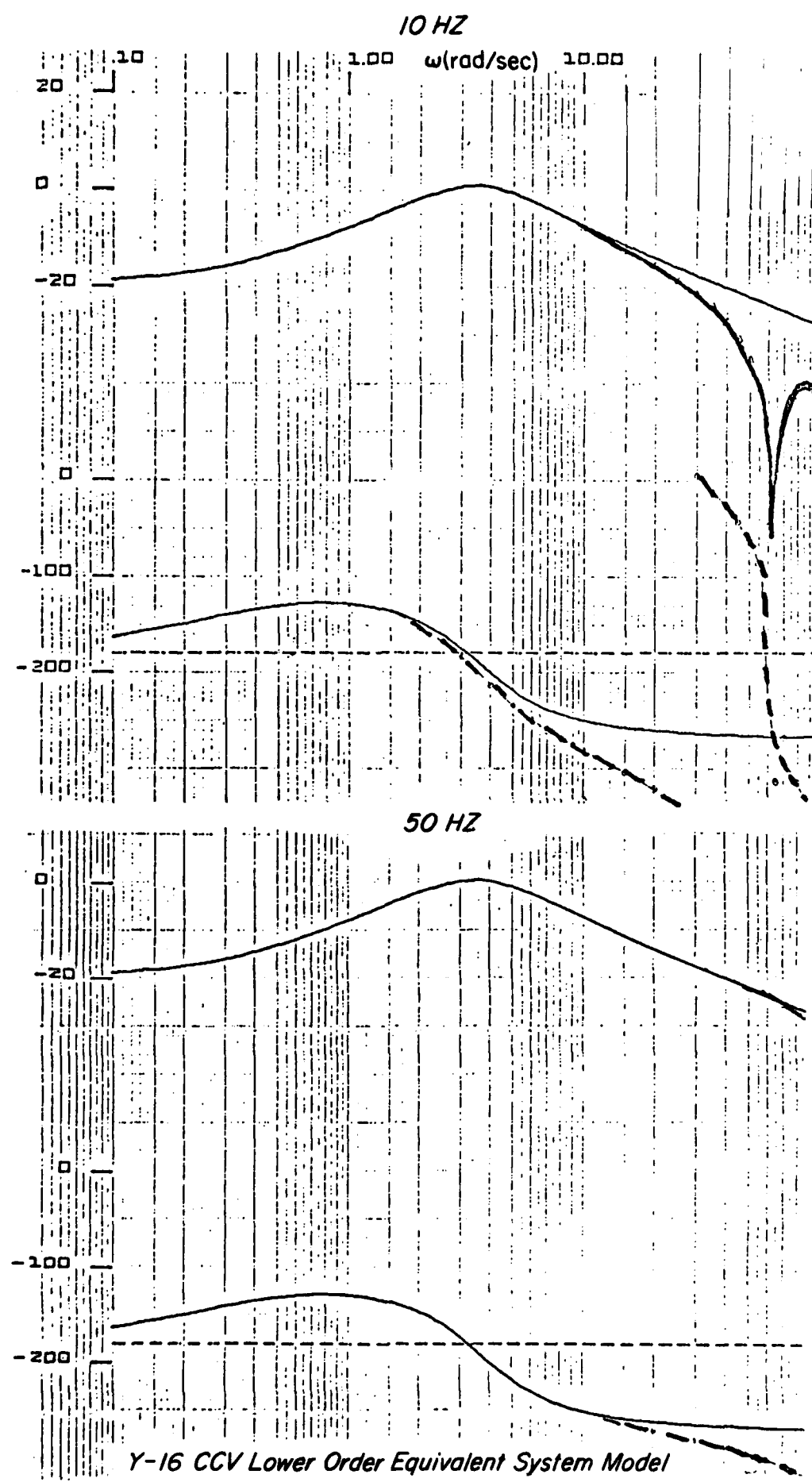


Figure 29. Bode Plot  $\psi/\delta_R$ , 10 Hz, 50 Hz

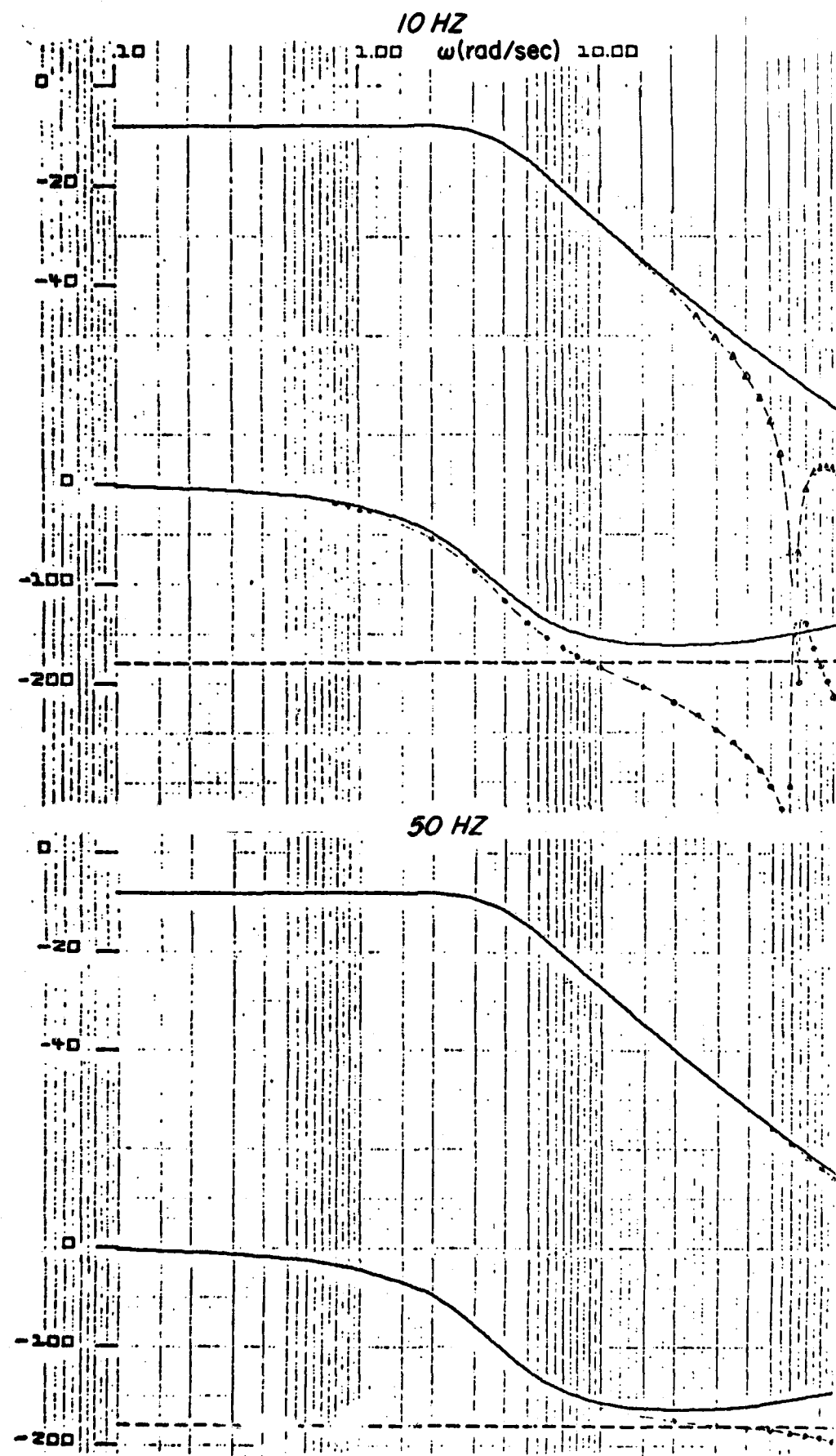


Figure 30. Bode Plot  $\beta/\delta_R$

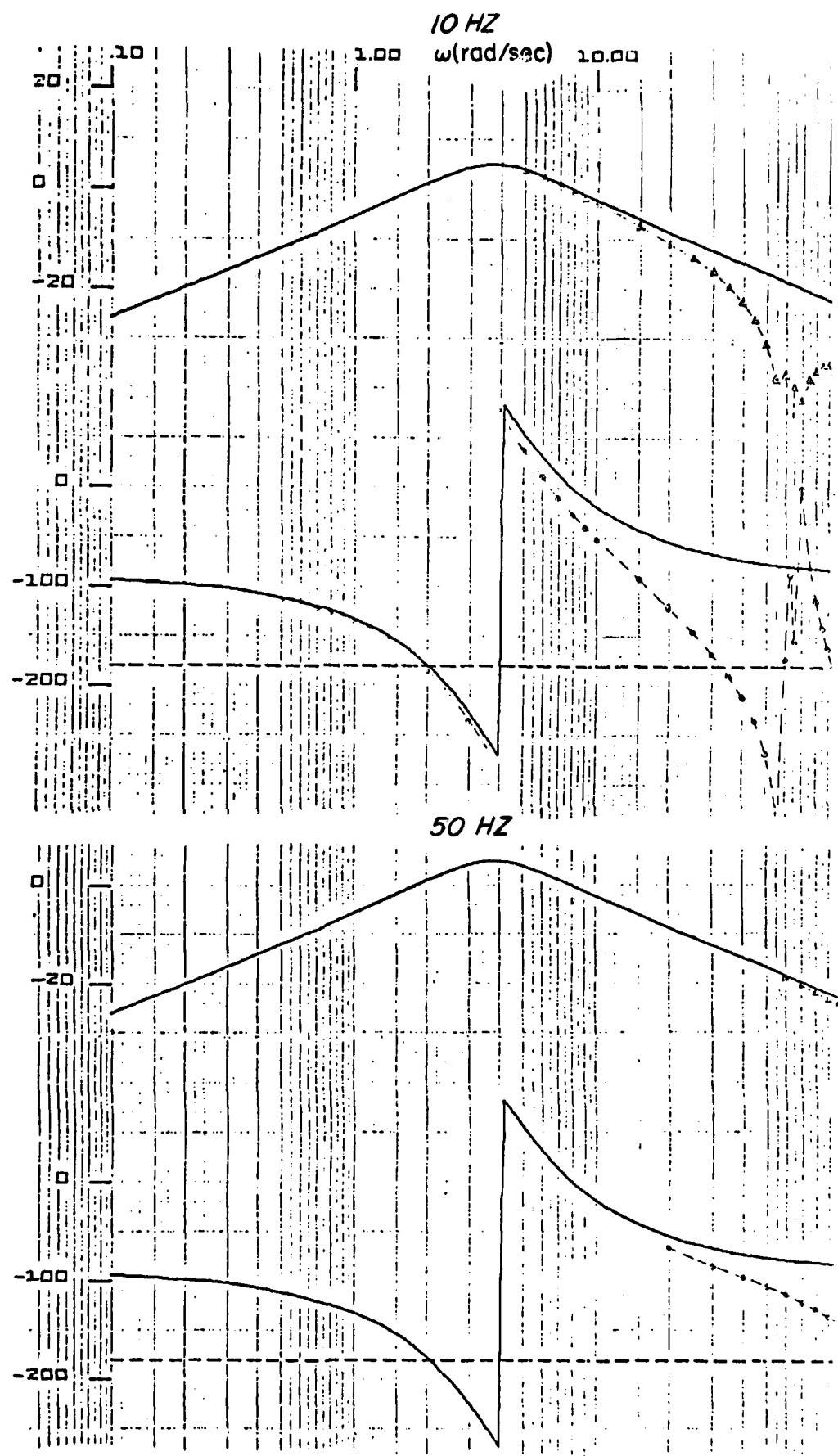


Figure 31. Bode Plot  $p/\delta_R$

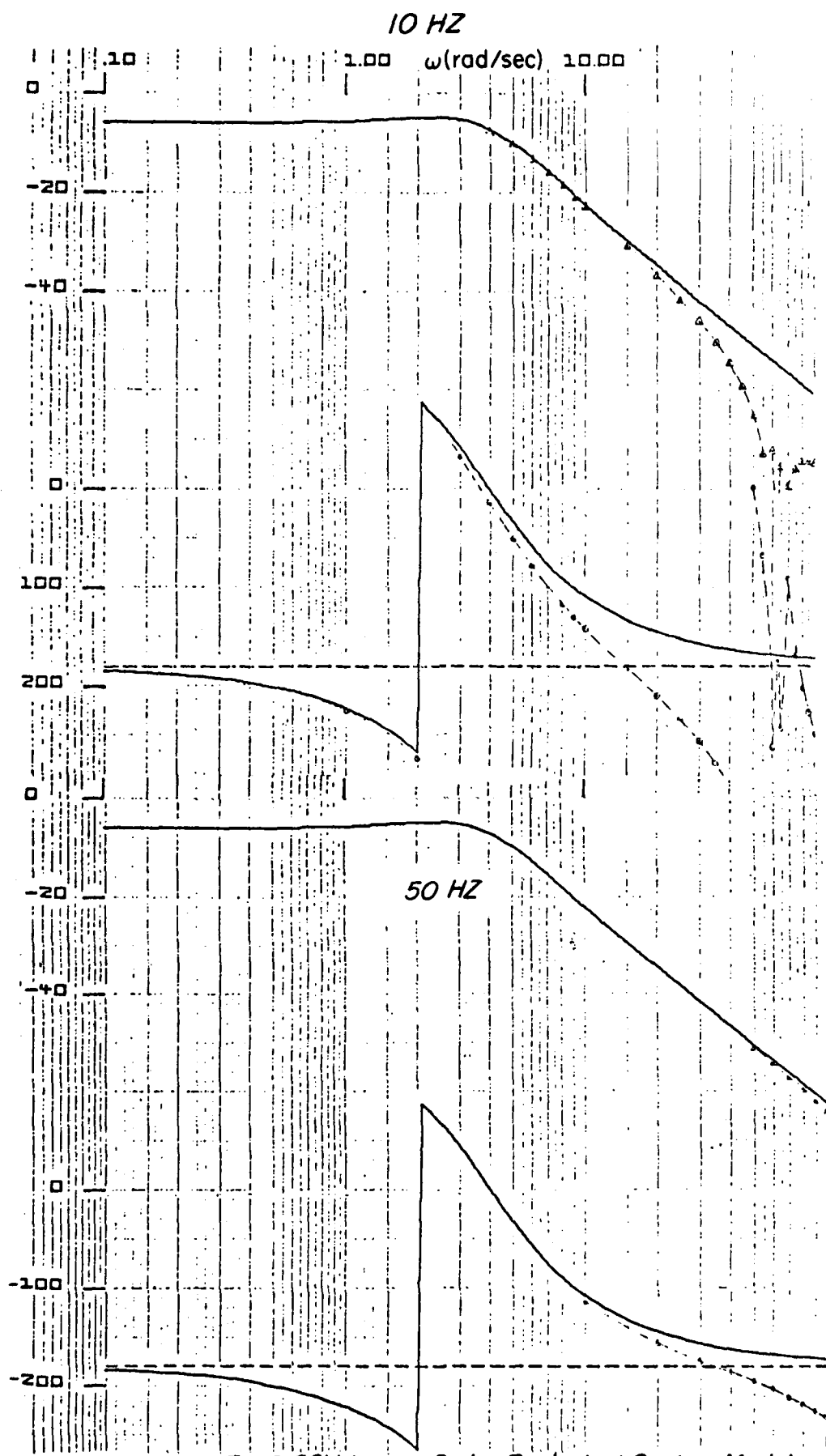


Figure 32. Bode Plot  $\phi/\delta_R$

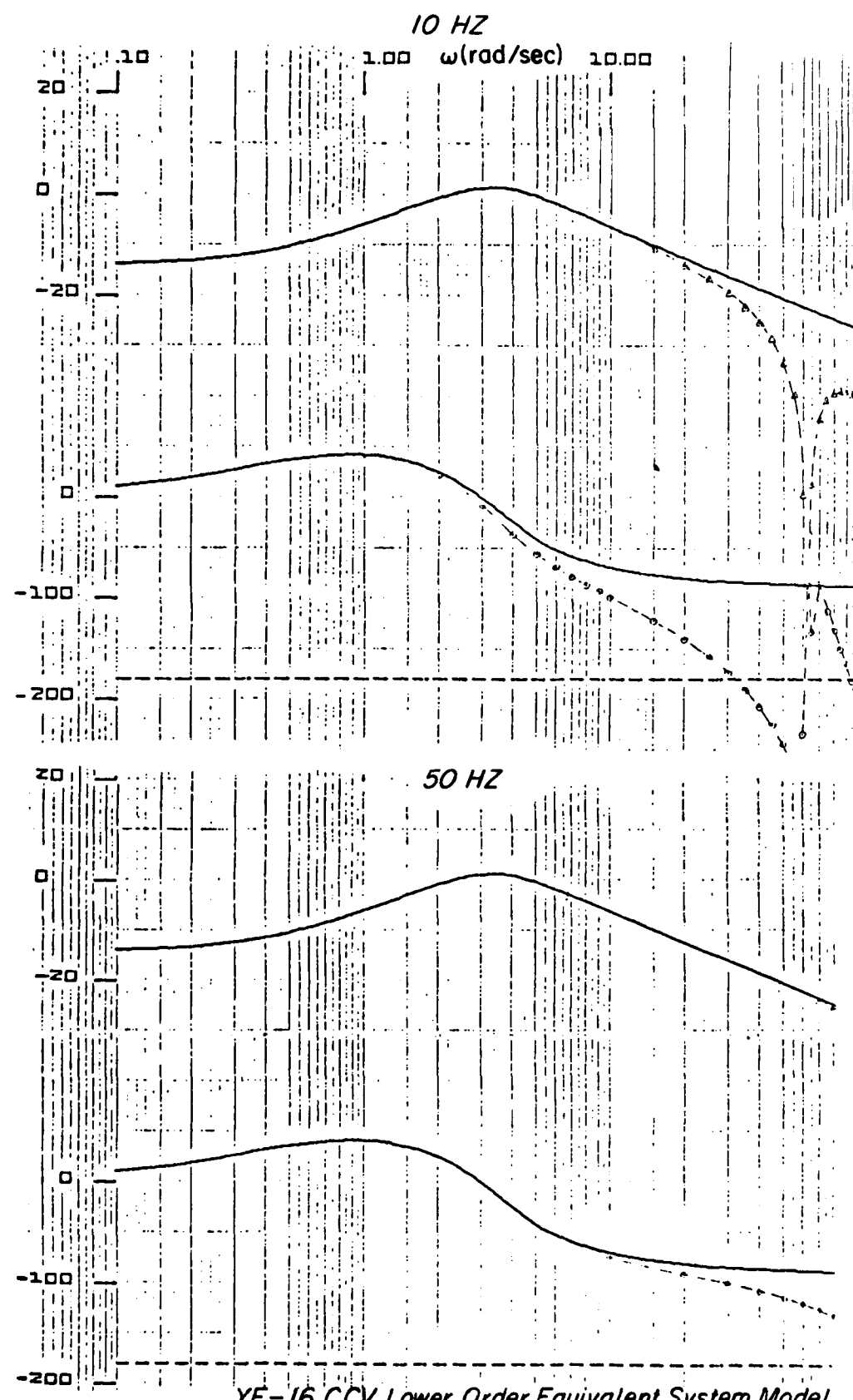


Figure 33. Bode Plot  $r/\delta_C$

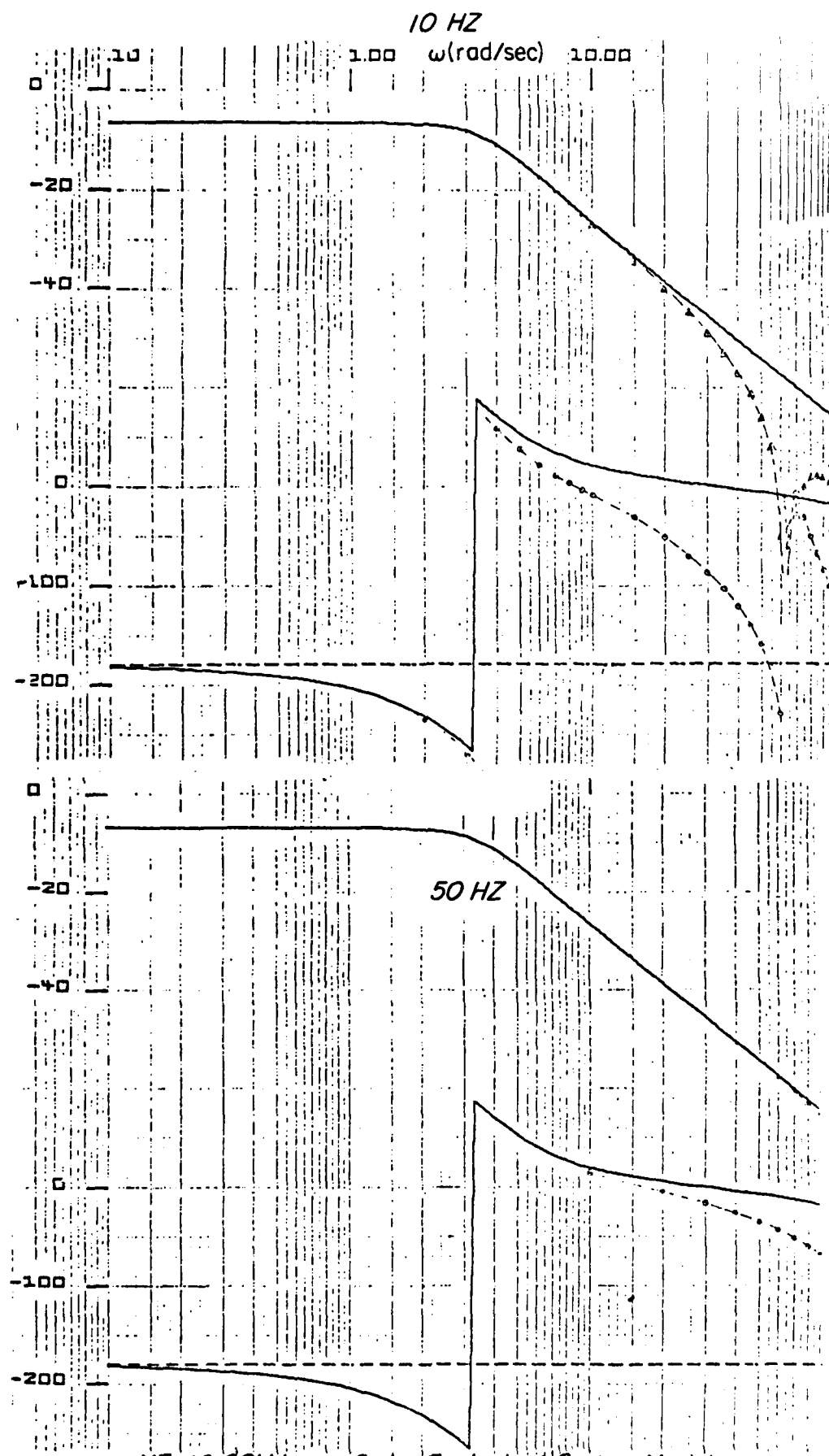


Figure 34. Bode Plot  $\beta/\delta_C$

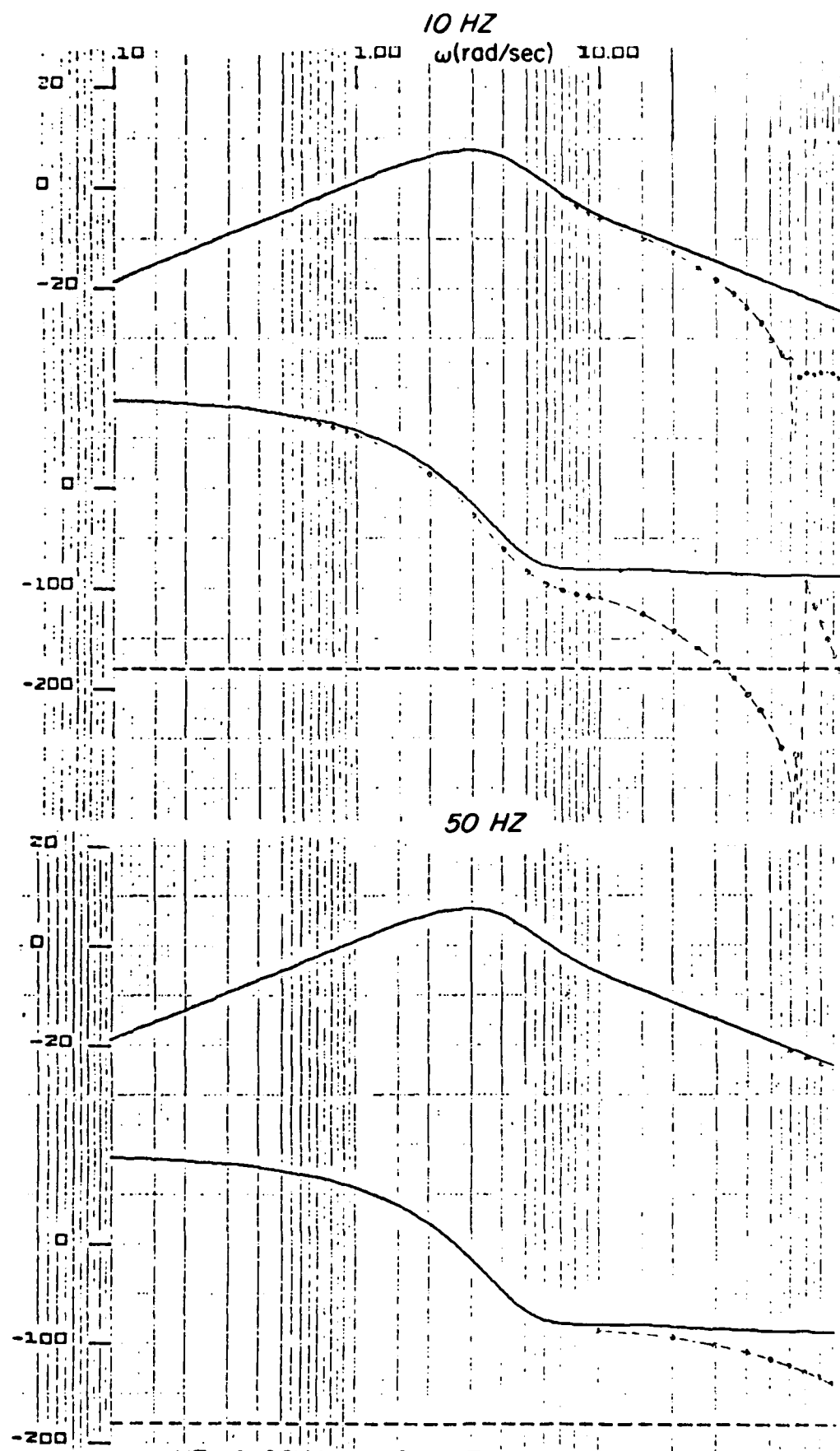
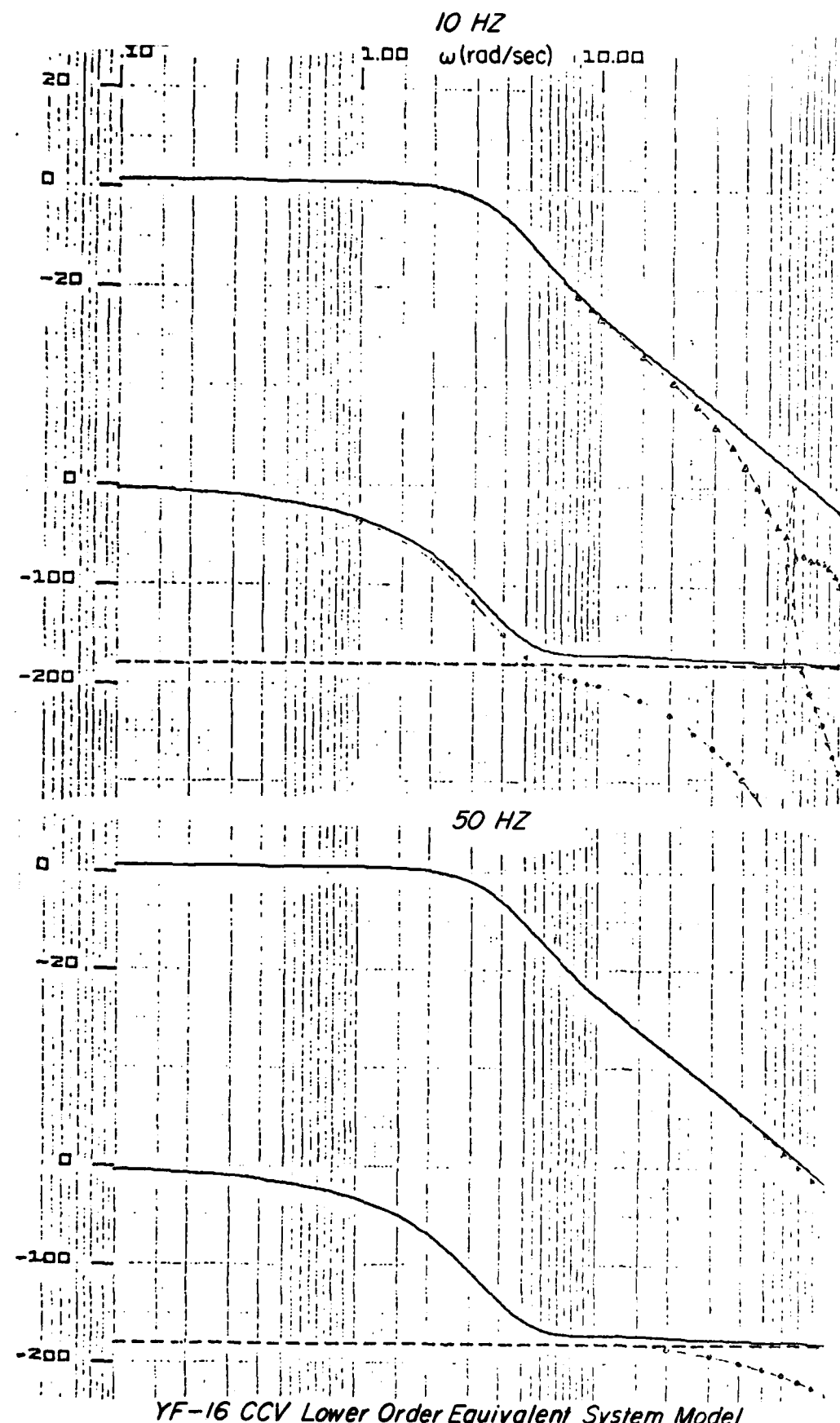


Figure 35. Bode Plot  $p/\delta_C$



YF-16 CCV Lower Order Equivalent System Model

Figure 36. Bode Plot  $\phi/\delta_C$

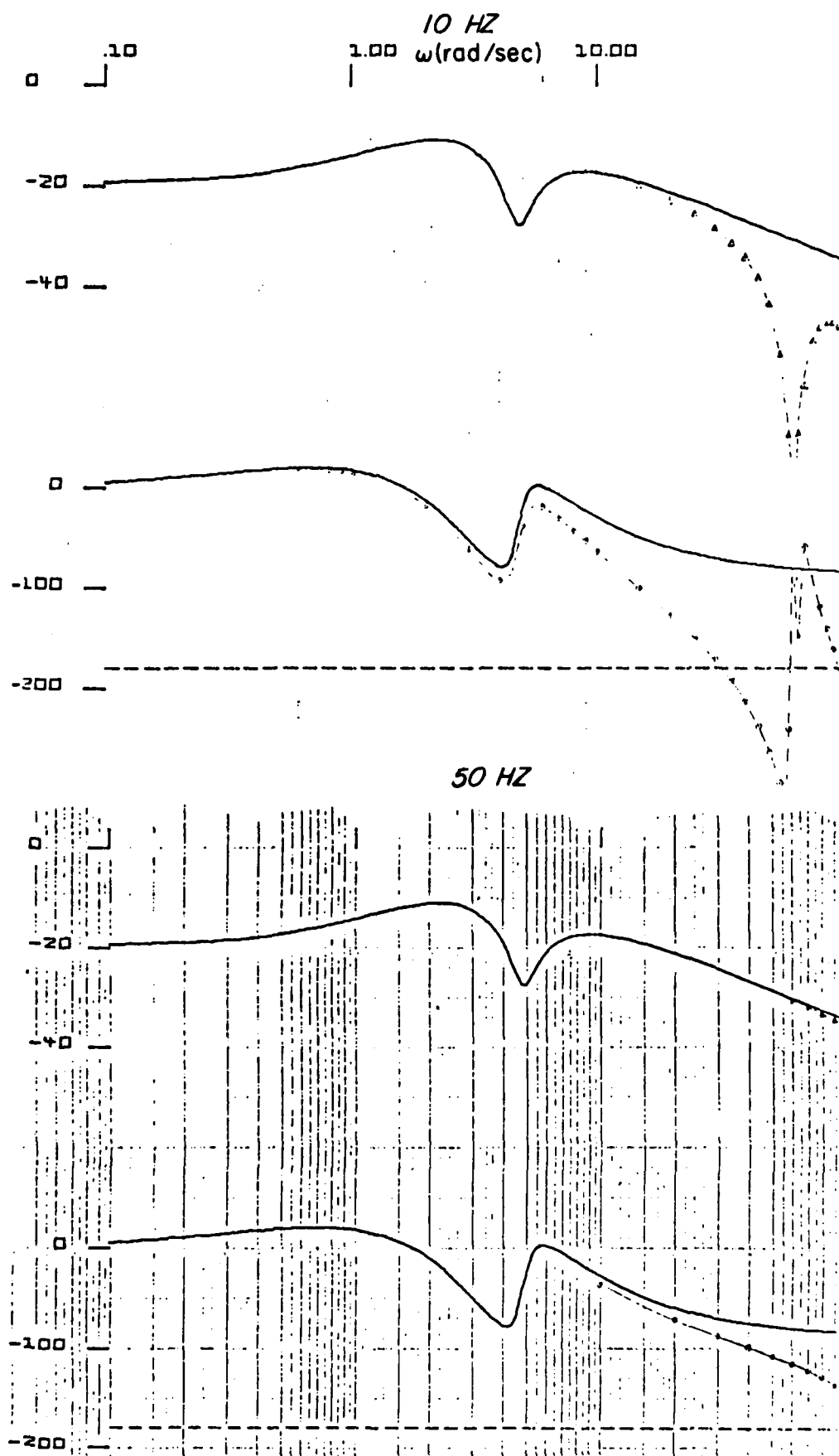
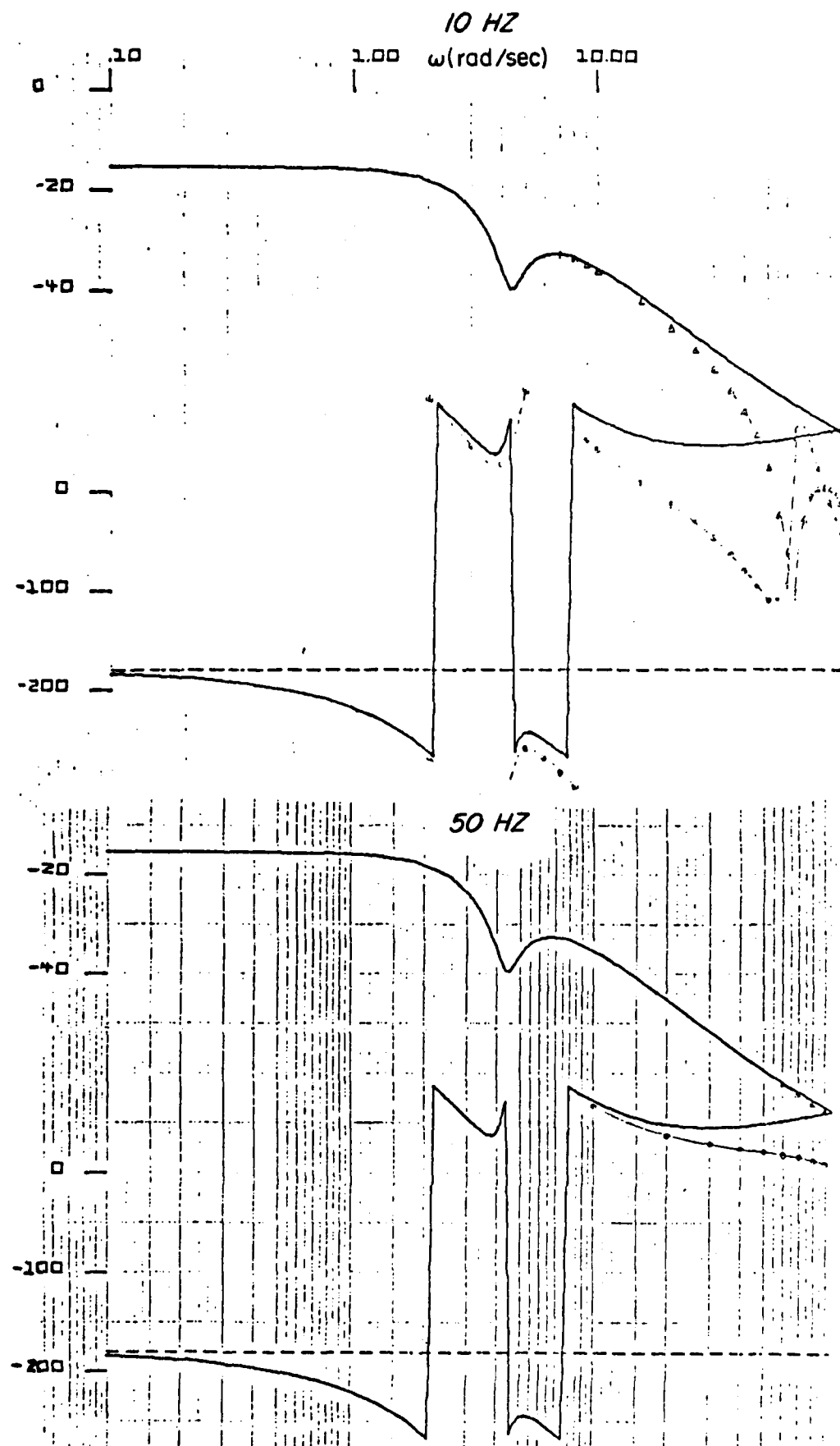
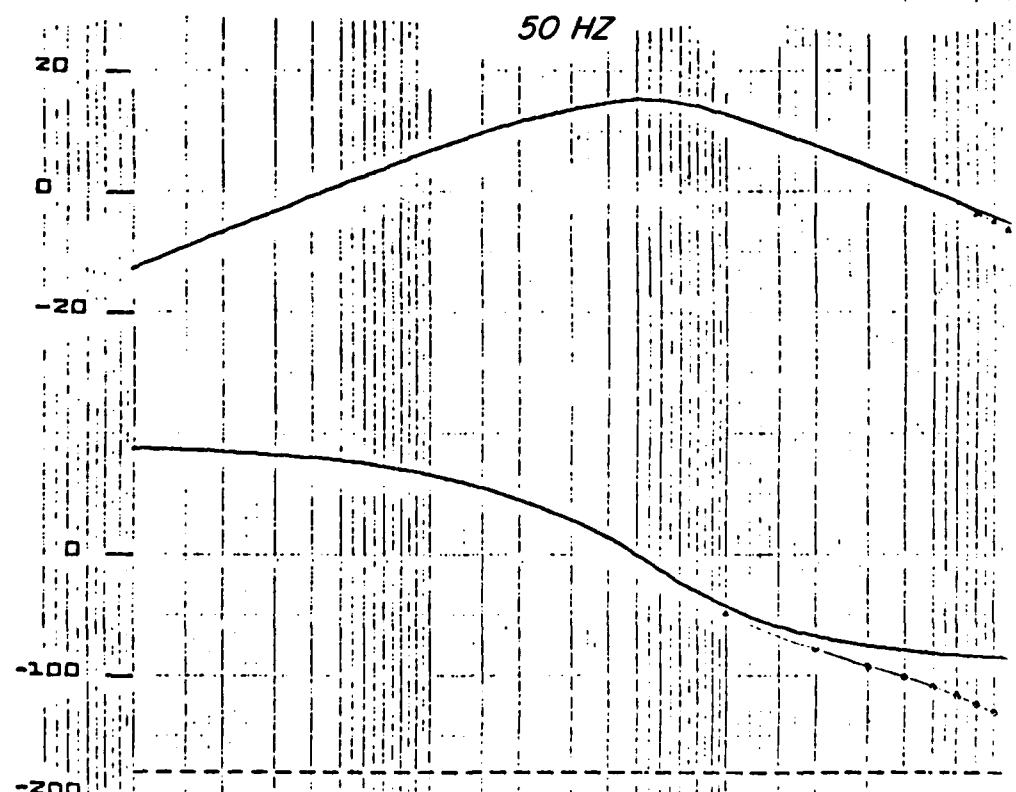
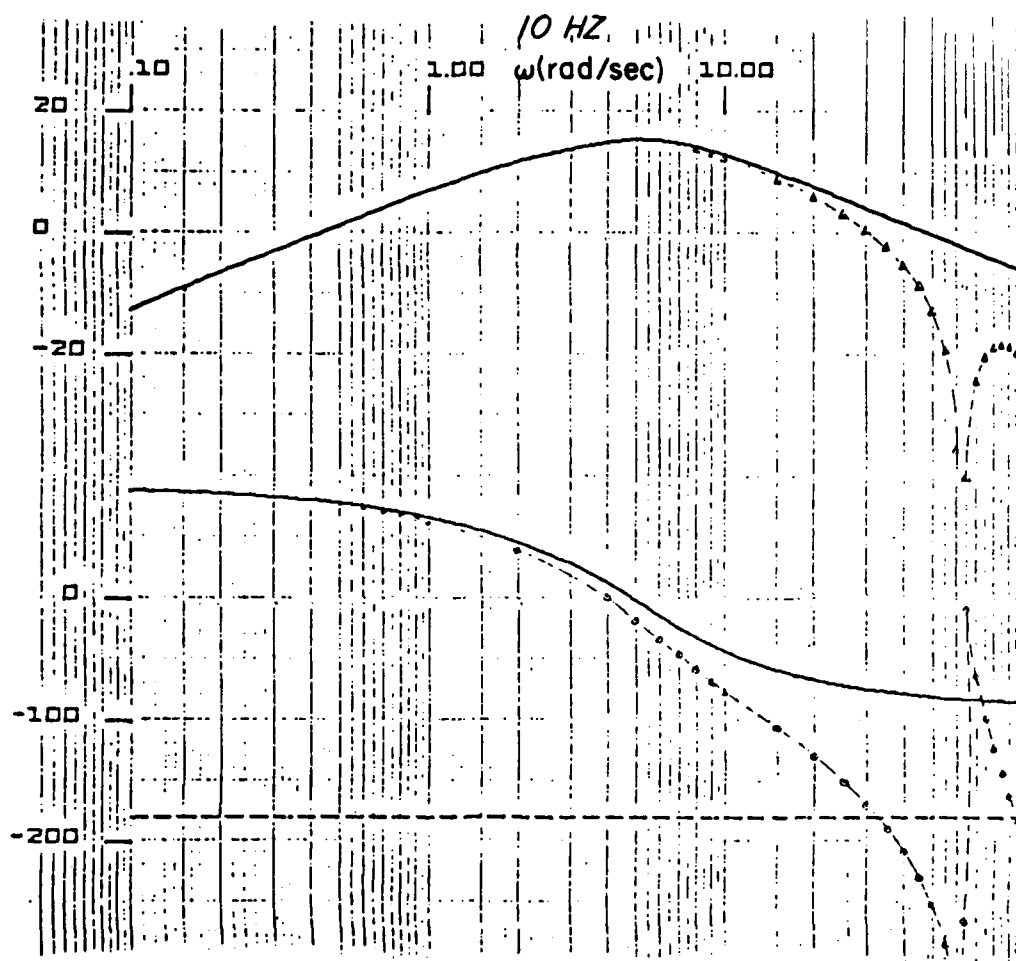


Figure 37. Bode Plot  $r/\delta_A$



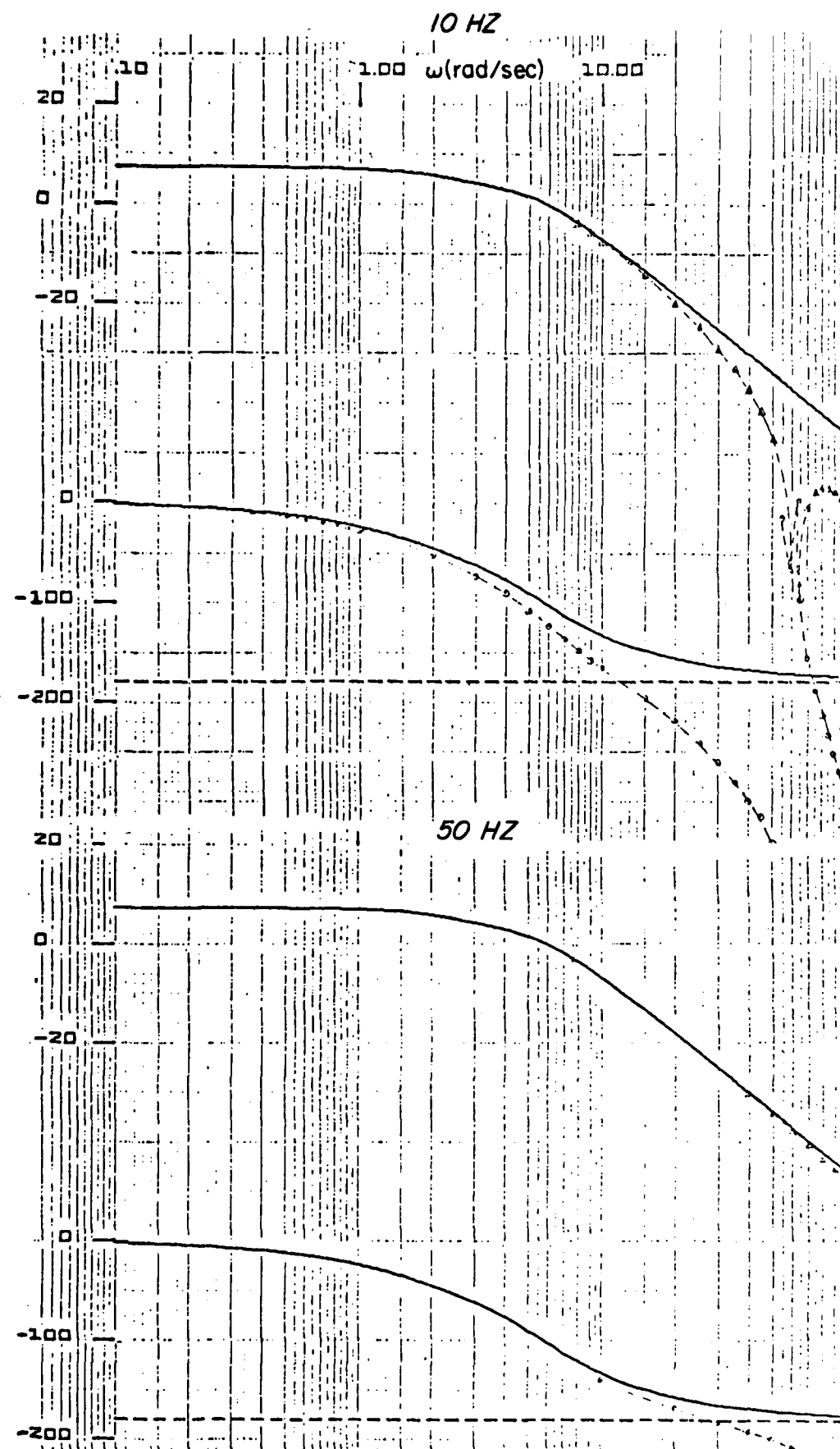
YF-16 CCV Lower Order Equivalent System Model

Figure 38. Bode Plot  $\beta/\delta_A$



YF-16 CCV Lower Order Equivalent System Model

Figure 39. Bode Plot  $p/\delta_A$



YF-16 CCV Lower Order Equivalent System Model

Figure 40. Bode Plot  $\phi/\delta_A$

**APPENDIX E**  
**SLEWER FIRST-ORDER FORM**

**Given**

$$\dot{x} = Ax + Bu \quad (122)$$

**the Laplace transform is**

$$X(s) = [Is - A]^{-1}x(0) + [Is - A]^{-1}Bu \quad (123)$$

**If the continuous control vector is a reconstructed signal, using slew data holds, then**

$$U(s) = M(s)R^T(s) \quad (124)$$

**where  $M$  is the  $s$ -plane transform of the data hold. For the slew, if  $R^T$  is the sampled input,**

$$\begin{aligned} U(s) &= \left[ \frac{(1 - e^{-sT})^2}{Ts^2} \right] R^T \\ &= \left[ \frac{1 - e^{-sT}}{Ts^2} - \frac{e^{-sT}}{s} \right] R^T + \left[ \frac{1}{s} - \frac{1 - e^{-sT}}{Ts^2} \right] e^{-sT} R^T \\ &= M_1(s)R^T + M_2(s)(R^T e^{-sT}) \end{aligned} \quad (125)$$

**The motivation for partitioning Equation 125 in this particular manner is clear when the impulse responses of  $M_1$  and  $M_2$  are plotted.**

From Equation 125 write the impulse responses:

$$M_1(t) = \begin{cases} t/T & 0 < t < T \\ 0 & \text{Elsewhere} \end{cases} \quad (126)$$

$$M_2(t) = \begin{cases} 1 - (t/T) & 0 < t < T \\ 0 & \text{Elsewhere} \end{cases} \quad (127)$$

From Equation 125,

$$x(s) = [Is - A]^{-1}x(0) + [Is - A]^{-1}B[M_1R^T + M_2R^Te^{-sT}] \quad (128)$$

Let

$$[Is - A]^{-1} = \phi(t) \quad (129)$$

and write the inverse of Equation 123:

$$\begin{aligned} x(t) &= \phi(t)x(0) + \left[ \int_0^t \phi(t - \xi)BM_1(\xi) d\xi \right] R^T(t) \\ &+ \left[ \int_0^t \phi(t - \xi)BM_2(\xi) d\xi \right] R^T(t - T) \end{aligned} \quad (130)$$

Using the definition of Equation 126 and 127, substituted into Equation E-9, yields the explicit solution

$$\begin{aligned} x(t) &= \phi(t)x(0) + \left[ \int_0^t \phi(t - \xi) \frac{B}{T} \xi d\xi \right] R^T(t) \\ &+ \left[ \int_0^t \phi(t - \xi)B \left[ 1 - \frac{\xi}{T} \right] d\xi \right] R^T(t - T) \end{aligned} \quad (131)$$

Next, turn the integral equation into an integro-recursion equation by setting

$$t = kT + \tau, \quad k = 0, 1, \dots, 0 < \tau \leq T \quad (132)$$

Clearly, in the recursion

$$\begin{aligned} x(0) &\Rightarrow x(T) \\ x(T) &\Rightarrow x(2T) \\ &\vdots \\ x(kT) &\Rightarrow x[(k+1)T] \end{aligned}$$

Substituting Equation 132 into 131 gives the first-order form

$$\begin{aligned} x(kT + \tau) &= \phi(\tau)x(kT) + \left[ \int_0^0 \phi(t - \xi) \frac{B}{T} \xi \, d\xi \right] R^T(kT + \tau) \\ &+ \left[ \int_0^t \phi(t - \xi) B [1 - (\xi/T)] \, d\xi \right]_{t=T} R^T[kT] \quad (133) \end{aligned}$$

Finally, suppress the redundant notation with regard to  $T$ , and thus verify the simpler first-order form

$$x_{k+1} = \phi x_k + \Gamma_1 r_k + \Gamma_2 r_{k-1} \quad (134)$$

where

$$\phi = [Is - A]_{t=T}^{-1} \quad (135)$$

$$\Gamma_1 = \frac{1}{T} \int_0^t \phi(t - \xi) B \, d\xi = \mathcal{L}^{-1} \left[ \frac{1}{T} \frac{[Is - A]^{-1} B}{s^2} \right]_{t=T} \quad (136)$$

$$\Gamma_2 = \frac{1}{T} \int_0^T [\phi(t - \xi) B[1 - (\xi/T)] d\xi]_{t=T} \quad (137)$$

In going from Equation 133 to Equation 134 we make use of the discrete nature of  $R^T$ , specifically,

$$\left. \begin{array}{l} R^T[(k+1)T] \equiv R(kT) \\ R^T[(k-1)T] \equiv R(kT) \end{array} \right\} \quad (138)$$

since the sampling value is determined at the start of the frame time.

Finally, observe

$$\Gamma_2 \triangleq \Gamma_{ZOH} - \Gamma_1 \quad (139)$$

**APPENDIX F**  
**SLEWER WIENER-HOPF EQUATIONS**

Given a discrete set of equations of motion for the model

$$x_{m_{k+1}} = \phi_m x_{m_k} + \Gamma_m \delta_{m_k} \quad (140)$$

one desires to modify the simulator, modeled by the slewed data hold equations

$$x_{s_{k+1}} = \phi_s x_{s_k} + \Gamma_1 \delta_{s_k} + \Gamma_2 \delta_{s_{k-1}} \quad (141)$$

to match the model. Take the z-transforms, setting the initial condition vector equal to zero:

$$[Iz - \phi_m]x_m = \Gamma_m \delta_m \quad (142)$$

$$[Iz - \phi_s]x_s = [\Gamma_1 + \Gamma_2 z^{-1}] \delta_s \quad (143)$$

Given a control law of the form

$$\delta_s = C_F \delta_m + C_B x_s \quad (144)$$

Equation 143 becomes

$$[Iz - \phi_s - (\Gamma_1 + \Gamma_2 z^{-1}) C_B] x_s = [\Gamma_1 + \Gamma_2 z^{-1}] C_F \delta_m \quad (145)$$

The relationships

$$[\Gamma_1 + \Gamma_2 z^{-1}] C_F = \Gamma_m \quad (146)$$

and

$$[\Gamma_1 + \Gamma_2 z^{-1}] C_B = \phi_m - \phi_s \quad (147)$$

cannot be identically satisfied, since  $[\Gamma_1 + \Gamma_2 z^{-1}]^{-1}$  does not, in general, exist. Taking a mean-square approach, form the vector  $E$  according to Equation 148,

$$E = [\Gamma_1 + \Gamma_2 z^{-1}] \begin{bmatrix} C_F \\ C_B \end{bmatrix} - \begin{bmatrix} \Gamma_m \\ \phi_m - \phi_s \end{bmatrix} \quad (148)$$

to set up the integrand of the performand index

$$J = \frac{1}{2\pi j} \int_{\Gamma} E'(z) E(z) \frac{dz}{z} \quad (149)$$

The gradient of  $E'(z)E(z)$  with respect to  $[C_F(1/z) \mid C_B(1/z)]$  gives the W-H equation:

$$\frac{1}{z} [\Gamma'_1 + \Gamma'_2 z] \left\{ [\Gamma_1 + \Gamma_2 z^{-1}] \begin{bmatrix} C_F \\ C_B \end{bmatrix}' - \begin{bmatrix} \Gamma_m \\ \phi_m - \phi_s \end{bmatrix}' \right\} = \psi \quad (150)$$

This verifies the W-H equation given for the slewer in the text.

## APPENDIX G

$$\text{PROOF, } C_F^{-1} C_B = (\Gamma'_1 \Gamma_m)^{-1} \Gamma'_1 (\phi_m - \phi_s)$$

The relationship

$$C_F^{-1} C_B = (\Gamma'_1 \Gamma_m)^{-1} \Gamma'_1 (\phi_m - \phi_s) \quad (151)$$

can be proven by using the properties of spectral factorization. Let

$$\frac{(\Gamma'_1 + \Gamma_2 z)(\Gamma_1 + \Gamma_2 z^{-1})}{z} = \phi \quad (152)$$

have the factorization

$$\phi = \phi_{1*} \phi_1 \quad (153)$$

and write

$$\phi_{1*} \phi_1 [C_F \mid C_B] - \frac{[\Gamma'_1 + \Gamma_2 z]}{z} [\Gamma_m \mid \phi_m - \phi_s] = \psi \quad (154)$$

The symbolic solution is

$$[C_F \mid C_B] = \phi_1^{-1} \left[ \phi_{1*}^{-1} \frac{[\Gamma'_1 + \Gamma_2 z]}{z} [\Gamma_m \mid \phi_m - \phi_s] \right]_+ \quad (155)$$

But  $\phi_{1*}^{-1}$  and  $\Gamma'_1 + \Gamma_2 z$  have no poles interior to the unit circle. Therefore, only the pole at the origin can contribute to the partial fraction expansion. Thus,

$$[C_F \mid C_B] = \phi_1^{-1} \left[ \phi_{1*}^{-1}(0) \Gamma'_1 \Gamma_m \mid \phi_{1*}^{-1}(0) \Gamma'_1 (\phi_m - \phi_s) \right] \quad (156)$$

Since

$$c_F^{-1} = (\Gamma'_1 \Gamma_m)^{-1} \phi_{1*}(0) \phi_1$$

then

$$c_F^{-1} c_B = (\Gamma'_1 \Gamma_m)^{-1} \phi_{1*}(0) \phi_1 \phi_1^{-1} \phi_{1*}^{-1} \Gamma'_1 (\phi_n - \phi_s)$$

or

$$c_F^{-1} c_B = (\Gamma'_1 \Gamma_m)^{-1} \Gamma'_1 (\phi_m - \phi_s)$$

**APPENDIX H**  
**PHYSICAL REALIZATION OF THE SLEWER COUPLER**

This appendix reviews the conversion of a sampled sequence to a continuous variable using a zero-order hold. One particular realization of the ZOH can be considered to be an incremental hold.

**A. CONVENTIONAL ZERO-ORDER HOLD**

Consider the impulse sampling of a time signal  $x = t$ , with a transform of

$$x = 1/s^2 \quad (157)$$

Reconstruction, via a ZOH (Fig. 41a) gives

$$\begin{aligned} Y &= \frac{1 - e^{-sT}}{s} X(s) = \frac{1 - e^{-sT}}{s} \frac{Tz}{(z - 1)^2} \\ &= \frac{1 - e^{-sT}}{s} \times T \frac{1}{z} + \frac{2}{z^2} + \frac{3}{z^3} + \dots \end{aligned} \quad (158)$$

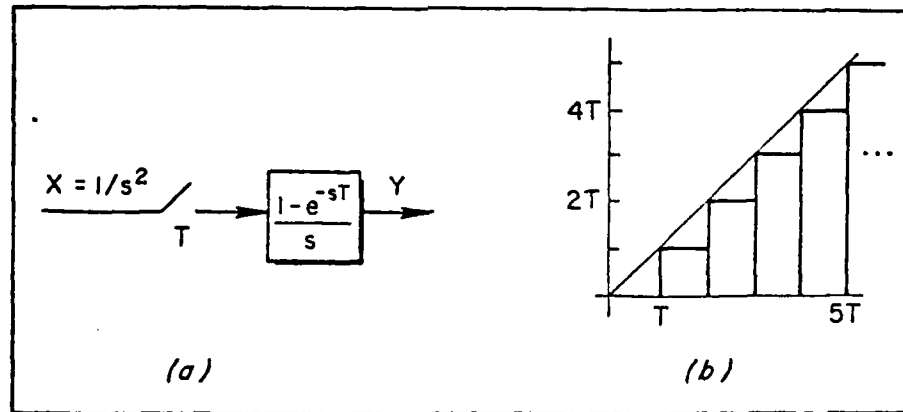


Figure 41. Zero-Order Hold Reconstruction

The reconstruction, using Eq. 158, is represented schematically in Fig. 41b.

Figure 41b represents a hardware implementation using a clamping circuit. That is, a constant level of voltage (or current) is held for  $T$  seconds and then (physically) removed. The control law then (essentially instantaneously) supplies a new pulse, which is clamped (held) for the next  $T$  second interval. The data hold is  $(1 - e^{-sT})/s$ .

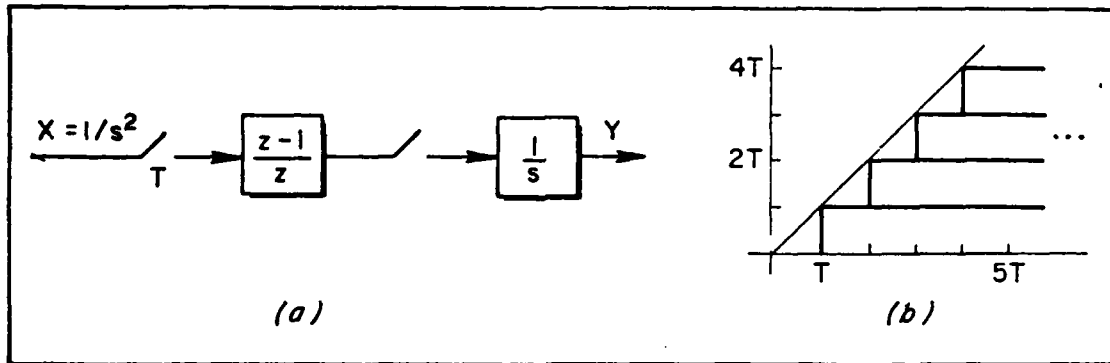


Figure 42. An Incremental Implementation

#### B. A PARTIAL SOFTWARE IMPLEMENTATION

Suppose the decision is made to relegate the transcendental element of the clamping circuit to software (Fig. 42). The describing equation is

$$Y = \frac{1}{s} \frac{z - 1}{z} \left[ \frac{Tz}{(z - 1)^2} \right] = \frac{T}{s} \left[ \frac{1}{z} + \frac{1}{z^2} + \frac{1}{z^3} + \dots \right] \quad (159)$$

The implication is (Fig. 42b) that each  $T$  second an increment to the control action is added to the signal already present. The data hold is  $1/s$ .

### C. THE SLEWER DATA HOLD

The preceding viewpoints transfer readily to the slew data hold.

$$M_{\text{slew}} = \frac{M_0^2}{T} = \frac{(1 - e^{-sT})}{T s^2} \quad (160)$$

The hardware implementation (Fig. 43) interprets the output

$$Y = \frac{(1 - e^{-sT})^2}{T s^3} \frac{Tz}{(z - 1)^2} = \frac{(1 - e^{-sT})^2}{T s^2} \frac{1}{z} + \frac{1}{z^2} + \frac{3}{z^3} + \dots \quad (161)$$

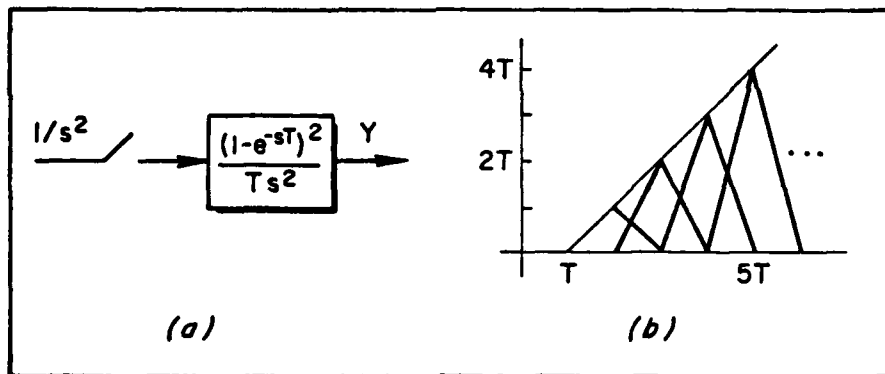


Figure 43. A Hardware Slew

as being built from shifted triangles while a more software-oriented implementation might retain an integrator and a ZOH (in hardware) and relegate the remainder to software (Fig. 44). This tends (Fig. 44) to have the appearance of an incremental controller.

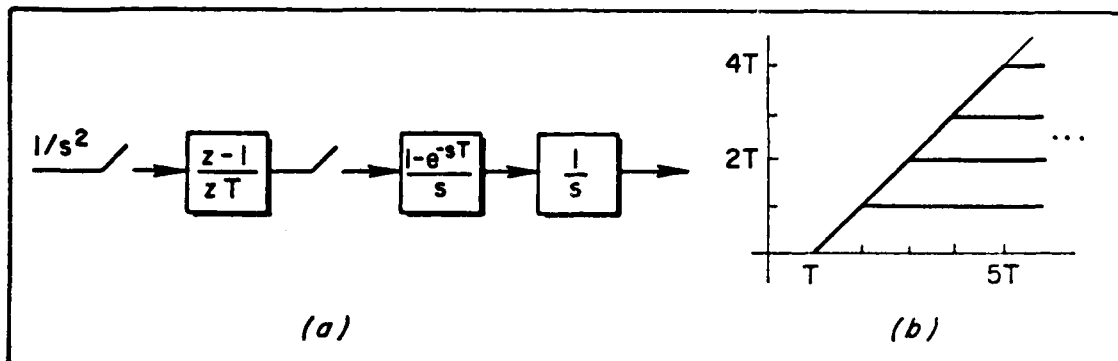


Figure 44. Partially Software Implemented Slewrate

The point we wish to make at this juncture is simple. The analytical model used in the synthesis process can differ from the physical implementation; however, the derived control law properties remain intact.

## APPENDIX I

### ADDITIONAL SLEWER DATA AND TABULAR LISTING OF STEP RESPONSES

The matrices involved in the slewер solution are  $\phi_s$ ,  $\phi_m$ ,  $\Gamma_m$ ,  $\Gamma_1$ , and  $\Gamma_2$ . These are, with the exception of  $\Gamma_1$  and  $\Gamma_2$ , listed in Appendix A. Define

$$\Gamma_1 = \begin{bmatrix} R_{101} & R_{102} & R_{103} \\ R_{104} & R_{105} & R_{106} \\ R_{107} & R_{108} & R_{109} \\ R_{110} & R_{111} & R_{112} \end{bmatrix}, \quad \Gamma_2 = \begin{bmatrix} R_{121} & R_{122} & R_{123} \\ R_{124} & R_{125} & R_{126} \\ R_{127} & R_{128} & R_{129} \\ R_{130} & R_{131} & R_{132} \end{bmatrix} \quad (162)$$

Data for Equation 162 are listed in Table 7.

TABLE 7

#### DATA FOR $\Gamma_1$ , $\Gamma_2$

$R_{101} = -0.283742140$	$R_{121} = -0.197317335$
$R_{102} = 0.115668810$	$R_{122} = 0.218682553$
$R_{103} = 0.102104000$	$R_{123} = 0.095739417$
$R_{104} = 0.008363868$	$R_{124} = 0.014969735$
$R_{105} = -0.006567369$	$R_{125} = -0.013856154$
$R_{106} = -0.005131947$	$R_{126} = -0.008120770$
$R_{107} = 0.332982000$	$R_{127} = 0.277639404$
$R_{108} = 0.294238000$	$R_{128} = 0.300734839$
$R_{109} = 2.287250000$	$R_{129} = 2.132551283$
$R_{110} = 0.010283700$	$R_{130} = 0.022925586$
$R_{111} = 0.009357000$	$R_{131} = 0.020065493$
$R_{112} = 0.076482000$	$R_{132} = 0.152324084$

In addition, the step transient responses of the closed-loop system, in increments of 0.1 seconds, are listed in Table 8. In this table,

$$\begin{array}{ll} R_{01} = x_1 = \beta & R_{13} = \delta_1 = \delta_R \\ R_{02} = x_2 = r & R_{14} = \delta_2 = \delta_{SF} \\ R_{03} = x_3 = p & R_{15} = \delta_3 = \delta_A \\ R_{04} = x_4 = \phi & \end{array} \quad (163)$$

TABLE 8. SLEWER STEP RESPONSES

R01= 0.000000000	0.065737053	R01= 0.067496061	0.060167828	0.060434960	0.060677115	0.060788469	0.060839083
R02= 0.000000000	0.008117652	R02= 0.001243138	0.000360214	0.000621534	0.000822119	0.000646129	0.000762000
R03= 0.000000000	-0.013466723	R03= 0.025416892	0.005729389	-0.002199976	-0.000103033	0.000021235	0.000085064
R04= 0.000000000	-0.015747090	R04= -0.008983560	-0.000804114	-0.000726351	-0.001329984	-0.001265243	-0.001272412
R13= 1.533456216	0.696242196	R13= 1.147232834	0.894189300	1.037649412	0.972434251	0.977715535	1.014113040
R14= 1.667517094	0.665216749	R14= 1.229729217	0.894826302	1.107724311	0.987333531	1.034175438	1.040527945
R15= -0.450530559	-0.172884186	R15= -0.333396952	-0.245968690	-0.297762217	-0.271497306	-0.277453132	-0.235834349
0.	5.	10.	15.	20.	25.	30.	35.
R01= 0.017370935	0.070002452	R01= 0.065105378	0.060130317	0.060366755	0.060864974	0.060629684	0.060744902
R02= 0.004292115	0.006428972	R02= 0.000365533	0.000254143	0.000348812	0.000656734	0.000762639	0.000660051
R03= -0.030702223	0.000608122	R03= 0.023563805	0.000201990	-0.001553394	-0.000215081	0.000233023	-0.000096414
R04= -0.003052635	-0.016446332	R04= -0.006496718	-0.000427312	-0.000928712	-0.001313972	-0.001290036	-0.001233136
R13= 0.562121392	1.168622941	R13= 0.348037595	1.070152247	0.944910031	0.996671023	1.001599991	0.953749276
R14= 0.548256696	1.249503669	R14= 0.835675474	1.155334865	0.954267110	1.057959539	1.023927932	1.00903263
R15= -0.139155544	-0.334843938	R15= -0.229132429	-0.311752351	-0.262222740	-0.283984441	-0.281518494	-0.270829095
1.	6.	11.	16.	21.	26.	31.	36.
R01= 0.034367119	0.071133194	R01= 0.0635568400	0.059793901	0.060713305	0.060676733	0.060761370	0.060641053
R02= 0.007522752	0.005140056	R02= 0.000249189	0.000534925	0.000672744	0.000795131	0.000652156	0.000750592
R03= -0.039460099	0.0136539621	R03= 0.018731427	0.000344493	-0.001594104	0.000237276	-0.000034755	0.000057272
R04= -0.006292239	-0.015661312	R04= -0.004339958	-0.000316309	-0.001964322	-0.001345226	-0.001241732	-0.001275305
R13= 1.249711064	0.754954354	R13= 1.126732450	0.912353795	1.021350008	0.933746710	0.970210206	1.018726043
R14= 1.351269724	0.729347837	R14= 1.209111466	0.916146310	1.038715797	1.001209371	1.024476647	1.046942329
R15= -0.360440470	-0.194004198	R15= -0.327836099	-0.251714261	-0.292388530	-0.275369146	-0.274357915	-0.287523465
2.	7.	12.	17.	22.	27.	32.	37.
R01= 0.043053173	0.071052527	R01= 0.061817274	0.060121379	0.060532210	0.060829573	0.060624718	0.060743003
R02= 0.000024367	0.003401572	R02= 0.000327604	0.000479761	0.000647060	0.000646621	0.000764762	0.000674233
R03= -0.033307352	0.021176209	R03= 0.014521491	-0.001438822	-0.000781215	0.000066470	0.000145483	-0.000089615
R04= -0.010240044	-0.013946238	R04= -0.002722226	-0.000369937	-0.001297846	-0.001293267	-0.001275251	-0.001236833
R13= 0.641608235	1.160535731	R13= 0.872900715	1.056326891	0.959443506	0.98650160	1.008447001	0.954604253
R14= 0.613594065	1.241854598	R14= 0.869407833	1.129996734	0.971583620	1.045306317	1.032901599	1.003294229
R15= -0.155571322	-0.335335001	R15= -0.239390097	-0.304193961	-0.267085948	-0.238461021	-0.28397092	-0.269340399
3.	8.	13.	18.	23.	28.	33.	38.
R01= 0.052904422	0.069200005	R01= 0.061072210	0.060026565	0.060547403	0.060864931	0.060748993	0.060650019
R02= 0.003774122	0.002435093	R02= 0.000072326	0.000761434	0.000672025	0.000777323	0.000668323	0.000754335
R03= -0.023722649	0.025330534	R03= 0.009217262	-0.001629209	-0.000763155	0.000301295	-0.000024191	0.000049819
R04= -0.013674109	-0.011530742	R04= -0.001549529	-0.000542409	-0.001257643	-0.001310256	-0.001232690	-0.001276961
R13= 1.184973982	0.906327102	R13= 1.102411100	0.929134823	1.000353222	0.993421795	0.963917495	1.022339442
R14= 1.271057036	0.739155121	R14= 1.102705753	0.935729663	1.072311410	1.013446629	1.01614047	1.052250213
R15= -0.333276443	-0.214575353	R15= -0.328024325	-0.257063697	-0.287030363	-0.273695153	-0.272657047	-0.200649013
4.	9.	14.	19.	24.	29.	34.	39.

END

FILMED

283

DTIC